TABLE OF CONTENTS

TABLE OF CONTENTS
(Continued)

TABLE OF CONTENTS
(Continued)

TABLE OF CONTENTS
(Continued)

LIST OF TABLES

LIST OF TABLES
(Continued)

LIST OF FIGURES

LIST OF FIGURES
(Continued)

LIST OF FIGURES
(Continued)

NASA Contractor Report 2946

Analytical Study of a Free-Wing/Free-Trimmer Concept

Richard F. Porter, David W. Hall,
Joe H. Brown, Jr., and Gerald M. Gregorek

CONTRACT NAS4-2378
FEBRUARY 1978

NASA

Blank
Page

NASA Contractor Report 2946

Analytical Study of a Free-Wing/Free-Trimmer Concept

Richard F. Porter, David W. Hall,
Joe H. Brown, Jr., and Gerald M. Gregorek
Battelle Columbus Laboratories
Columbus, Ohio

Prepared for
Dryden Flight Research Center
under Contract NAS4-2378

National Aeronautics
and Space Administration

Scientific and Technical
Information Office

1978

Blank
Page

ANALYTICAL STUDY OF A FREE-WING/FREE-TRIMMER CONCEPT

Richard F. Porter, David W. Hall, Joe H. Brown, Jr.,
and Gerald M. Gregorek

Battelle Columbus Laboratories

SUMMARY

Previous studies have indicated several benefits, including substantial gust alleviation, for aircraft employing an unconventional wing, free to pivot about a spanwise axis forward of its aerodynamic center and subject only to aerodynamic pitching moments imposed by lift and drag forces and a trailing-edge control surface. A disadvantage of this basic free-wing concept is the relatively low wing lift coefficient available, since there is no mechanism to overcome the powerful negative pitching moments associated with the deflection of high-lift trailing-edge flaps.

The free-wing/free-trimmer is a NASA-conceived extension of the basic free-wing concept intended to provide sufficient trimming power to permit the use of high-lift trailing-edge flaps on free-wing aircraft. The wing is controlled by the pitching moment produced about its hinge axis by the aerodynamic forces on a smaller, external trimmer surface attached to the wing by a boom or equivalent structure. Furthermore, the trimmer itself is free to pivot about a spanwise hinge axis forward of its aerodynamic center. Pitch control of the entire assembly is effected by deflection of a trailing-edge flap on the trimming surface.

This report describes an analytical study of the longitudinal behavior of representative small free-wing/free-trimmer aircraft. It includes an assessment of the response to symmetric vertical turbulence, the nature of the characteristic longitudinal stick-fixed modes of motion, and the maximum trimmed

lift coefficients obtainable. Both forward- and aft-mounted trimming surfaces are considered.

Although the permissible trimmer moment arm is limited by adverse dynamic effects, it is concluded that configurations with trimmer surfaces mounted aft of the wing hinge can be designed that provide excellent alleviation of vertical gust loads yet exceed the maximum lift capability of pure free-wing aircraft and meet fundamental criteria for the stick-fixed longitudinal stability. Forward trimmer configurations were found to have inferior gust alleviation characteristics.

While the allowable center of gravity range for the fuselage assembly is comparable to conventional aircraft, the wing/trimmer assembly should be mass-balanced about the wing hinge to facilitate smooth landings. Close mass-balancing of the free trimmer surface, with respect to its hinge axis, is mandatory to preclude short-period dynamic instabilities.

INTRODUCTION

Background

Low wing loading has long been synonymous with poor ride quality in turbulence, a fact which has probably been a significant deterrent to widespread acceptance of light aircraft as a practical means of transportation. The problem is compounded by the fact that light aircraft spend a major portion of their flight time at the lower altitudes where measurable turbulence is most likely to be encountered, even in good weather.

An increase in wing loading can be expected to produce ride improvement, but this approach is constrained by the need to maintain low minimum flying speeds. Not only is a low speed capability desirable from an operational standpoint for aircraft in this class, but Federal airworthiness standards (FAR Part 23) require a minimum speed of 61 knots or less for single engine aircraft. Even with well designed mechanical high-lift devices, it appears that a wing loading of 1900 N/M^2 (40 lb/ft^2) is an approximate practical upper limit; this may be compared to wing loadings of 4300 N/M^2 to 5300 N/M^2 (90 lb/ft^2 to 110 lb/ft^2) typical of the commercial jet transport aircraft which have enjoyed wide acceptance by the traveling public.

The free-wing concept is a novel and very effective approach to gust alleviation which would appear to have other benefits as well, but a disadvantage of the concept is the relatively low maximum lift coefficient obtainable.

The free-wing/free-trimmer is a NASA-conceived extension of the basic free-wing concept intended to provide sufficient trimming power to permit the use of high-lift trailing-edge flaps on the free wing.

Free-Wing Concept

The basic concept of the free wing was disclosed in U.S. Patent No. 2,347,230. This patent, now expired, was issued in 1944 to Daniel R. Zuck, who built a small prototype aircraft in 1945 as a private venture. This aircraft was never successfully flown.

As conceived by Zuck, a free-wing aircraft differs from a conventional airplane in that the two panels of the fuselage-mounted wing are free to move independently about a spanwise axis and are controlled by means of trailing-edge control surfaces. Each wing panel is completely free to rotate about its spanwise axis, subject to aerodynamic moments but otherwise unrestricted by mechanical constraints. To provide static pitching stability, the axis of rotation is located forward of the chordwise aerodynamic center of the wing panel, as shown in figure 1. The wing is brought to an equilibrium angle of attack through a balance of moments created by the trailing-edge surface, which is controlled by the pilot, and the torques produced by the lift and drag forces.

The gust alleviation feature of the free wing is caused by the fact that a stable lifting surface tends to maintain a prescribed lift coefficient by responding to natural pitching moments which accompany changes in flow direction. While all stable aircraft tend to relieve the lift increment due to a vertical gust by pitching into the relative wind, the rapidity of the alleviating motion depends upon the pitching moment of inertia. Because of the greatly reduced inertia of the wing panel, compared to the aircraft as a whole, the free-wing concept produces a significant reduction in turbulence responses.

Previous Work

The first known analytical study to predict the fundamental dynamic behavior of free-wing aircraft permitted independent motion of the left and

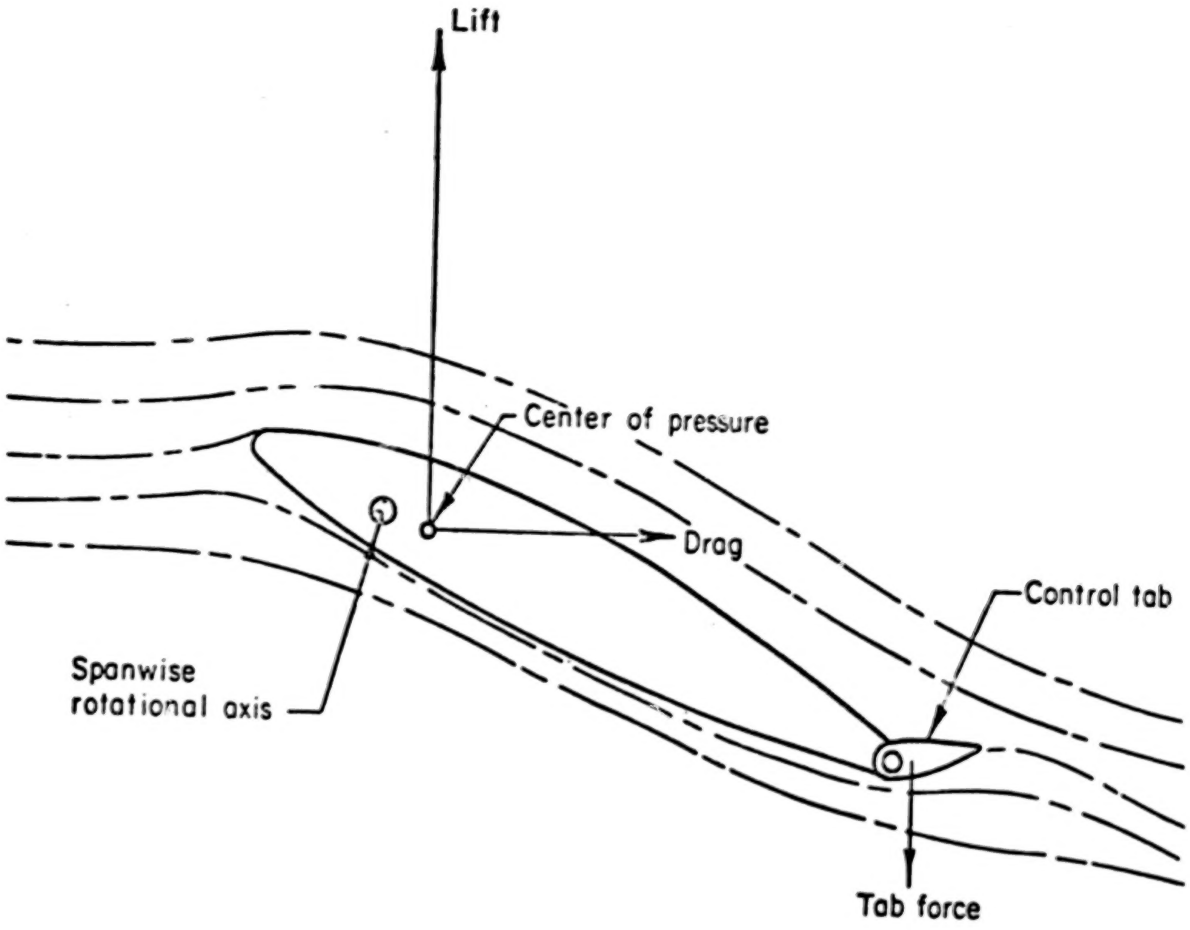

FIGURE 1. CROSS-SECTIONAL ILLUSTRATION OF THE FREE WING

right wing panels and is reported in reference 1. The following conclusions were drawn from this earlier work:

(1) Most atmospheric turbulence effects were greatly reduced, particuarly in the root-mean-square (rms) load factor (62 percent reduction) and rolling disturbances (25 percent reduction). On the other hand, the rms fuselage pitch rate was increased about 180 percent in comparison with equivalent fixed-wing aircraft.

(2) All stick-fixed modes of motion were stable except for the spiral mode, where the rate of divergence was found to be excessively high in the approach condition.

(3) The lateral-directional handling qualities were unsatisfactory because of the combination of low roll damping and spiral divergence.

(4) Artificial stability augmentation, in the form of a simple roll damper, provided excellent lateral control and turbulence penetration characteristics.

As a result of the very substantial gust alleviation predicted in reference 1, a second study was performed to provide a realistic and

comprehensive assessment of the practical aspects of implementation of the free-wing concept for light, general aviation aircraft.

The second investigation is reported in reference 2. This study, while analytical, was supported by limited wind-tunnel experiments.

From the results of the second study, the following conclusions were drawn:

(1) The free-wing concept can be applied to unsophisticated low wing loading light aircraft to provide a ride quality, based on normal load factor attenuation, equal or superior to that of aircraft employing much higher wing loadings. Compared to similar light aircraft in cruise flight, reductions of about 54 percent can be realized in the rms load factor increments in continuous turbulence.

(2) For free-wing aircraft without differential wing panel freedom, all pertinent handling qualities and certification criteria can be met without recourse to stability augmentation, either active or passive.

(3) Differential pitch freedom between the left and right wing panels should not be permitted for aircraft in this class, although it appears that passive mechanical devices can be applied to correct the serious lateral deficiencies which accompany such freedom.

(4) Leading-edge slats are necessary for takeoff and landing to compensate for the inherent low maximum trimmed lift coefficients obtained with trailing-edge control surfaces.

(5) The free-wing panels should be balanced about the spanwise hinge axis with leading-edge slats retracted. A ballast weight penalty is incurred which might range from 1.5 percent to 7.0 percent of the aircraft gross weight, depending on the detailed design.

Purpose of this Investigation

The purpose of this work was to perform an analytical evaluation of the dynamic characteristics of an aircraft employing a NASA-conceived concept of a wing and wing-trimmer assembly. In this concept, the wing is free to pivot freely in pitch forward of its aerodynamic center, and pitch control is achieved by a trimming surface, which is trimmed by trailing-edge flaps. The trimming surface is also free to pivot freely in pitch forward of its aerodynamic center but is connected to the wing by a rigidly attached boom. This report describes an analytical study of the longitudinal behavior of representative small free-wing/free-trimmer aircraft. It includes an assessment of the response to symmetric vertical turbulence, the nature of the characteristic longitudinal stick-fixed modes of motion, and the maximum trimmed lift

coefficients obtainable. Both forward- and aft-mounted trimming surfaces are considered. To avoid the lateral-directional instability problems found in previous free-wing studies, the left and right wing panels were constrained to symmetrical deflections only, roll control being achieved by the differential operation of wing flaps. Body attitude adjustment was provided, as in the previous studies, by a separate horizontal stabilizer.

Scope

The research effort described in this report is limited to an analytical study of the stick-fixed longitudinal motion and gust alleviation characteristics of a representative light aircraft employing the free-wing/free-trimmer concept. The analysis was supported by the design of several conceptual free-wing/free-trimmer aircraft to provide representative dimensional and mass parameters.

Since both the free-wing and free-trimmer panels were constrained to symmetrical pitching motion, only the longitudinal behavior was analyzed. With no differential freedom permitted, the aircraft could be expected to behave similarly to conventional fixed-wing aircraft in the lateral-directional modes.

Attention was confined to linear analyses of the responses to symmetric vertical gusts and the basic longitudinal flying qualities as indicated by the characteristic roots associated with the stick-fixed longitudinal modes.

The turbulence responses were evaluated by computing rms values of pertinent variables in response to continuous atmospheric turbulence, but no attempt was made for a direct evaluation of riding qualities as affected by human tolerance factors.

The fundamental strategy of this investigation was to:

(1) derive the equations of motion applicable to an aircraft using the free-wing/free-trimmer concept;

(2) create a family of conceptual aircraft designs to provide realistic parameters for the mathematical models; and

(3) perform a linear analysis of the gust alleviation characteristics, handling qualities, and other features peculiar to the overall concept.

SYMBOLS

$\bar{c}$	mean aerodynamic chord, meters (feet)
$C_{l_{max}}$	maximum section lift coefficient
C_{L_c}	free-trimmer lift coefficient
C_{L_w}	wing lift coefficient
$C_{L_{max_w}}$	maximum wing lift coefficient
$C_{m_{a.c}}$	moment coefficient about aerodynamic center
$C_{m_{hinge}}$	moment coefficient about hinge axis
$F_{x_{c\to b}}$, $F_{z_{c\to b}}$	components of force transmitted from free trimmer to boom, newtons (pounds)
$F_{x_{w\to f}}$, $F_{z_{w\to f}}$	components of force transmitted from wing to fuselage, newtons (pounds)
HM	hinge margin, distance from aerodynamic center forward to hinge axis, expressed as fraction of chord length
S	wing reference area, meters^2 (feet^2)
S_c	free-trimmer reference area, meters^2 (feet^2)
u	increment in airspeed divided by equilibrium airspeed
X_c'	distance of free-trimmer hinge forward of wing hinge, meters (feet)
α_c	angle of attack of free-trimmer surface, radians
α_f	angle of attack of fuselage assembly, radians
α_w	angle of attack of wing, radians
δ_c	angular displacement of free trimmer with respect to wing, radians
δ_f	wing flap deflection, degrees
δ_p	angular displacement of wing with respect to fuselage, radians
θ	pitch angle of fuselage with respect to horizon, radians
σ_{n_z}	rms normal load factor response, g's
λ	Laplace operator, 1/sec

PROCEDURE

Mathematical Models

Although the original plan was to modify the computer programs used in the previous free-wing analyses, it soon became apparent that the additional complexity introduced by the free-trimmer dynamics dictated the development of

new mathematical models. Furthermore, whereas the linear models used in the previous analyses were derived directly from the complete nonlinear equations by limiting the motion to small disturbances from straight and level equilibrium, the current task required an unorthodox form of the linear model.

The development of the inertial force and moment terms for the complete nonlinear equations with eight degrees of freedom is given in appendix A to provide documentation for possible future studies. The linear development, which is confined to longitudinal motion, is described separately in appendix B.

The longitudinal system has five degrees of freedom. Three variables are required to define the spatial position and orientation of the fuselage in the vertical plane, and two additional variables are required to define the angular displacements of the wing and trimmer surfaces. With unsteady aerodynamic effects included for both lifting surfaces, the linear longitudinal system is of tenth order*.

The linearized set of equations describing the longitudinal motion of the aircraft in response to vertical gust velocities and control tab displacement is given by the following equation:

$$[A]\,\overline{X} = [B]\,\delta_t + [C]\,\frac{V_g}{U_o} \qquad (1)$$

Where [A] is a 13 by 13 matrix of the coefficients of the homogeneous equations, and [B] and [C] are column matrices.

The state variable $\overline{X}$ has 13 components: α_c, C_{L_c}, δ_c, $F_{\substack{x \\ c\to b}}$, $F_{\substack{z \\ c\to b}}$, α_w, C_{L_w}, δ_p, $F_{\substack{x \\ w\to f}}$, $F_{\substack{z \\ w\to f}}$, θ, u, and α_f.

It is the number of components of the state vector which constitutes the primary departure from convention. Since the system has five independent degrees of freedom, it would have been possible to combine most of the equations to arrive at a set using only five independent variables. These would logically have been u, α_f, θ, δ_p, and δ_c. Unfortunately, the elimination of the eight remaining variables involves considerable algebraic manipulation which would have obscured the physical significance and origins of the individual terms in the final equations.

* The linear approximations of reference 5 were used to model the unsteady lift phenomena, as discussed in appendix B.

Although the retention of 13 variables in the equations of motion seems ponderous, and incurs certain penalties in computation time, it has the overriding advantage of greatly facilitating the verification of each of the terms in the individual equations -- an advantage of some importance, since no prior analysis of such a system was in existence to provide a standard for checking the correctness of the model. Since time did not permit the restructuring of the model in condensed, more conventional form, the 13 equations were retained as they were derived.

Conceptual Aircraft Designs

In this study, attention was confined to families of airplanes based upon two light aircraft configurations in order to assess some benefits, if any, accruing to light aircraft of markedly different missions. The first was a two seat light aircraft having tricycle gear, pusher propeller, and a high free wing with a free trimmer placed two chord lengths ahead of the wing hinge line and fixed to the wing by two rigid booms. The second aircraft was a single seat agricultural airplane having conventional gear and a tractor propeller. The free wing was mounted lower on the fuselage and the free trimmers were mounted aft of the wing on two rigid booms.

For purposes of direct comparison and parametric analysis of the penalty and benefit of free trimmer control volume, both forward and aft of the wing, the first configuration was fitted with a forward free trimming surface, referred to in this work as a forward trimmer, two separate aft free trimming surfaces referred to as aft trimmers, a pure free wing, and a comparable fixed wing.

Design summary. - Following accepted procedures for the conceptual design of light aircraft, the two types of aircraft were designed in enough detail to allow the calculation of weights and moments of inertia. Steps in this process common to both were the identification of aircraft mission, the calculation of the flying surface sizes necessary to fulfill their missions, a first weight estimate based on mission requirements, an estimate of wing maximum trimmed lift, tail sizing, development of a cockpit design that conformed to MIL-STD-1333, first layout, revision of the weight estimate, iterations to reduce weight, and the calculation of moments of inertia. Common features to

both aircraft are an aspect ratio 6 rectangular wing with a NACA 23012 section, wing loading comparable to existing aircraft of the same class, a total free trimmer area that is one-sixth the wing area, a horizontal tail sized strictly for fuselage pitch attitude control, wing panels and trimmer panels that are constrained to symmetrical deflections only, and 19 percent chord hinge lines for all free surfaces.

Previous work dictated that the free-wing/boom/trimmer combination balance about the hinge point of the wing. This is an important design constraint which was maintained in the conceptual configurations by carrying all disposable items in the fuselage. Variations of the center of gravity of the trimmer, wing/boom/trimmer, and fuselage were permitted for parametric analyses during the investigation.

First concept - a two place light aircraft. - This is a two place aircraft with the free trimmer in a forward position ahead of its free wing. The basic mission for sizing is fair weather training. Payload is similar to existing aircraft in this mission category and includes two crew and enough fuel for a 3 hour flight. Fixed wing gross weight is in the 680 kilogram (1500 pound) class. Other features are two place side by side seating ahead of the wing, a shoulder wing, typical general aviation wing loading, an 86 kilowatt (115 BHP) engine in a pusher arrangement, 20 percent chord flaps on the free wing and free trimmer, and a two wing-chord-length arm on the free trimmer.

The family of configurations is listed in table I and figures 2(a) to 2(c) are multiview drawings of each of the parametric variations described in table I below:

TABLE I. FAMILY OF TWO-PLACE LIGHT AIRCRAFT

Configuration	Figure	Description
1A	2(a)	Forward free surface
1B	2(b)	Pure free wing
1C	2(c)	Aft free surface
1D	(Not shown)	Fixed-wing equivalent to configuration 1B

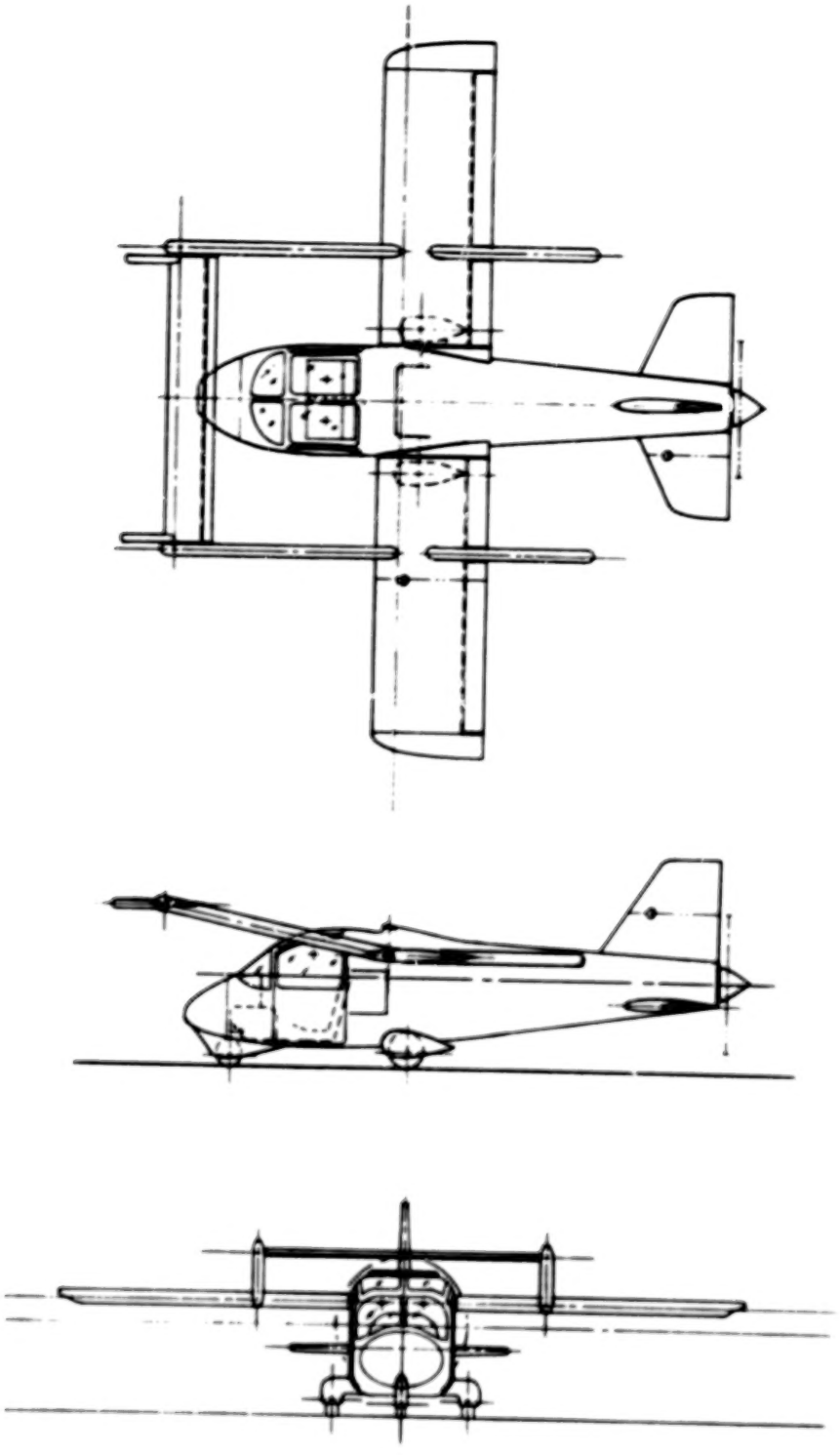

FIGURE 2(a). TWO SEAT LIGHT AIRCRAFT (CONFIGURATION 1A--
FREE WING/FORWARD FREE TRIMMER).

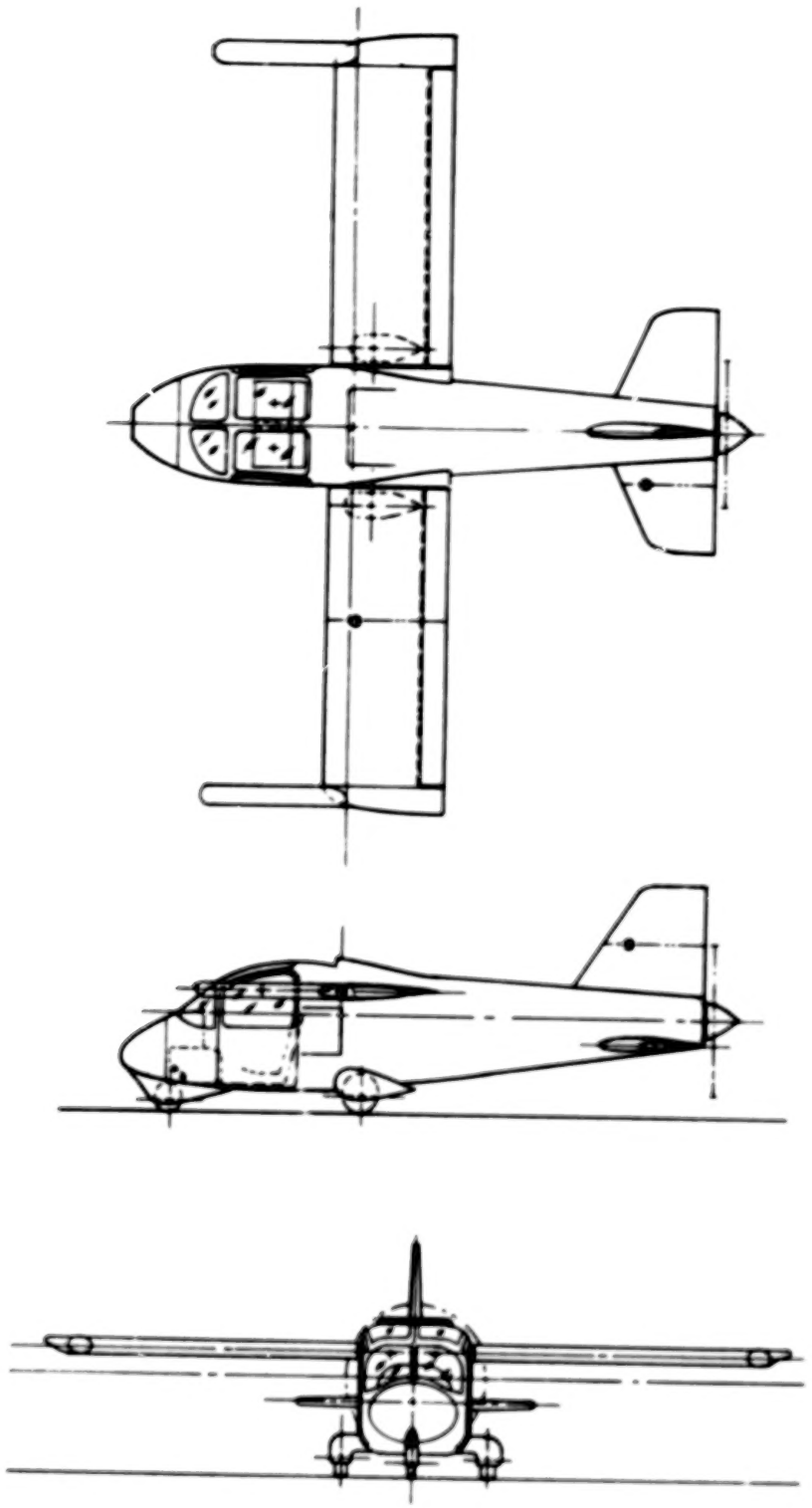

FIGURE 2(b). TWO SEAT LIGHT AIRCRAFT (CONFIGURATION 1B--PURE FREE WING). FIXED WING CONFIGURATION 1D EXTERNALLY IS SIMILAR TO THIS LESS EXTERNAL BALANCES ON WING.

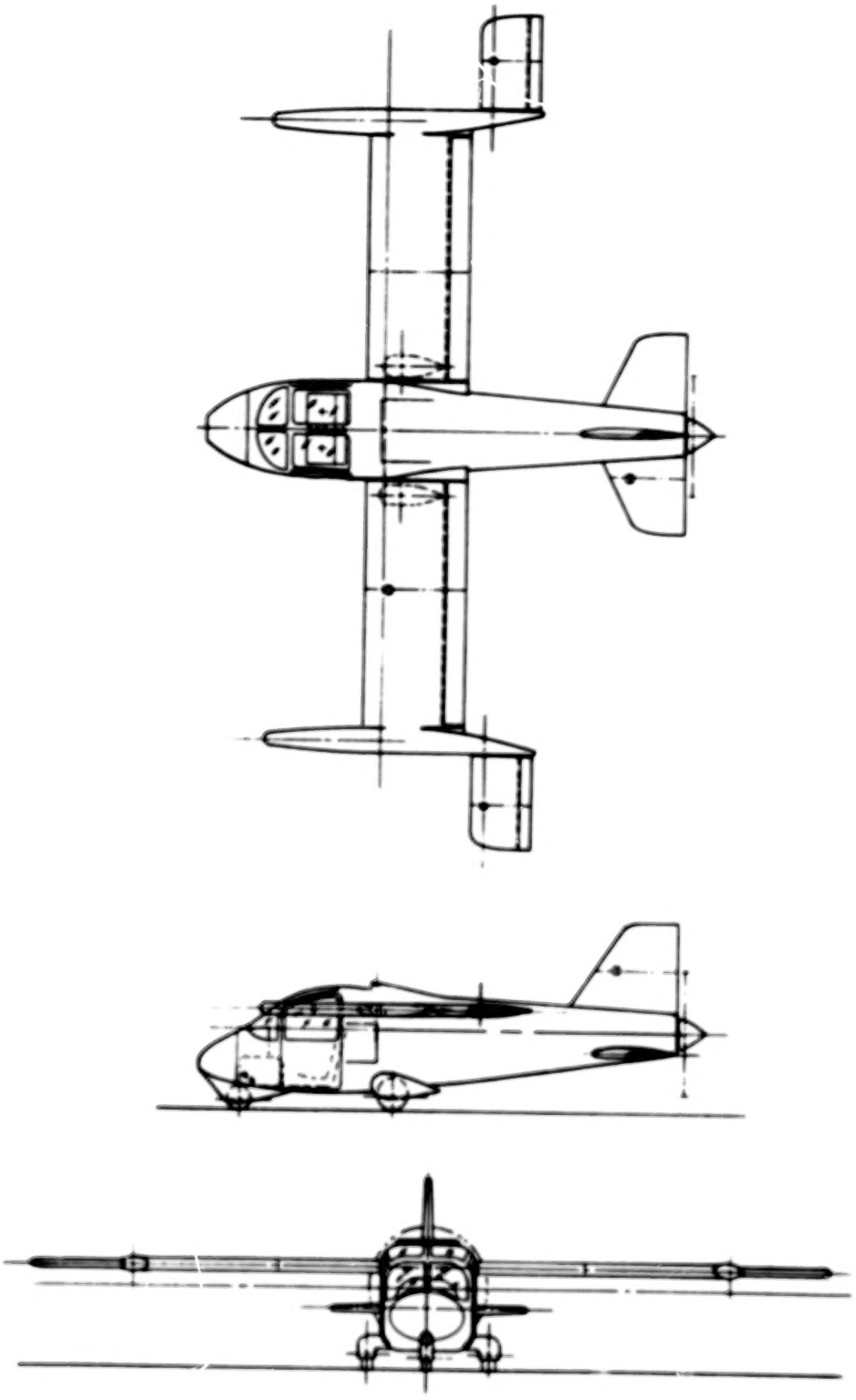

FIGURE 2(c). TWO SEAT LIGHT AIRCRAFT (CONFIGURATION 1C--FREE WING/AFT FREE TRIMMER).

Table II is a summary of geometric data, and table III is a weight summary for each of the configurations in table I. No attempt was made to minimize the counterbalancing weight penalty due to static balance requirements to provide a direct comparison of benefits and penalties from one configuration to another.

These configurations are strictly conceptual and address only the most obvious practical design constraints. The propeller and engine placement, for instance, may not be practical in a real aircraft because of lack of propeller ground clearance.

Second concept - a single place agricultural aircraft. - This aircraft was sized to be comparable to existing American agricultural aircraft in the 1700 kilogram (3800 pound) weight range with about a 0.5 cubic meter (17 cubic foot) hopper capacity. Features of this aircraft design are a single place air conditioned and pressurized cockpit surrounded by 40g crash-resistant shell, a 0.45 cubic meter (16 cubic foot) hopper (approximately 590 kilogram (1300 lb) payload), a 227 kilowatt (305 BHP) engine with a constant speed propeller, a fully cantilevered wing, spray bars carried in external struts under each wing and hinged on the wing main spar, conventional gear, and a mid-wing to eliminate the need for geometric dihedral.

The family of parametric configurations examined is shown in figures 3(a) and 3(c) and their designations are explained in table IV. Geometric data are presented in table V, and weight data are shown in table VI.

TABLE II. SUMMARY OF GEOMETRIC DATA FOR TWO SEAT AIRCRAFT VARIATIONS

Item	Configuration 1A	1B	1C	1D
Fuselage -				
Length, m (ft)	6.44 (21.13)	6.44 (21.13)	6.44 (21.13)	6.44 (21.13)
Maximum width, m (ft)	1.19 (3.9)	1.19 (3.9)	1.19 (3.9)	1.19 (3.9)
Maximum height, m (ft)	1.31 (4.3)	1.31 (4.3)	1.31 (4.3)	1.31 (4.3)
Surface area, m^2 (ft^2)	18.247 (196.4)	18.247 (196.4)	18.247 (196.4)	18.247 (196.4)
Wing -				
Span, m (ft)	7.77 (25.5)	7.77 (25.5)	7.77 (25.5)	7.77 (25.5)
Reference area, m^2 (ft^2)	10.09 (108.6)	10.09 (108.6)	10.09 (108.6)	10.09 (108.6)
Exposed area, m^2 (ft^2)	8.54 (91.9)	8.54 (91.9)	8.54 (91.9)	8.54 (91.9)
Wetted area, m^2 (ft^2)	17.38 (187.1)	17.38 (187.1)	17.38 (187.1)	17.38 (187.1)
Aspect ratio	6.00	6.00	6.00	6.00
Taper ratio	1.00	1.00	1.00	1.00
Thickness ratio	0.12	0.12	0.12	0.12
Mean geometric chord, m (ft)	1.30 (4.25)	1.30 (4.25)	1.30 (4.25)	1.30 (4.25)
Airfoil	NACA 23012	NACA 23012	NACA 23012	NACA 23012
Hinge point (percent chord)	19.0	19.0	19.0	None
Free stabilizer (each surface if more than one) -				
Span, m (ft)	3.17 (10.4)	----------	1.14 (3.8)	----------
Reference area, m^2 (ft^2)	1.68 (18.1)	----------	0.871 (9.4)	----------
Exposed area, m^2 (ft^2)	1.68 (18.1)	----------	0.871 (9.4)	----------
Wetted area, m^2 (ft^2)	3.42 (36.8)	----------	1.77 (19.1)	----------
Aspect ratio	6.0	----------	1.50	----------
Taper ratio	1.0	----------	1.00	----------
Thickness ratio	0.12	----------	0.12	----------
Mean geometric chord, m (ft)	0.52 (1.7)	----------	0.76 (2.5)	----------
Airfoil	NACA 23012	----------	NACA 23012	----------
Hinge point (percent chord)	19.00	----------	19.00	----------
Control arm (hinge point to hinge point), m (ft)	-2.53 (-8.3)	----------	1.31 (4.3)	----------
Control volume (hinge point to hinge point)	-0.33	----------	0.18	----------
Horizontal tail -				
Span, m (ft)	2.44 (8.0)	2.44 (8.0)	2.44 (8.0)	2.44 (8.0)
Reference area, m^2 (ft^2)	2.14 (23.0)	2.14 (23.0)	2.14 (23.0)	2.14 (23.0)
Exposed area, m^2 (ft^2)	1.49 (16.0)	1.49 (16.0)	1.49 (16.0)	1.49 (16.0)

TABLE II. (Continued)

Item	Configuration 1A	1B	1C	1D
Wetted area, m^2 (ft^2)	3.03 (32.6)	3.03 (32.6)	3.03 (32.6)	3.03 (32.6)
Aspect ratio	2.78	2.78	2.78	2.78
Taper ratio	0.50	0.50	0.50	0.50
Thickness ratio	0.09	0.09	0.09	0.09
Mean geometric chord, m (ft)	0.951 (3.12)	0.951 (3.12)	0.951 (3.12)	0.951 (3.12)
Airfoil	NACA 0009	NACA 0009	NACA 0009	NACA 0009
Control arm (hinge point to one-quarter chord), m (ft)	3.05 (10.0)	3.05 (10.0)	3.05 (10.0)	3.05 (10.0)
Control volume (hinge point to one-quarter chord)	0.50	0.50	0.50	0.50
Vertical tail -				
Span, m (ft)	1.02 (3.3)	1.02 (3.3)	1.02 (3.3)	1.02 (3.3)
Reference area m^2 (ft^2)	2.02 (21.7)	2.02 (21.7)	2.02 (21.7)	2.02 (21.7)
Exposed area m^2 (ft^2)	2.02 (21.7)	2.02 (21.7)	2.02 (21.7)	2.02 (21.7)
Wetted area m^2 (ft^2)	4.097 (44.1)	4.097 (44.1)	4.097 (44.1)	4.097 (44.1)
Aspect ratio	0.51	0.51	0.51	0.51
Taper ratio	0.50	0.50	0.50	0.50
Thickness ratio	0.09	0.09	0.09	0.09
Mean geometric chord, m (ft)	1.04 (3.42)	1.04 (3.42)	1.04 (3.42)	1.04 (3.42)
Airfoil	NACA 0009	NACA 0009	NACA 0009	NACA 0009
Control arm (hinge point to one-quarter chord), m (ft)	2.92 (9.6)	2.92 (9.6)	2.92 (9.6)	2.92 (9.6)
Control volume (hinge point to one-quarter chord)	0.08	0.08	0.08	0.08
Pitch moment of inertia -				
Forward trimmer about trimmer hinge line, kg-m^2 (slug-ft^2)	1.2 (1.637)	----------	----------	----------
Aft trimmer about trimmer hinge line, kg-m^2 (slug-ft^2)	----------	----------	36.0 (48.839)	----------
Wing/boom/balances about wing hinge line, kg-m^2 (slug ft^2)	129.7 (175.894)	34.1 (46.283)	56.8 (77.027)	----------
Total aircraft about aircraft center of gravity, kg-m^2 (slug-ft^2)	----------	----------	----------	779.1 (1056.35)

TABLE III. WEIGHT SUMMARY

Item	Configuration 1A	1B	1C	1D
Total Structure -	353 (779)	311 (685)	338 (746)	236 (521)
Wing group including balances	148 (326)	116 (255)	158 (349)	84 (185)
Tail group:				
Horizontal	10 (21)	10 (21)	10 (21)	10 (21)
Vertical	5 (11)	5 (11)	5 (11)	5 (11)
Body group	88 (193)	88 (193)	88 (193)	88 (193)
Alighting gear group:				
Main	24 (54)	24 (54)	24 (54)	24 (54)
Auxiliary	5 (10)	5 (10)	5 (10)	5 (10)
Surface controls	21 (47)	21 (47)	21 (47)	21 (47)
Engine section	----------	----------	----------	----------
Booms	15 (33)	----------	32 (71)	----------
Trimmer including balances	38 (84)	----------	38 (84)	----------
Propulsion Group -	156 (345)	156 (345)	156 (345)	156 (345)
Engine (as installed)	111 (244)	----------	----------	----------
Accessories	2 (5)	----------	----------	----------
Air induction system	5 (10)	----------	----------	----------
Exhaust system	1 (2)	----------	----------	----------
Cooling and drain provisions	1 (3)	----------	----------	----------
Lubricating system	1 (2)	----------	----------	----------
Fuel system	7 (15)	----------	----------	----------
Engine controls	1 (2)	----------	----------	----------
Starting system	11 (24)	----------	----------	----------
Propeller installation	12 (26)	----------	----------	----------
Drive shaft	5 (12)	----------	----------	----------
Fixed Equipment -	59 (129)	59 (129)	59 (129)	59 (129)
Instruments	23 (50)	----------	----------	----------
Electrical group	13 (29)	----------	----------	----------
Furnishings	23 (50)	----------	----------	----------
Total Weight Empty -	568 (1253)	483 (1065)	596 (1314)	451 (995)
Crew	154 (340)	----------	----------	----------
Fuel:				
Internal	54 (120)	----------	----------	----------
Trapped	3 (6)	----------	----------	----------
Oil:				
Engine	3 (7)	----------	----------	----------
Trapped	0.5 (1)	----------	----------	----------
Total Useful Load	215 (474)	215 (474)	215 (474)	215 (474)
Takeoff Gross Weight	783 (1727)	698 (1539)	811 (1788)	666 (1469)
Flight Design Gross Weight	761 (1679)	676 (1491)	789 (1740)	644 (1421)
Landing Design Gross Weight	740 (1631)	654 (1443)	767 (1692)	623 (1373)

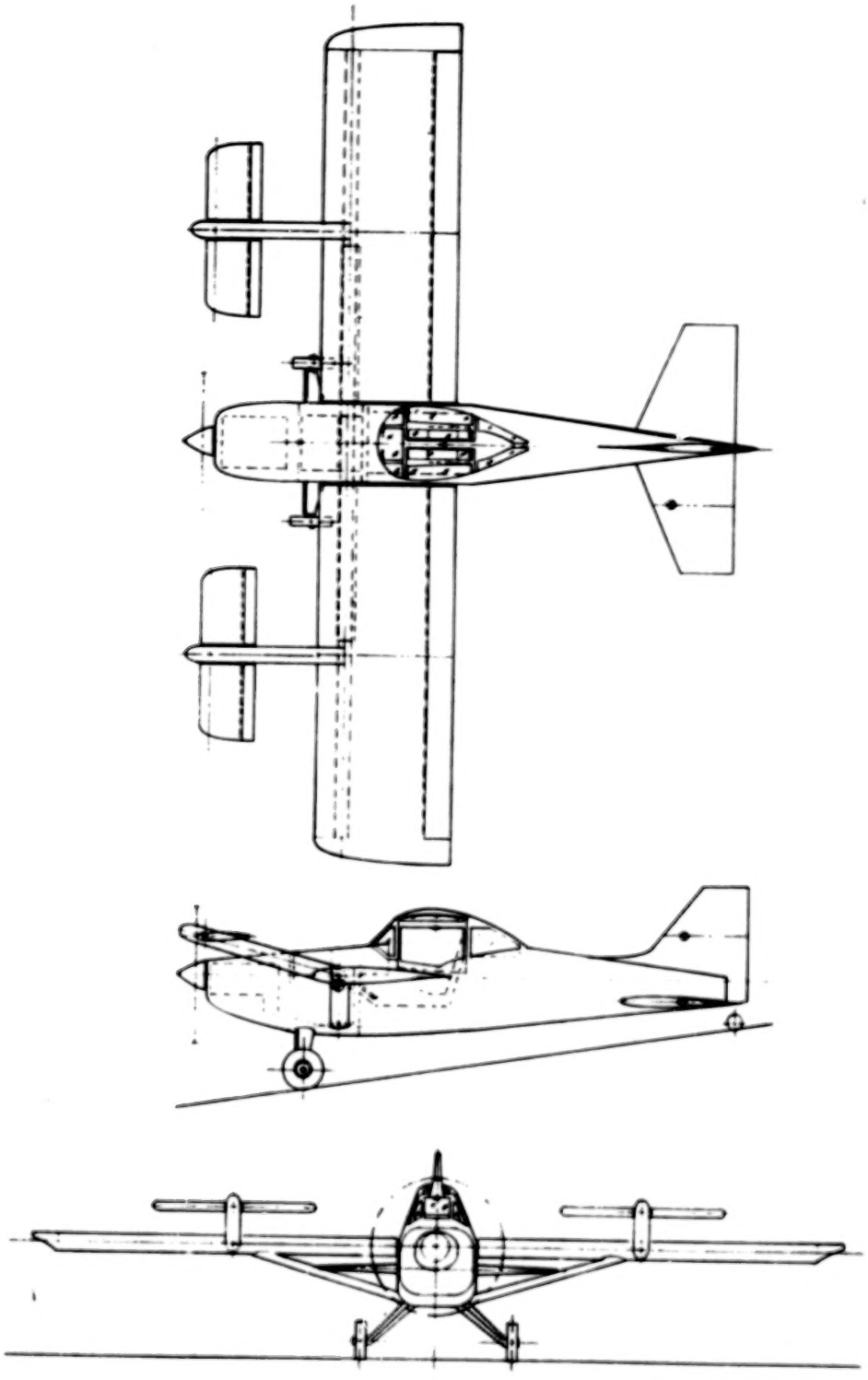

FIGURE 3(a). SINGLE SEAT AGRICULTURAL AIRCRAFT (CONFIGURATION 2A--FREE WING/ FORWARD FREE TRIMMER.

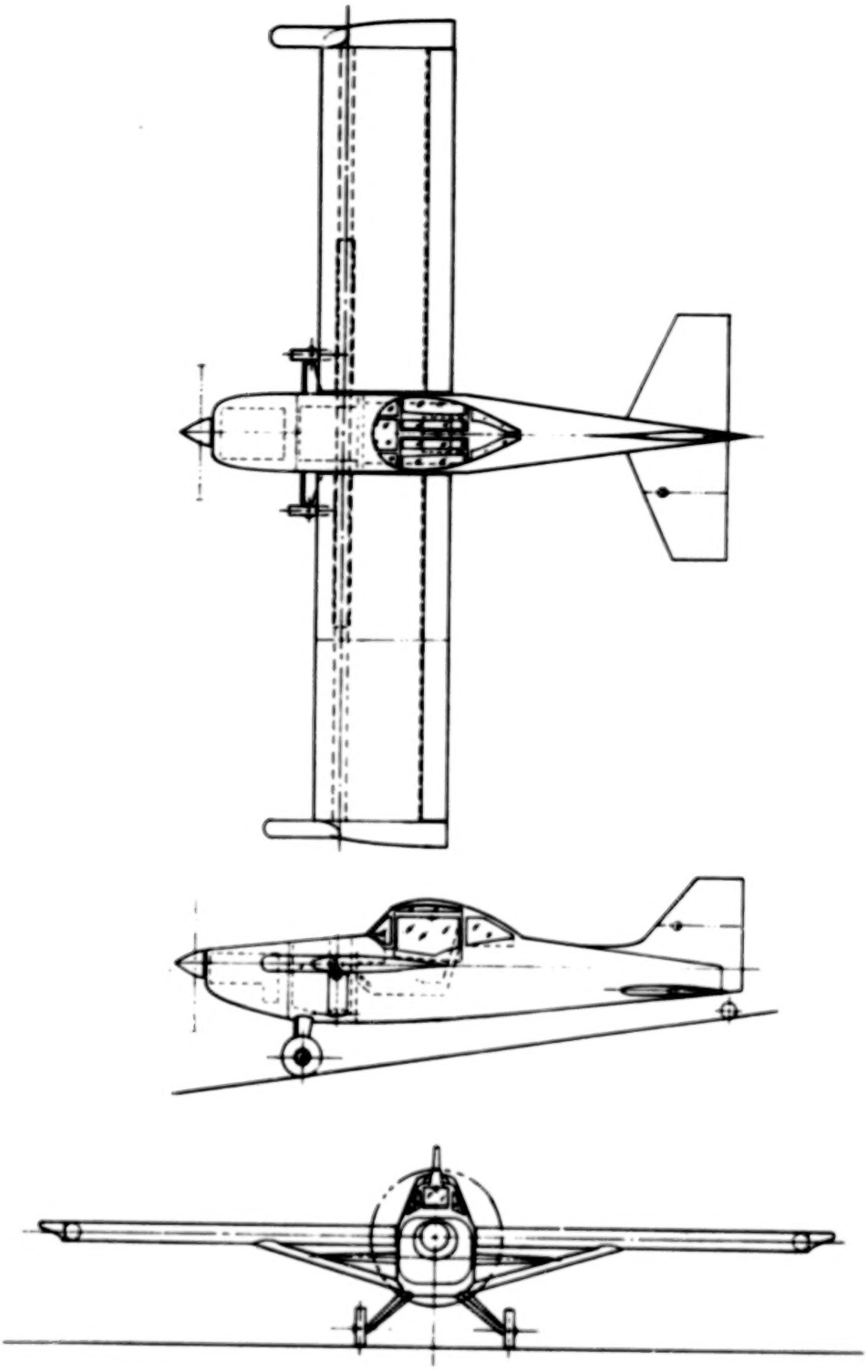

FIGURE 3(b). SINGLE SEAT AGRICULTURAL AIRCRAFT (CONFIGURATION 2B -- PURE FREE WING). FIXED WING CONFIGURATION 2D IS EXTERNALLY SIMILAR TO THIS LESS EXTERNAL BALANCES ON WING.

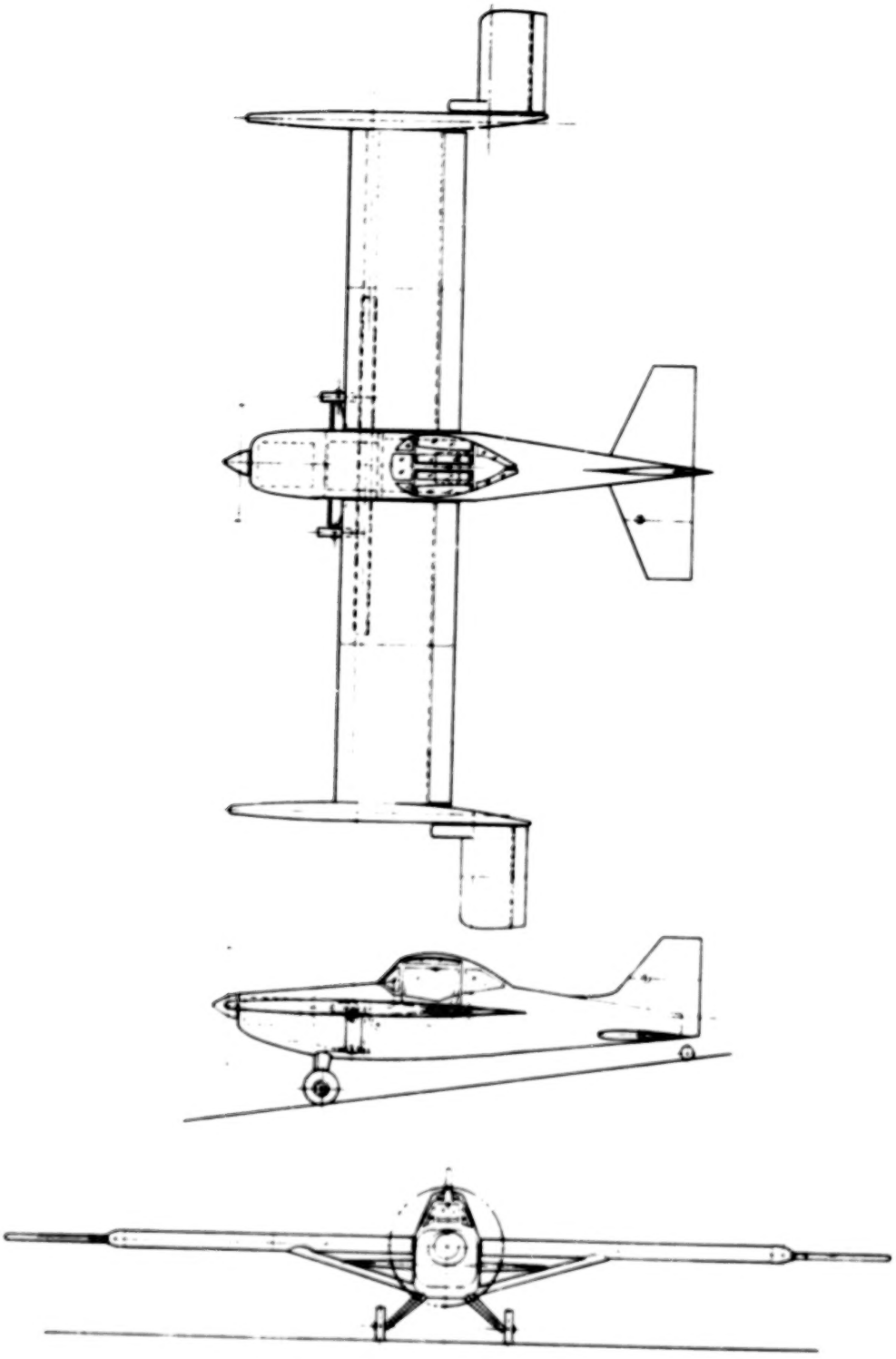

FIGURE 3(c). SINGLE SEAT AGRICULTURAL AIRCRAFT (CONFIGURATION 2C--FREE WING/AFT FREE TRIMMER).

TABLE IV. FAMILY OF AGRICULTURAL AIRCRAFT

Configuration	Figure	Description
2A	3(a)	Forward free surface
2B	3(b)	Pure free wing
2C	3(c)	Aft free surface
2D	Not shown	Fixed-wing equivalent to Configuration 2B

TABLE V. SUMMARY OF GEOMETRIC DATA FOR SINGLE SEAT AGRICULTURAL AIRCRAFT VARIATIONS

Item	Configuration			
	2A	2B	2C	2D
Fuselage -				
Length, m (ft)	7.5 (24.50)	7.5 (24.50)	7.5 (24.50)	7.5 (24.50)
Maximum width, m (ft)	1.0 (3.25)	1.0 (3.25)	1.0 (3.25)	1.0 (3.25)
Maximum height, m (ft)	1.6 (5.25)	1.6 (5.25)	1.6 (5.25)	1.6 (5.25)
Surface area, m^2 (ft^2)	20.1 (215.92)	20.1 (215.92)	20.1 (215.92)	20.1 (215.92)
Wing -				
Span, m (ft)	10.5 (34.6)	10.5 (34.6)	10.5 (34.6)	10.5 (34.6)
Reference area, m^2 (ft^2)	19.3 (207.5)	19.3 (207.5)	19.3 (207.5)	19.3 (207.5)
Exposed area, m^2 (ft^2)	17.5 (188.8)	17.5 (188.8)	17.5 (188.8)	17.5 (188.8)
Wetted area, m^2 (ft^2)	35.7 (384.1)	35.7 (384.1)	35.7 (384.1)	35.7 (384.1)
Aspect ratio	6.0	6.0	6.0	6.0
Taper ratio	1.0	1.0	1.0	1.0
Thickness ratio	0.12	0.12	0.12	0.12
Mean geometric chord, m (ft)	1.8 (5.76)	1.8 (5.76)	1.8 (5.76)	1.8 (5.76)
Airfoil	NACA 23012	NACA 23012	NACA 23012	NACA 23012
Hinge point (percent chord)	19.0	19.0	19.0	19.0
Free stabilizer (each surface if more than one) -				
Span, m (ft)	2.2 (7.1)	----------	1.5 (5.0)	----------
Reference area, m^2 (ft^2)	1.6 (16.8)	----------	1.6 (16.7)	----------
Exposed area, m^2 (ft^2)	1.4 (15.2)	----------	1.6 (16.7)	----------
Wetted area, m^2 (ft^2)	2.9 (31.0)	----------	3.1 (33.9)	----------
Aspect ratio	3.0	----------	1.5	----------
Taper ratio	1.0	----------	1.0	----------
Thickness ratio	0.12	----------	0.12	----------
Mean geometric chord, m (ft)	0.7 (2.4)	----------	1.0 (3.3)	----------

TABLE V. (Continued)

Item	Configuration 2A	2B	2C	2D
Airfoil	NACA 23012	----------	NACA 23012	----------
Hinge point (percent chord)	19.0	----------	19.000	----------
Control arm (hinge point to hinge point), m (ft)	-1.7 (-5.5)	----------	1.8 (5.8)	----------
Control volume (hinge point to hinge point)	-0.15		0.16	
Horizontal tail -				
Span, m (ft)	3.1 (10.3)	3.1 (10.3)	3.1 (10.3)	3.1 (10.3)
Reference area, m^2 (ft^2)	3.2 (34.6)	3.2 (34.6)	3 2 (34.6)	3.2 (34.6)
Exposed area, m^2 (ft^2)	2.9 (31.3)	2.9 (31.3)	2.9 (31.3)	2.9 (31.3)
Wetted area, m^2 (ft^2)	5.9 (63.7)	5.9 (63.7)	5.9 (63.7)	5.9 (63.7)
Aspect ratio	3.0	3.0	3.0	3.0
Taper ratio	0.5	0.5	0.5	0.5
Thickness ratio	0.09	0.09	0.09	0.09
Mean geometric chord	1.1 (3.5)	1.1 (3.5)	1.1 (3.5)	1.1 (3.5)
Airfoil	NACA 0009	NACA 0009	NACA 0009	NACA 0009
Control arm (hinge point to one-quarter chord), m (ft)	4.2 (13.92)	4.2 (13.92)	4.2 (13.92)	4.2 (13.92)
Control volume (hinge point to one-quarter chord)	0.4	0.4	0,4	
Vertical tail -				
Span, m (ft)	1.1 (3.5)	1.1 (3.5)	1.1 (3.5)	1.1 (3.5)
Reference area, m^2 (ft^2)	2.1 (22.5)	2.1 (22.5)	2.1 (22.5)	2.1 (22.5)
Exposed area, m^2 (ft^2)	2.1 (22.5)	2.1 (22.5)	2.1 (22.5)	2.1 (22.5)
Wetted area, m^2 (ft^2)	4.2 (45.7)	4.2 (45.7)	4.2 (45.7)	4.2 (45.7)
Aspect ratio	0.5	0.5	0.5	0.5
Taper ratio	0.5	0.5	0.5	0.5
Thickness ratio	0.09	0.09	0.09	0.09
Mean geometric chord, m (ft)	1.1 (3.5)	1.1 (3.5)	1.1 (3.5)	1.1 (3.5)
Airfoil	NACA 0009	NACA 0009	NACA 0009	NACA 0009

TABLE VI. WEIGHT SUMMARY

Item	Configuration 2A	2B	2C	2D
Total Structure -	537 (1184)	586 (1291)	654 (1441)	465 (1026)
Wing group including balances	(461)	(726)	(674)	(461)
Tail group:				
Horizontal	25 (56)	25 (56)	25 (56)	25 (56)
Vertical	7 (16)	7 (16)	7 (16)	7 (16)
Body group	121 (266)	121 (266)	121 (266)	121 (266)
Alighting gear group:				
Main	64 (141)	64 (141)	64 (141)	64 (141)
Auxiliary	5 (11)	5 (11)	5 (11)	5 (11)
Surface controls	24 (54)	24 (54)	24 (54)	24 (54)
Engine section	10 (21)	10 (21)	10 (21)	10 (21)
Booms	(68)	----------	(112)	----------
Trimmer including balances	(90)	----------	(90)	----------
Propulsion Group -	268 (591)	268 (591)	268 (591)	268 (591)
Engine (as installed)	----------	----------	205 (452)	----------
Accessories	----------	----------	3 (7)	----------
Air induction system	----------	----------	1 (2)	----------
Exhaust system	----------	----------	1 (2)	----------
Cooling & drain provisions	----------	----------	1 (2)	----------
Lubricating system	----------	----------	2 (5)	----------
Fuel system	----------	----------	10 (22)	----------
Engine controls	----------	----------	1 (2)	----------
Starting system	----------	----------	11 (24)	----------
Propeller installation	----------	----------	33 (73)	----------
Fixed Equipment -	154 (340)	154 (340)	(154 (340))	154 (340)
Instruments	----------	----------	18 (40)	----------
Electrical group	----------	----------	11 (25)	----------
Electronics group	----------	----------	16 (35)	----------
Furnishings	----------	----------	23 (51)	----------
Air conditioning equipment	----------	----------	34 (76)	----------
Auxiliary gear (spray tank and nozzles)	----------	----------	51 (113)	----------
Total Weight Empty -	959 (2115)	1008 (2222)	1076 (2372)	888 (1957)
Crew	----------	----------	77 (170)	----------
Fuel:				
Internal	----------	----------	106 (234)	----------
Trapped	----------	----------	3 (6)	----------
Oil:				
Engine	----------	----------	6 (14)	----------
Trapped	----------	----------	1 (2)	----------
Equipment (AG spray or dust)	----------	----------	590 (1300)	----------
Total Useful Load	783 (1726)	783 (1726)	793 (1726)	783 (1726)
Takeoff Gross Weight	1742 (3841)	1790 (3948)	1859 (4098)	1670 (3683)
Flight Design Gross Weight	1699 (3747)	1748 (3854)	1816 (4004)	1628 (3589)
Landing Design Gross Weight	1657 (3654)	1706 (3761)	1774 (3911)	1585 (3496)

Handling Qualities

Handling qualities criteria were based upon the requirements of the revised military handling qualities specification, MIL-F-8785B (ASG), and were confined to an examination of the damping of the phugoid and longitudinal short-period modes for stick-fixed motion. Compliance with the standards was determined by examining the characteristic roots of the system of equations. It is recognized that the applicability of the conventional handling qualities criteria has not been established for free-wing aircraft.

When represented as a polynomial in the operator λ, the determinant of the matrix of coefficients of equation (1) becomes a tenth degree expression with eleven polynomial coefficients. To compute these coefficients, eleven arbitrary real values of the operator were selected, and the corresponding values of the determinant were computed. Then a set of eleven simultaneous equations was formed and solved for the eleven coefficients. The roots of this polynomial were then obtained by a standard computer subroutine to arrive at the characteristic roots of the system. The 10 roots were typically divided into four complex pairs and two heavily damped real roots.

Responses to Atmospheric Turbulence

The responses to atmospheric turbulence were computed by using the techniques outlined in appendix C. A power spectral density technique was used to obtain the statistical responses to continuous turbulence, and a discrete gust technique was used to examine the details of an encounter with an isolated gust disturbance. Only vertical gust components were considered.

DISCUSSION OF RESULTS

Longitudinal Characteristic Modes

In this section, the characteristic modes of a free-wing/free-trimmer aircraft are discussed by the use of specific numerical examples, and comparisons are made with the natural motions of conventional fixed-wing aircraft and the pure free-wing aircraft analyzed in references 1 and 2.

It is well known that the longitudinal motion of a conventional rigid aircraft with controls fixed is adequately described by a set of equations

yielding four characteristic roots. These four roots are typically divided into two complex pairs, one pair defining the long-period phugoid motion, and the other pair representing the longitudinal short-period mode.

For a pure free-wing aircraft with trim provided by trailing-edge control surfaces, the previous analyses have shown that an additional oscillatory mode appears. The new oscillatory mode, which was termed the symmetric wing panel mode in reference 1, was easy to distinguish from the usual short-period mode because of its higher frequency of oscillation (a consequence of the low pitching inertia of the wing panels), and it was the dominant mode with regard to normal load factor responses to control inputs and vertical gust excitation. The roots associated with the conventional short-period mode, on the other hand, described a motion almost totally confined to the pitching of the fuselage assembly. From an analysis standpoint, the clear physical and numerical separation of these modes permitted a relatively straightforward assessment of the significance of parametric changes in the motions of the aircraft.

In the current analysis, the addition of a separate free trimming surface creates yet another oscillatory mode that is related to the pitching motion of the trimmer surface. Although the new mode is easily identified by its high natural frequency and has a readily understood physical significance, the addition of the separate surface complicates the analysis because of the much greater coupling which it introduces between the motions of the fuselage and wing/trimmer assemblies. Not only does the increased pitching inertia of the wing/trimmer place the natural frequencies of the wing and fuselage into closer proximity; but in addition, the transient aerodynamic trimmer forces caused by the vertical motion of the entire aircraft create significant pitching moments about the wing hinge axis. As a consequence, in the terminology of reference 1, the symmetric wing panel mode and the short-period mode cannot, in general, be easily distinguished with regard to their physical manifestation in the behavior of the aircraft. For this reason, the two modes are simply termed mode A and mode B in the discussion which follows.

The set of linearized equations derived in appendix B defines a tenth order dynamic system for controls-fixed motion. Typically, the 10 characteristic roots include four complex pairs denoting oscillatory modes and two heavily damped aperiodic modes related to unsteady aerodynamic forces.

To provide an illustration of modal behavior, table VII lists the numerical values of the characteristic roots for two configurations which differ primarily in the location of the trimming surface. The first (forward trimmer, configuration 1A, fig. 2(a)) has a trimming surface located two wing chord lengths forward of the wing hinge axis. The second configuration has the same trimmer area and moment arm, but the trimmer is aft of the wing hinge. Both configurations have a mass balanced fuselage, wing assembly, and trimmer about their respective hinge axes. Calculations were made for a normal cruise condition of 241.4 kilometers per hour (150 miles per hour) at an altitude of 1829 meters (6000 feet).

TABLE VII. COMPARISON OF CHARACTERISTIC ROOTS FOR FORWARD AND AFT TRIMMING SURFACES

$\left|\frac{X'_c}{\bar{c}}\right| = 2.0$, CRUISE FLIGHT

Mode	Forward trimmer	Aft trimmer
Phugoid	$-0.0509 \pm j\ 0.321$	$-0.0676 \pm j\ 0.313$
Mode A	$-0.171 \pm j\ 2.42$	$-1.890 \pm j\ 2.35$
Mode B	$-2.38 \pm j\ 5.12$	$-0.119 \pm j\ 4.42$
Trimmer mode	$-6.60 \pm j\ 17.2$	$-7.57 \pm j\ 17.7$
Aperiodic	-30.4, -75.3	-30.5, -75.1

Figure 4 is a comparison of the responses to step displacements, of equal magnitude, of trailing-edge control flaps on the trimmer surfaces, and illustrates the inadvisability of attempting to assign a simple physical significance to either mode A or mode B.

Even though modes A and B are the respective generic equivalents of the short-period and symmetric wing panel modes identified in references 1 and 2, they are clearly not uniquely related to either the fuselage or to wing motion alone. One of these modes is much more heavily damped than the other, but the relative damping is reversed between the two configurations. Furthermore, the mode with the lighter damping ratio appears to dominate the response. The forward trimmer response displays the relatively long period of mode A, while

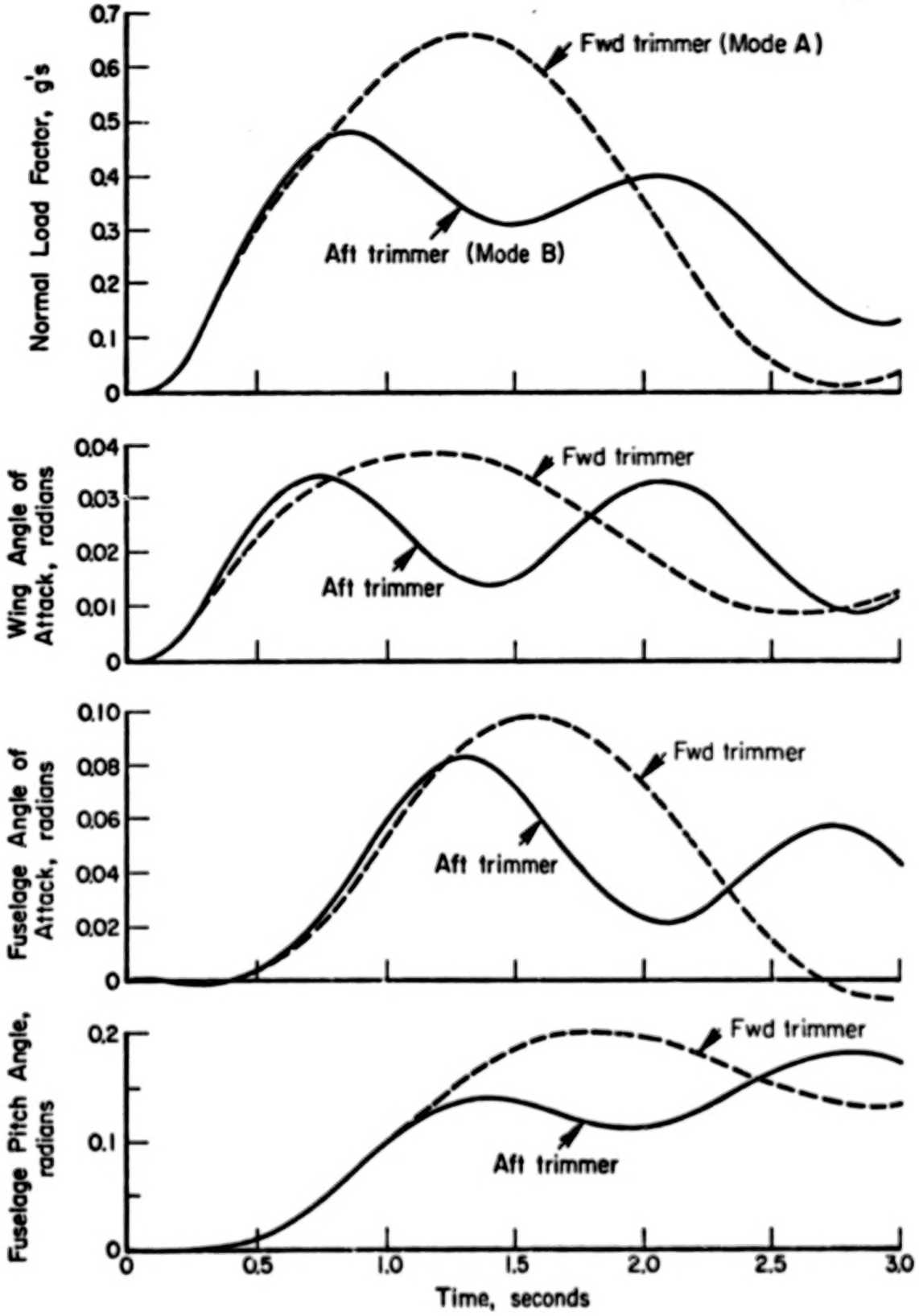

FIGURE 4. COMPARISON OF RESPONSES TO STEP CONTROL INPUTS FOR FREE TRIMMING SURFACES WITH LARGE MOMENT ARMS (TWO WING CHORDS).

the aft trimmer response is governed by the shorter period of mode B; the dominant mode in either case is the one with the lighter damping.

It should be noted that these cases are shown only for illustration, and it is recognized that neither represents acceptable response characteristics from a handling qualities standpoint. The shortcomings of configurations such as these, with large trimmer moment arms, will be discussed in the following sections.

Configuration Options and Limitations

The most fundamental design feature of the free-wing/free-trimmer concept is the size and location of the trimming surface relative to the wing. A key portion of this investigation was therefore an assessment of the gross effects of wing/trimmer geometry.

For this evaluation, the pure free-wing aircraft version of the light aircraft of figure 2(b) (configuration 1B) was used as a baseline. The fuselage and basic wing were unchanged, and the trimming surface and its supporting structure, as well as the necessary counterweights, were added to the wing. For this portion of the analysis, mass balance was maintained about the hinge axes of the trimmer surface and the wing/boom/trimmer assembly. In this way, the general effects of trimmer geometry on wing assembly moment of inertia were implicitly included in the parametric changes, and the relative weight penalties for the various configurations could be evaluated.

In assessing the merits of each configuration, four criteria were used: gust alleviation, handling qualities, maximum obtainable trimmed lift coefficient, and relative weight penalty incurred by mass balancing.

The gust alleviation characteristics of each configuration were evaluated by comparing its vertical gust response to the vertical gust response of the baseline pure free-wing aircraft and to a geometrically similar fixed wing airplane. The comparison criteria were the rms normal load factor response to continuous vertical turbulence and the peak load factor values computed for an encounter with a discrete 1-cosine gust with a wavelength of 25 wing chords and a peak magnitude of 3.048 meters per second (10 feet per second).

For the continuous turbulence analysis, the velocity degree of freedom was eliminated from the equations of motion to avoid large contributions

at very low frequencies near the phugoid mode, since these are easily controlled by pilot action. The Dryden turbulence spectrum was used with a scale length of 533 meters (1750 feet) for consistency with the previous work of references 1 and 2. Details of the procedure for computing turbulence responses are contained in appendix C.

Although the continuous turbulence analysis is probably the more meaningful of the two, the discrete gust calculations, in time history form, provided valuable insight into the detailed behavior of the aircraft during gust encounters. The 25 chord length gust was used to conform to the standards of the Federal Air Regulations (FAR 23.333(2)(2)(i)), which specify this type of discrete gust for analytical proof of compliance with the structural gust load criterion. A comparison of the peak discrete gust loads with the loads of the equivalent fixed-wing aircraft therefore yields a rapid, first order estimate of the relative structural gust loads which each aircraft would be required to withstand for certification purposes.

With regard to handling qualities, the primary criterion was the damping ratio of the more poorly damped of the two short-period modes. The military handling qualities criterion, MIL-F-8785B(ASG), requires the damping ratio of the short-period motion to lie between 0.35 and 1.30 for level 1 performance.* For level 3 flying qualities, a damping ratio of 0.15 is permitted.

Forward trimmer configurations. - Since the trimming force with forward trimming surfaces is in an upward direction, thereby augmenting wing lift, the forward trimmer configurations were initially expected to offer the most promise. The investigation began, therefore, with an analysis of Configuration 1A (fig. 2(a)), with a forward trimmer moment arm of two wing chord lengths and an area ratio of 1/6.

---

*MIL-F-8785B(ASG) defines three levels of acceptability:

Level 1: Flying qualities clearly adequate.

Level 2: Flying qualities adequate to accomplish the mission... but some increase in pilot work load or degradation of mission effectiveness exists.

Level 3: Flying qualities such that the airplane can be controlled safely but pilot workload is excessive or mission effectiveness is inadequate, or both.

The response to continuous turbulence of unit intensity was computed for the cruise condition of 241.4 kilometers per hour (150 miles per hour) at an altitude of 1829 meters (6000 feet). The response proved to be disappointing - higher than the equivalent fixed-wing aircraft. Table VIII compares the rms responses to continuous turbulence as well as the peak load factor responses to discrete gusts for the free-wing/forward free trimmer of Configuration 1A, the pure free-wing version of Configuration 1B (fig. 2(b)), and the fixed wing equivalent, Configuration 1D. The input magnitude used for the Dryden model of continuous turbulence is not related to the discrete gust input magnitude. Instead, a value of 1 foot per second, or unity, was selected as the rms value for reasons of simplicity. As a consequence, the rms load factors shown are appreciably less than would actually be measured in turbulence.

TABLE VIII. COMPARISON OF TURBULENCE RESPONSES

Configuration	Rms load factor per unit turbulence intensity	Peak load factor response to discrete gust
Free wing/ free forward trimmer (conf. 1A)	0.0273	0.730
Free wing (conf. 1B)	0.00989	0.348
Fixed wing (conf. 1D)	0.0191	0.675

The poor gust response of the forward free-trimmer configuration can be explained by an examination of the response histories in figure 5. For these encounters, all three of the aircraft of Table VIII were subjected to the standard 25 chord-length 1 - cosine gust velocities shown at the bottom of the figure. In the pure free-wing version, the wing begins to deflect almost immediately after encountering the gust, thereby limiting the load factor response to the relatively low value shown in the upper trace. In contrast, the forward trimmer surface experiences an initial upward transient lift force before its downward pitching motion can relieve the load. The transient forward trimmer force, though lasting less than one-fifth of a second, imparts a pitch-up impuse to the wing assembly which not only delays the alleviating motion of the wing, but actually produces a small wing displacement in an

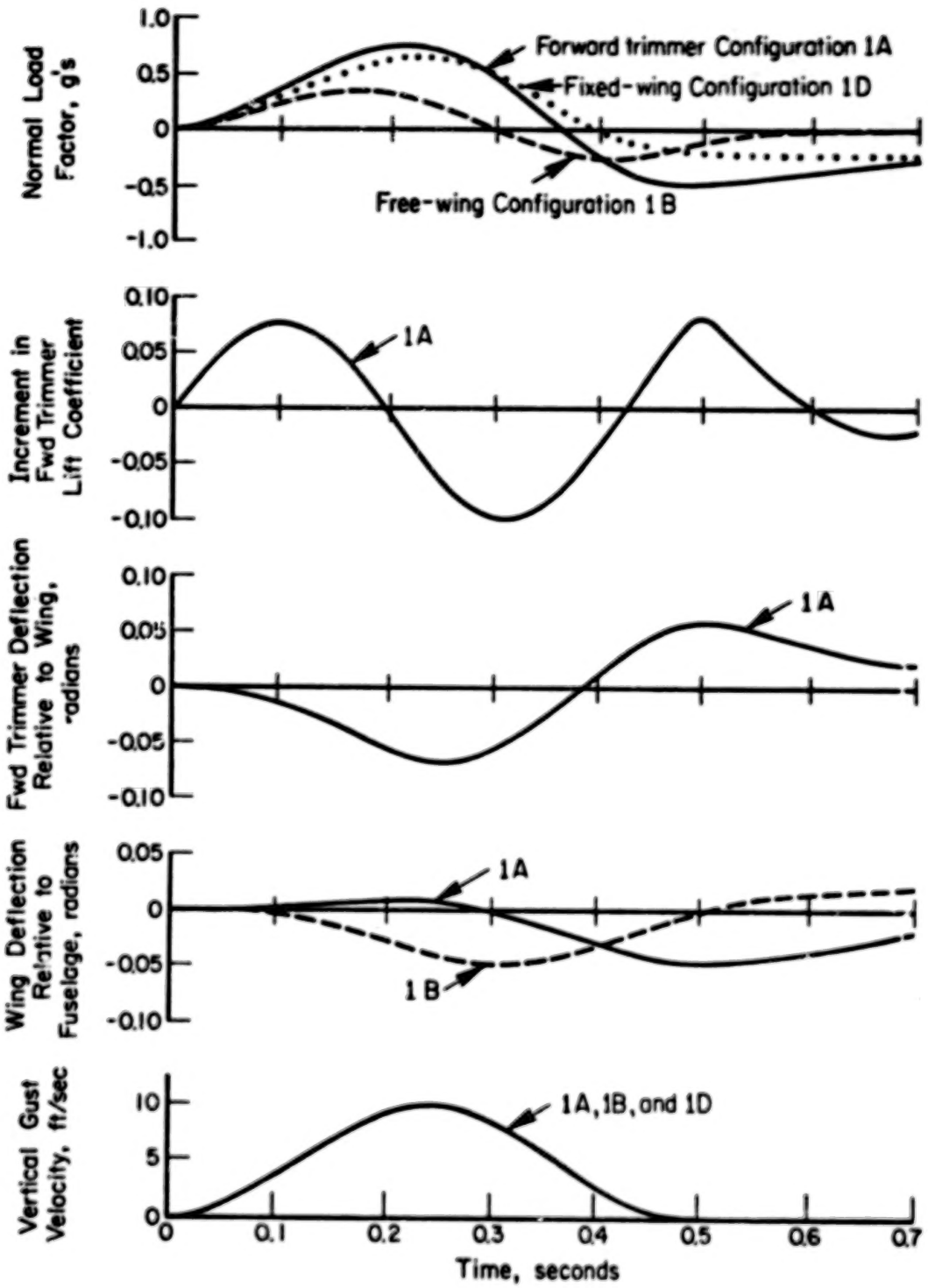

FIGURE 5. VERTICAL GUST RESPONSES ILLUSTRATING ADVERSE TRANSIENT EFFECT OF FORWARD TRIMMER.

adverse direction. In the case shown, the wing does not begin to pitch downward until the gust has already passed its peak value.

Aside from the poor gust response characteristics, Configuration 1A is unsatisfactory from a handling qualities standpoint because of the low damping of the dominant short-period oscillation. As noted in figure 4, the dominant short-period mode is the oscillation identified as mode A in table VII, and the damping ratio of this mode is only 0.0705, which is well below the lowest standard (level 3) of MIL-F-8785B(ASG).

The poor gust response of Configuration 1A is related to the trimmer volume (area times moment arm), while the low damping of the oscillatory mode may be a consequence of the relatively large rotational inertia of the wing/boom/forward trimmer system as compared to the small pitch damping provided by the free forward trimmer at the modal frequency.

To improve the behavior of the forward trimmer configurations, two changes were explored: the use of smaller moment arms and the relocation of the hinge axis on the forward trimmer surface.

With regard to the hinge axis, the nominal hinge margin for the forward trimmer surface of Configuration 1A is 6 percent; that is, the hinge axis is located 6 percent of the trimmer chord forward of the aerodynamic center. From earlier free-wing analyses it is known that the greater the hinge margin, the more rapid the alleviation of out-of-trim conditions. It might be expected that the unfavorable pitch impulse imparted by the trimmer, as in the gust encounter in figure 5, would be reduced by quickening the response of the trimmer surface. On the other hand, the larger the hinge margin the greater the control tab size and deflection required for trim, and the smaller the maximum trimmed lift coefficient of the free surface. In light of these factors, all subsequent analyses for forward trimmers were made with an assumed trimmer hinge margin of 20 percent, which would place the hinge axis at about 5 percent of the trimmer mean aerodynamic chord.

Table IX lists the results for two modified versions of Configuration 1A, with moment arms of 1.5 and 1.0 chord lengths. The free-trimmer hinge margin is 20 percent in both cases.

TABLE IX. RESPONSES OF MODIFIED FORWARD TRIMMER CONFIGURATIONS

Trimmer moment arm, wing chords	Rms turbulence response	Response ratio compared to fixed wing, percent	Mode A		Mode B	
			Roots	Damping ratio	Roots	Damping ratio
1.5	0.0178	98	$-0.431 \pm j\ 3.35$	0.131	$-3.09 \pm j\ 7.03$	0.402
1.0	0.0154	81	$-0.445 \pm j\ 3.29$	0.134	$-5.63 \pm j\ 10.67$	0.467

As a basis of comparison, the rms gust response for the pure free wing of Configuration 1B is 0.00989, or just 52 percent of the fixed-wing response. Even the smaller moment arm case falls far short of the basic free wing, from a gust alleviation standpoint, although a reduction of 19 percent from the fixed-wing response is significant.

It should be noted that the two oscillatory modes become more widely separated as the pitching inertia of the wing assembly decreases. With decreasing moment arm, the frequency of mode B increases, while mode A changes only slightly.

If the fuselage assembly is considered by itself, free to heave and pitch, its characteristic motion is defined by a cubic equation with a well-damped real root and an oscillatory mode with roots of $-0.712 \pm j\ 3.43$ at this flight condition. It appears that mode A of the complete aircraft is tending toward this isolated fuselage oscillatory mode; but despite the numerical separation of modes A and B, both modes are evident in the load factor response history shown in figure 6 for the one chord length moment arm case.

The handling qualities specification of MIL-F-8785B(ASG) is based upon the assumption that the short-period response is essentially that of a simple second order system. In the case at hand, the short-period motion is clearly the superposition of two separate oscillatory modes, raising a question of the direct application of the simplified standards to the free-wing/free-trimmer aircraft.

Aft-trimmer configurations. - The most powerful aft-trimmer configuration examined was one based upon Configuration 1A, but with the trimming surface mounted two wing chord lengths aft of the wing hinge axis.

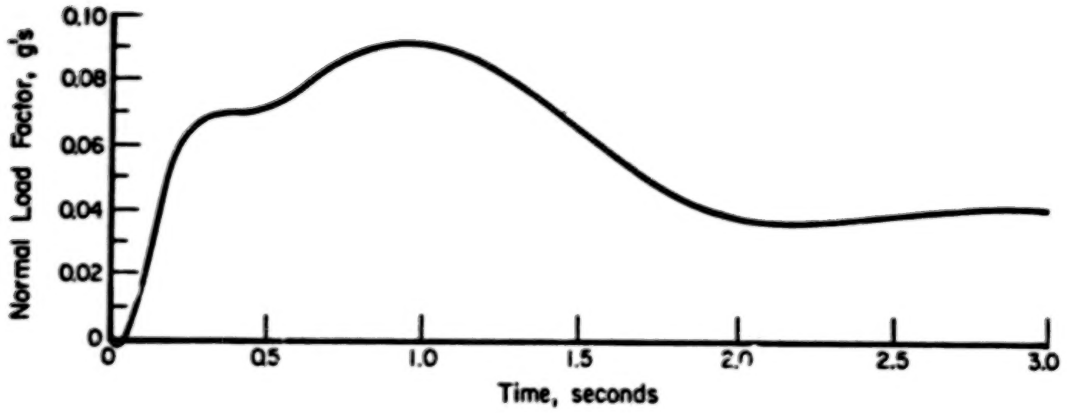

FIGURE 6. RESPONSE TO STEP CONTROL INPUT OF MODIFIED CONFIGURATION 1A AIRCRAFT WITH FORWARD TRIMMER MOMENT ARM OF ONE WING CHORD LENGTH.

The adverse short-period damping of this configuration has been mentioned previously under the discussion of longitudinal characteristic modes, and a time history of the response to a step control input is shown in figure 4.

The damping ratio of the dominant mode in figure 4 is only 0.027, which is obviously well below the standards of MIL-F-8785B(ASG), which requires at least 0.15 for level 3 flying qualities. The rms responses to continuous turbulence were not obtained for this configuration because of excessive computing time caused by the large spike in the power spectrum of the normal load factor response.

To improve the behavior of the aft-trimmer configurations, smaller moment arms were explored. Unlike the forward trimmer cases, however, the trimmer hinge margin was maintained at the 6 percent value to retain a relatively high value of maximum trimmer lift coefficient. Furthermore, the trimmers in all subsequent cases were assumed to be mounted on the wingtips, as seen in Configuration 1C (fig. 2(c)).

Aside from esthetic improvement, the tip-mounted trimmers are superior, from a gust alleviation standpoint, to surfaces mounted behind the wing. The aft trimmer experiences a transient lift change, upon gust penetration, just like the forward surface of Configuration 1A; but in this case the transient force on the aft trimmer is beneficial, since it produces a favorable

pitching moment on the main wing. With the outboard location, the trimmer is exposed to a strong upwash increment from increased circulation in the trailing vortex system of the wing. The upwash increases the magnitude of the transient trimmer force and enhances the relieving pitching moment on the wing. If the trimmer is mounted directly behind the wing, the influence of the wing appears as an increase in downwash (for an upward gust), and the alleviating transient moment from the trimmer is reduced.

Table X lists the behavior of aircraft in cruise flight with tip-mounted aft trimmers for two moment arm lengths and for an area ratio of 1/6, as before.

TABLE X. BEHAVIOR OF TIP-MOUNTED AFT-TRIMMER CONFIGURATIONS

Moment arm, wing chords	Rms turbulence response	Response compared to fixed wing, percent	Mode A		Mode B	
			Roots	Damping ratio	Roots	Damping ratio
-1.5	0.0132	69	$-0.509 \pm j\ 4.54$	0.111	$-1.77 \pm j\ 2.97$	0.512
-1.0	0.0104	54	$-1.11 \pm j\ 3.32$	0.317	$-1.67 \pm j\ 5.28$	0.302

The gust alleviation of the one chord length moment arm configuration (Configuration 1C, fig. 2(c)) is excellent, inasmuch as it is virtually identical to the pure free wing, which reduced the response to 52 percent of the fixed-wing value. Furthermore, the computed damping ratios of both modes exceed the level 3 requirements (0.15) of MIL-F-8785B (ASG), and almost meet the level 1 standard (0.35).

The larger moment arm length (one and a half wing chords) is inferior to the smaller moment arm case with respect to both turbulence response and short-period damping.

Since the literal application of the MIL-F-8785B (ASG) short-period damping standards is open to question because of the bimodal nature of the response, time histories of load factor response to step control displacement were computed and are shown in figure 7. The response of the smaller moment arm configuration, in particular, would appear to be acceptable from an intuitive viewpoint.

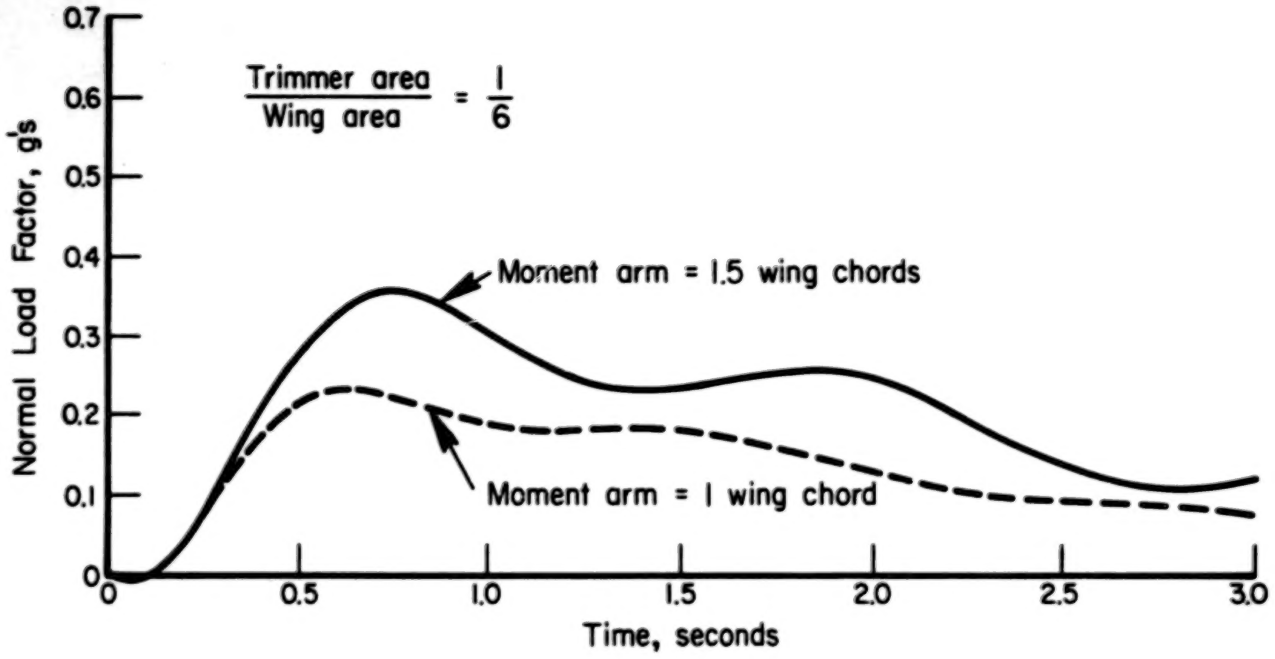

FIGURE 7. COMPARISON OF LOAD FACTOR RESPONSES TO STEP CONTROL INPUT FOR TWO CONFIGURATIONS WITH TIP-MOUNTED AFT TRIMMERS

Effect of configuration on maximum lift coefficient. - The principal advantage of the external trimmer concept over the basic free wing is the feasibility of improving the maximum trimmed lift coefficient of the aircraft. If this were the only consideration, the forward trimmer configuration with a large moment arm would be attractive, because it would permit the use of relatively powerful wing flaps and would contribute an upward force to augment the wing lift.

Unfortunately, very powerful external trimming surfaces, mounted either forward or aft of the wing, have been found to have adverse dynamic characteristics within the scope of this study, as previously discussed. These circumstances prompted a brief investigation of the methods of increasing the trimming power with relatively modest moment arms.

The fundamental problem is the large negative pitching moment, which inevitably accompanies the trailing-edge flap deflection required for high wing lift coefficients. The wing pitching moment about its hinge axis is given by the following equation:

$$C_{m_{hinge}} = C_{m_{a.c.}} - (HM)\, C_{L_w} \qquad (2)$$

$C_{m_{a.c.}}$ is always large and negative for large trailing-edge flap deflections; for example, it has a value of about -0.40 for 20 percent flaps deflected 40°.

The moment available from the external trimming surface to counter the wing moment of equation (2) is as follows:

$$C_{m_{trimmer}} = \frac{X'_c}{\bar{c}} \frac{S_c}{S} C_{L_c} \tag{3}$$

Since the maximum lift coefficient of a free trimming surface controlled by a trailing-edge tab can be expected to be about 1.0, the maximum trimmer pitching moments which can be obtained are given in table XI.

TABLE XI. MAXIMUM TRIM MOMENT CAPABILITY FOR PLAIN TRIMMERS

$\frac{X'_c}{\bar{c}}$	$\frac{S_c}{S}$	$C_{m_{trimmer}}$
1.0	1/6	0.167
1.5	1/6	0.250
2.0	1/6	0.333
1.0	1/5	0.200
1.5	1/5	0.300
2.0	1/5	0.400

It should be noted that only the last case listed in table XI could provide sufficient power to trim the constant pitching moment ($C_{m_{a.c.}}$) of a wing with 20 percent flaps deflected 40°, should large deflection be required. In that case, no excess moment would be available to counter the moment due to lift in equation (2).

In reference 2, the lift capability of a pure free-wing aircraft was improved by using a leading-edge Handley-Page slat on the NACA 23012 airfoil section, using data from reference 3. This device yielded a computed maximum trimmed C_L of 1.46 for a rectangular wing of aspect ratio 6. If such a device were used on the free-trimmer surfaces, the increased trimmer power would produce the maximum moments given in table XII.

Although the trimming power is increased significantly by the trimmer leading-edge slat (46 percent), large wing flap deflections still cannot be

TABLE XII. MAXIMUM TRIM MOMENT CAPABILITY FOR TRIMMERS EQUIPPED WITH HANDLEY-PAGE LEADING-EDGE SLAT

$\left\lvert\frac{X_c'}{\bar{c}}\right\rvert$	$\frac{S_c}{S}$	$C_{m_{trimmer}}$
1.0	1/6	0.243
1.5	1/6	0.365
2.0	1/5	0.487
1.0	1/5	0.292
1.5	1/5	0.438
2.0	1/5	0.584

tolerated for moment arms of 1.5 chord lengths or less. For this reason, only smaller flap deflections are considered in the following calculations.

To provide parametric information, the data in figure 119 of reference 4 were used to derive a simple, approximate relationship between the maximum section lift and pitching moment coefficients of the NACA 23012 airfoil with variation in the deflection of a 20 percent slotted flap. This relationship is:

$$C_{m_{a.c.}} = 0.35 - 0.24\, C_{l_{max}} \qquad (C_{l_{max}} \geq 1.5) \tag{4}$$

If it is assumed that the finite wing lift coefficient is 80 percent of the maximum section lift coefficient, equation (4) becomes

$$C_{m_{a.c.}} = 0.35 - 0.30\, C_{L_{max_w}} \tag{5}$$

If the flap is deflected just sufficiently to produce $C_{L_{max_w}}$, the substitution of equation (5) into equation (2) provides a convenient expression for the total pitching moment of the wing about its hinge axis at $C_{L_{max_w}}$. For the nominal hinge margin of 0.06, the expression is

$$C_{m_{hinge}} = 0.35 - 0.36\, C_{L_{max_w}} \tag{6}$$

Equating the hinge moment of equation (6) to the available trimmer moments of tables XI and XII provides an estimate of the maximum permissible wing lift coefficient. Ignoring the contribution of the fuselage assembly, which is a function of fuselage center of gravity and trimmed attitude, the

total trimmed airplane lift coefficient is

$$C_{L_{total}} = C_{L_w} \pm \frac{S_c}{S} C_{L_c} \tag{7}$$

where the plus sign is used for the forward trimmer configurations and the minus sign is used for aft trimmers.

Table XIII lists the total trimmed airplane lift coefficients obtainable with the 20 percent wing flaps deflected just enough to provide the usable maximum wing lift coefficient.

TABLE XIII. MAXIMUM AIRPLANE LIFT CAPABILITIES FOR WING EQUIPPED WITH 20 PERCENT SLOTTED FLAPS

$\frac{X'_c}{\bar{c}}$	$\frac{S_c}{S}$	Usable $C_{L_{max_w}}$	δ_f degrees	Total C_L	
				Forward trimmer	Aft trimmer
		[Plain trimmer]			
1.0	1/6	1.44	6.6	1.60	1.27
1.5	1/6	1.67	13.0	1.83	1.50
2.0	1/6	1.90	19.4	2.06	1.73
1.0	1/5	1.53	9.1	1.73	1.33
1.5	1/5	1.81	16.8	2.01	1.61
2.0	1/5	2.08	24.5	2.28	1.88
		[Leading-edge slat on trimmer]			
1.0	1/6	1.65	12.4	1.89	1.41
1.5	1/6	1.99	21.8	2.23	1.75
2.0	1/6	2.33	31.3	2.57	2.09
1.0	1/5	1.78	16.2	2.07	1.49
1.5	1/5	2.19	27.5	2.48	1.90
2.0	1/5	2.59	38.7	2.88	2.30

Another possible approach to a high-lift capability would be to provide a leading-edge slat on the wing itself, in combination with trailing-edge flaps.

Reference 3 provides data for the NACA 23012 airfoil with a Handley-Page leading-edge slat and a 26 percent slotted flap. From the data in figure 7 of reference 3, it may be deduced that the aerodynamic center of the

airfoil section shifts forward to about the 19 percent chord position as the leading-edge slat is extended. Since this is also the position of the nominal hinge axis location, it would be necessary to move the hinge forward to provide static wing stability with the slat extended. If a new hinge location is selected at 15 percent chord, the hinge margin would be 10 percent with the slat retracted and 4 percent with the slat extended.

Using the data in reference 3, and again assuming that the maximum wing lift coefficient is 80 percent of the maximum section value, the relationship between the pure pitching moment about the aerodynamic center ($0.19\bar{c}$) and the maximum lift coefficient (both of which are functions of flap deflection) is, with the leading-edge slat extended,

$$C_{m_{a.c.}} = 0.665 - 0.438\, C_{L_{max_w}} \tag{8}$$

If the new hinge margin is 0.04,

$$C_{m_{hinge}} = C_{m_{a.c.}} - 0.04\, C_{L_w} \tag{9}$$

Substituting equation (8) into equation (9), the hinge moment about the wing hinge when the wing is at the maximum lift coefficient as determined by flap deflection, is

$$C_{m_{hinge}} = 0.665 - 0.478\, C_{L_{max_w}} \tag{10}$$

Equating the hinge moment of equation (10) with the available trimmer power in tables XI and XII yields the data listed in table XIV.

The data for the various high-lift configurations are summarized in figure 8 for the smaller of the two area ratios considered. It may be seen that the maximum lift coefficient of the pure free wing is easily exceeded, even for aft trimmers with relatively small moment arms.

Weight penalties. - In an attempt to assess the weight penalties for each of the free-wing/free-trimmer combinations studied, each wing-trimmer combination was added to one basic fuselage incorporating all fixed and disposable weight items for both the two seat light aircraft and the single seat agricultural aircraft (tables III and VI).

For the two seat light aircraft, given a fixed-wing baseline (Configuration 1D in table III), the following rules were used: all non-wing/

TABLE XIV. MAXIMUM AIRPLANE LIFT CAPABILITIES FOR WING EQUIPPED WITH LEADING-EDGE SLAT AND FLAPS

$\frac{X'_c}{C}$	$\frac{Sc}{S}$	Usable $C_{L_{max_w}}$	δF degrees	Total C_L	
				Forward trimmer	Aft trimmer
		[Plain trimmer]			
1.0	1/6	1.90	6.9	2.07	1.74
1.5	1/6	2.09	12.8	2.26	1.92
2.0	1/6	2.28	18.8	2.45	2.11
1.0	1/5	1.98	9.3	2.18	1.78
1.5	1/5	2.21	16.4	2.41	2.01
2.0	1/5	2.43	23.6	2.63	2.23
		[Leading-edge slat on trimmer]			
1.0	1/6	2.08	12.3	2.32	1.83
1.5	1/6	2.35	21.1	2.60	2.11
1.0	1/5	2.19	15.8	2.48	1.90
1.5	1/5	2.52	26.3	2.81	2.23

trimmer weight items were to remain constant, wing area was to remain constant at 10.1 square meters (108.6 square feet), trimmer area was to remain constant at 1.7 square meters (18.1 square feet), wing/boom and trimmer free surfaces were to be externally counterbalanced, and useful load was to be constant. The free-wing/forward-trimmer configuration (configuration 1A in fig. 2(a)) had an empty weight 26 percent greater than its fixed-wing counterpart and 18 percent greater than a comparable pure free-wing aircraft. The free-wing/aft trimmer configuration (configuration 1C in fig. 2(c)) had an empty weight 32 percent greater than its fixed-wing counterpart and 23 percent greater than a comparable pure free wing. (These weights reflect no attempt to minimize the weight gain of various configurations by making efficient use of some items of fixed weight as counterweights for wings and trimmers.) These weights essentially reflect the penalties incurred in modifying a fixed- or pure free-wing aircraft to free-wing/free-trimmer configurations without redesigning the basic aircraft.

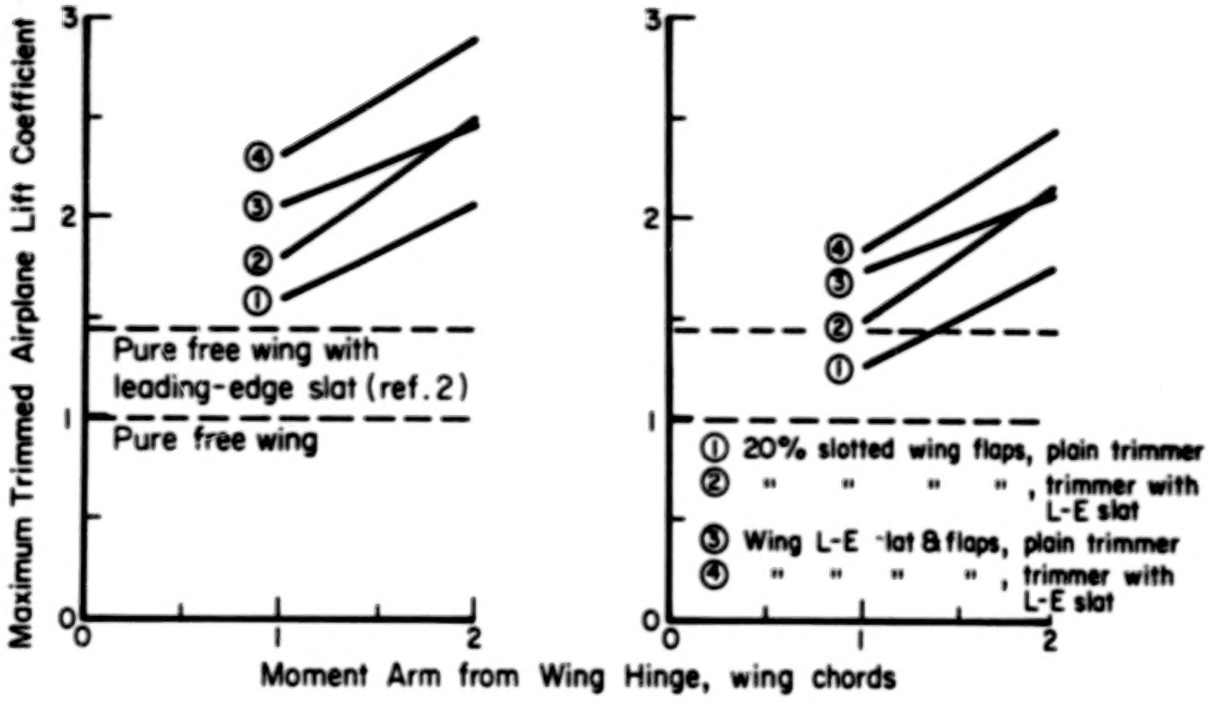

(a) Forward trimmers. (b) Aft trimmers.

FIGURE 8. MAXIMUM TRIMMED AIRPLANE LIFT COEFFICIENTS OF VARIOUS FREE-WING/FREE-TRIMMER CONFIGURATIONS.

Following the same rules for the single seat agricultural aircraft, the results are somewhat different. Considering the fixed-wing configuration (configuration 2D in table IV) as a baseline, the free-wing/aft-trimmer configuration (configuration 2C in fig. 3(c)) had an empty weight 21 percent greater than configuration 1A, its fixed-wing counterpart, and 7 percent greater than the comparable pure free-wing aircraft. The free-wing/forward-trimmer configuration (configuration 2A of fig. 3(a)) had an empty weight 8 percent greater than its fixed-wing counterpart but 5 percent less than a comparable pure free-wing aircraft.

This comparison brings up important design considerations. First, an aft-trimmer configuration incurs the highest weight penalty because the center of gravity of the trimmer surface is aft of the wing hinge line and does nothing to alleviate the counterweight needed to balance the free wing about its hinge line. Secondly, a forward-trimmer configuration is more efficient from a weight standpoint in that it incurs a lower weight penalty than an aft trimmer. Since the weight of the forward trimmer offsets the

weight needed to balance the wing about its hinge point, it can, if properly sized and placed, provide a lighter total wing weight than a pure free wing.

Obviously, a tradeoff must be made on a configuration-by-configuration basis to size the external trimming surface, and to decide whether one is, in fact, necessary. For static balance, the boom/trimmer combination must create just enough moment about the wing hinge axis to bring the wing/boom/trimmer center of gravity to the wing hinge axis. On the other hand, the wing/boom/trimmer pitch inertia must be as low as possible to provide acceptable handling qualities. The trimmer must also be close enough to the wing to provide a ride quality comparable to that of pure free-wing aircraft and far enough ahead of the wing to provide adequate control power for generating high trimmed wing lift coefficients.

Sensitivity to Mass Imbalance

All of the configurations examined to this point have incorporated the longitudinal mass balancing of the three major components. Although the fuselage center of gravity is calculated to be approximately 0.61 meter (2 feet) below the wing hinge, the longitudinal displacement with respect to the hinge axis is zero. The centers of gravity of the wing/boom/trimmer assembly and the trimming surface coincide exactly with their respective hinge axes.

The effects of mass imbalance in each of the three major components were examined by computing the loci of the characteristic roots as the centers of mass deviated in the fore and aft directions. For consistency, the aircraft in Configuration 1C was used throughout, with a tip-mounted aft trimmer positioned one wing chord length behind the wing hinge axis.

Two flight conditions were examined for each case: the nominal cruise condition, which was flight at 241.4 kilometers per hour (150 miles per hour) at an altitude of 1829 meters (6000 feet), and an approach condition, which was flight at 121.0 kilometers per hour (75 miles per hour) at sea level. The assumed approach speed is 30 percent above the minimum speed obtainable with a slatted trimmer and wing flaps and slats (case 4 in fig. 8(b)) at a gross weight of 810.88 kilograms (1788 pounds). For consistency with the high-lift configuration, the wing hinge margin is assumed to be 4 percent during approach, as discussed in the preceding section. The combination of low

airspeed and reduced wing hinge margin is intended to provide the highest sensitivity to mass imbalance because of the higher ratio of inertial forces to aerodynamic forces.

Fuselage center of gravity location. - While the wing assembly and trimming surface can be designed to have an invariant center of gravity, the fuselage assembly contains all variable and disposable load items, and provision must be made for a reasonable center of gravity range.

In cruise, the aircraft of Configuration 1C could tolerate a forward displacement of about 0.6 meter (2 feet), which is 47 percent of the mean aerodynamic chord, and an aft movement of even greater magnitude, according to the root locus plots in figure 9. At the forward limit, mode A damping deteriorates to the level 3 standards of MIL-F-8785B (ASG), and the phugoid mode becomes nearly neutrally stable. As the fuselage center of gravity moves aft from the wing hinge, the only adverse effect appears to be some degradation of the damping of mode B.

In the approach case, the effects are more pronounced, and the movement of the characteristic roots, as seen in figure 10, has little resemblance to the cruise condition. The damping ratio of mode A is slightly inferior to level 3 standards even for a mass balanced fuselage, and even a small aft movement is sufficient to cause a totally unacceptable dynamic instability. In addition, a forward displacement of less than 0.3 meters (1 foot) would be sufficient to produce an unstable phugoid motion.

As mentioned earlier, the coupling of fuselage and wing motion is much more in evidence with the external trimmer arrangements than with the pure free wing concept. For this reason, and because Configuration 1C appeared to be only marginally acceptable in approach, a brief excursion was made to explore the effects of changes in the aerodynamics of the fuselage assembly. Specifically, a large-tail version of Configuration 1C was hypothesized in which the fuselage stabilizer moment arm was held constant but the effective area of the stabilizer was doubled. This modification substantially increased the static angle of attack stability of the fuselage assembly, the fuselage pitch damping coefficient, and the slope of the fuselage lift curve.

The variation of fuselage center of gravity was then repeated for the large-tail version. The resulting root loci are plotted in figure 11 for

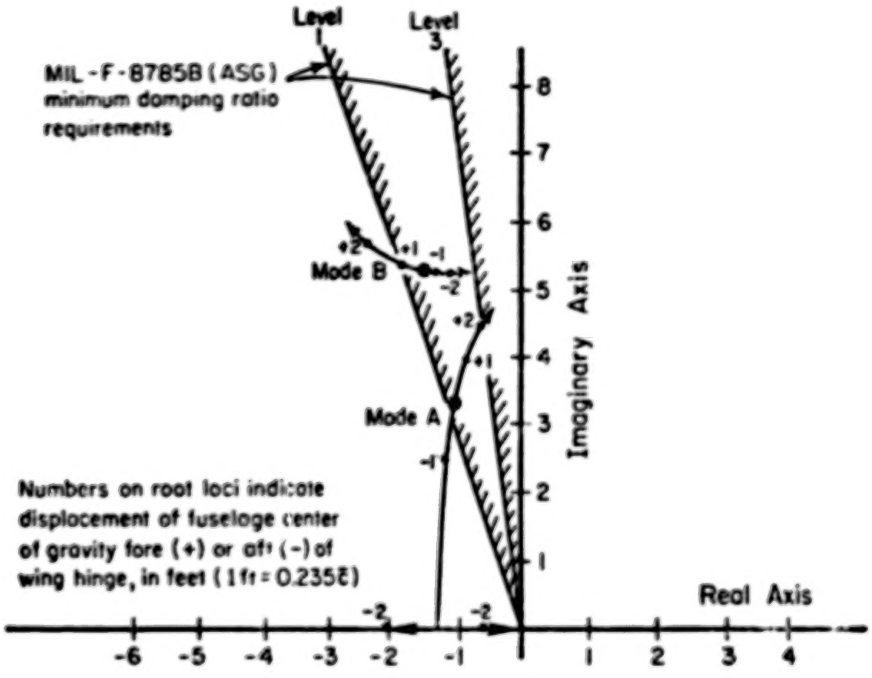

(a) Short-period modes.

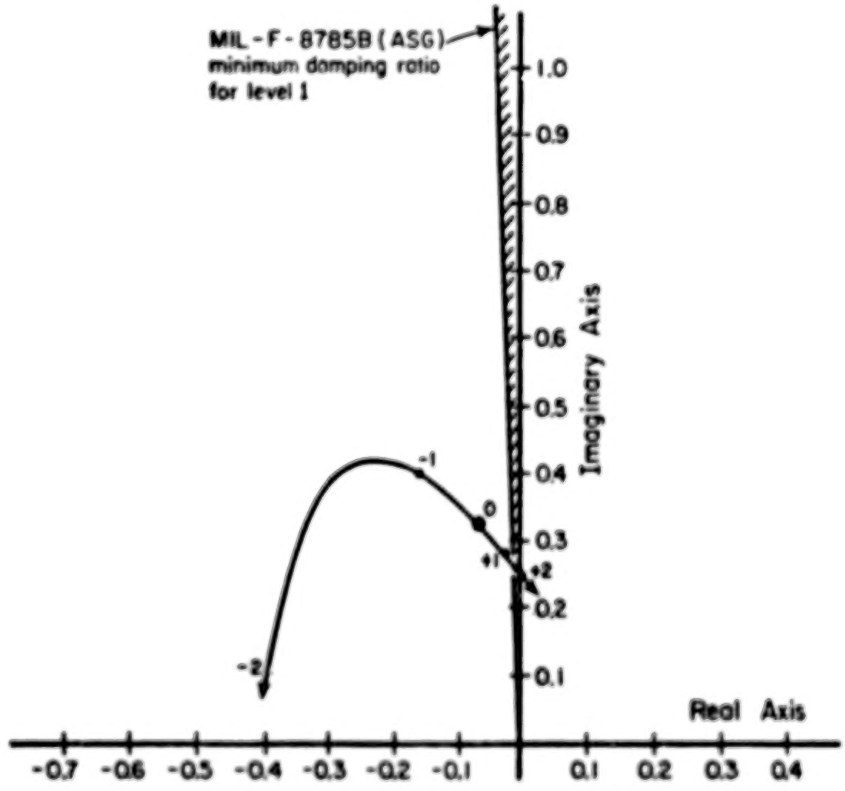

(b) Phugoid mode.

FIGURE 9. EFFECT OF FUSELAGE CENTER OF GRAVITY ON CHARACTERISTIC ROOTS OF CONFIGURATION 1C. CRUISE FLIGHT.

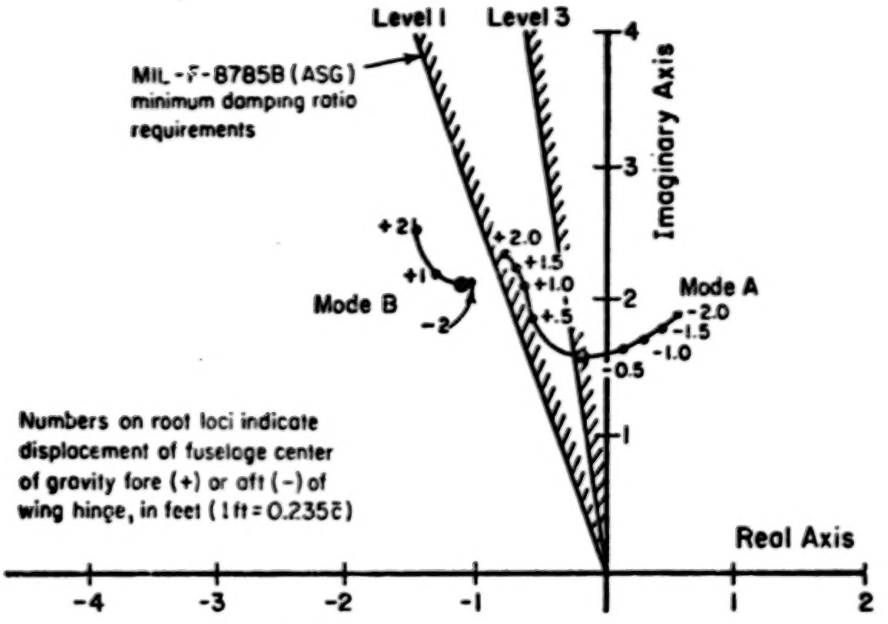

(a) Short-period modes.

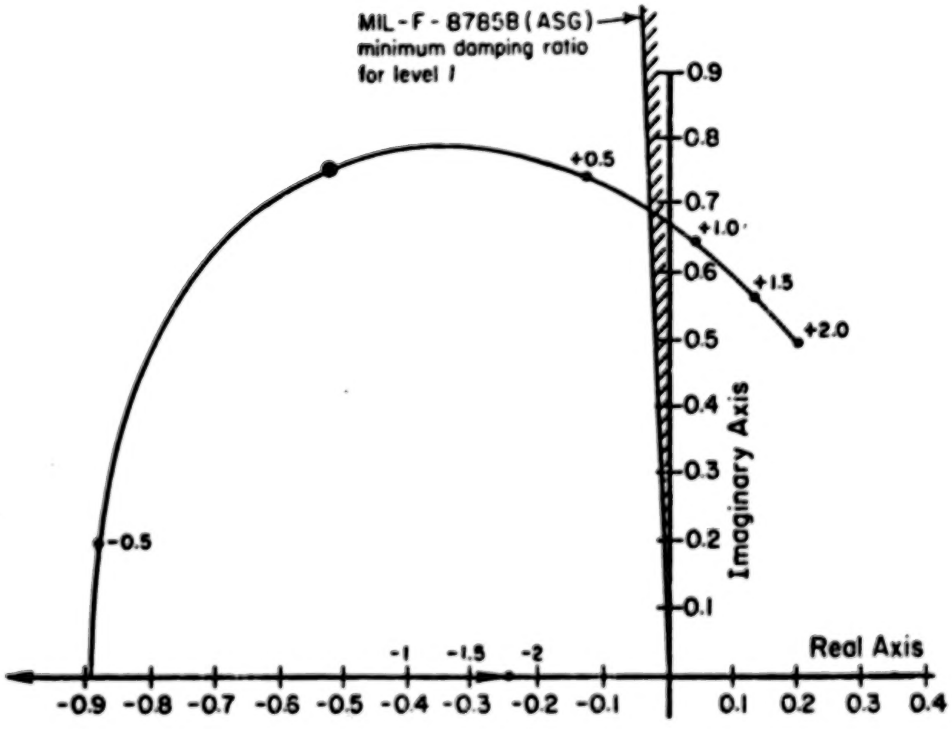

(b) Phugoid mode.

FIGURE 10. EFFECT OF FUSELAGE CENTER OF GRAVITY ON CHARACTERISTIC ROOTS OF CONFIGURATION 1C. APPROACH CONDITION WITH 4 PERCENT HINGE MARGIN.

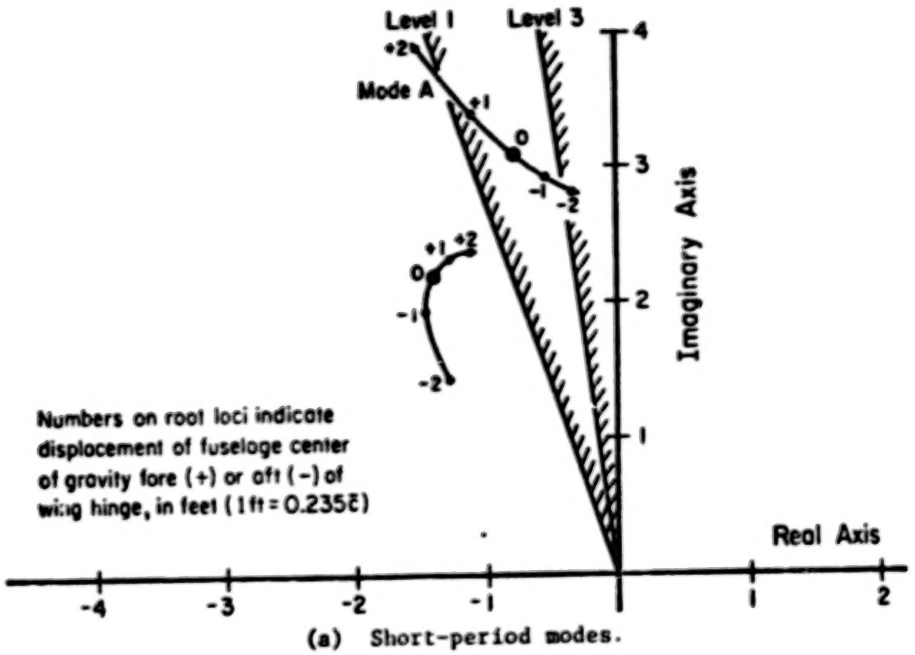

(a) Short-period modes.

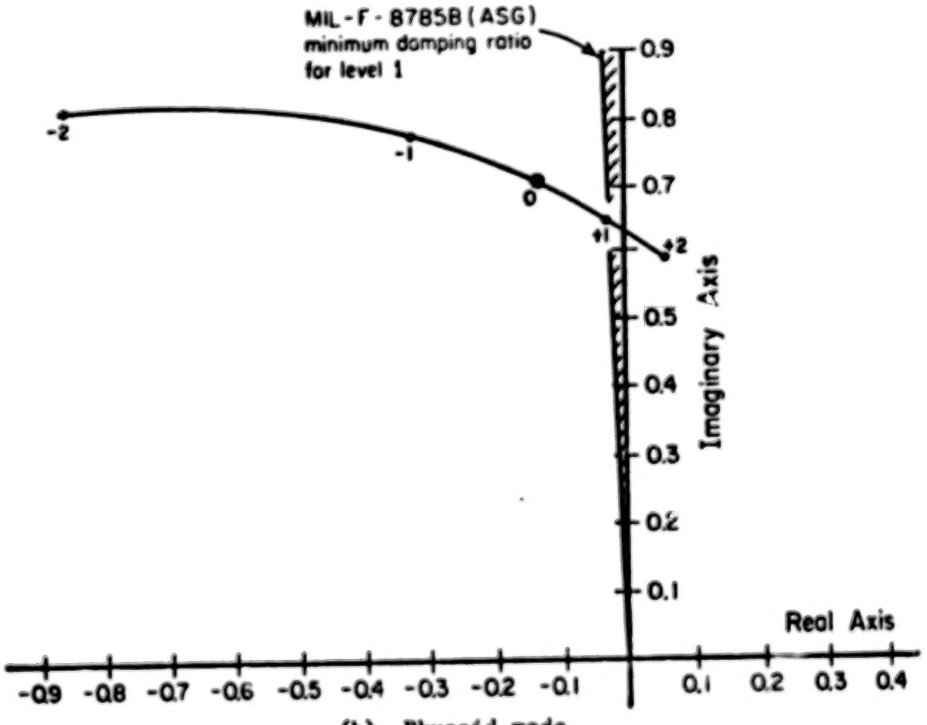

(b) Phugoid mode.

FIGURE 11. EFFECT OF FUSELAGE CENTER OF GRAVITY ON LARGE-TAIL VERSION OF CONFIGURATION 1C. APPROACH CONDITION WITH 4 PERCENT HINGE MARGIN.

approach and figure 12 for cruise. Again, the approach case is the more sensitive, but the fuselage center of gravity could deviate 0.3 meter (1 foot) forward and 0.6 meter (2 feet) aft before violating the level 1 phugoid standards or the level 3 short-period damping standards, respectively. These deviations would correspond to a fuselage center of gravity range of about 71 percent of the wing mean aerodynamic chord.

Although the approach dynamics of the large-tail version are improved and the sensitivity to fuselage imbalance is decreased, the modification would not be without its price. Comparing figures 9 and 12, the damping ratio of mode B in cruise flight is adversely affected; and more importantly, the turbulence response is inferior to the original configuration, Configuration 1C. The turbulence response will be covered in a subsequent section.

Because of the coupling between the dynamics of the fuselage and wing assembly with external trimmer, it is difficult to come to definite conclusions regarding the effects of fuselage center of gravity displacement. Nevertheless, from the four data points provided by the two flight conditions and two tail sizes, it may be concluded that forward displacement of the fuselage center of gravity decreases the damping of the phugoid mode and that aft displacement decreases the damping of one of the short-period modes, either A or B. Further, the effect of fuselage imbalance is more pronounced at low speeds and depends upon the aerodynamic design of the fuselage assembly. Significantly, however, the permissible range can be comparable to fixed-wing aircraft.

Wing assembly imbalance. - The center of gravity of the complete wing assembly, including the trimmer mass, was permitted to move through a distance of 15 percent of the wing chord fore and aft of the wing hinge. The resulting root loci are plotted in figure 13 for the cruise condition and figure 14 for the approach condition.

As shown by figure 13, the prescribed center of gravity displacement has no significant effect on any of the characteristic modes. For the approach condition, on the other hand, large forward center of gravity displacements (in excess of about 12 percent of wing chord) cause an instability in mode A. As plotted in figure 14, no serious detrimental effects are noted for aft displacements.

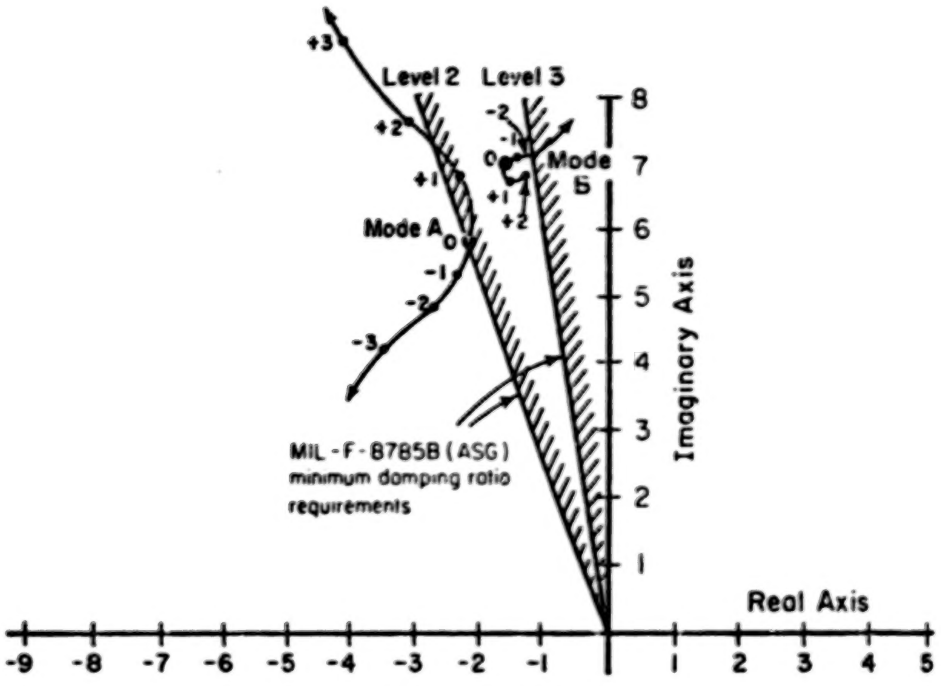

(a) Short-period modes.

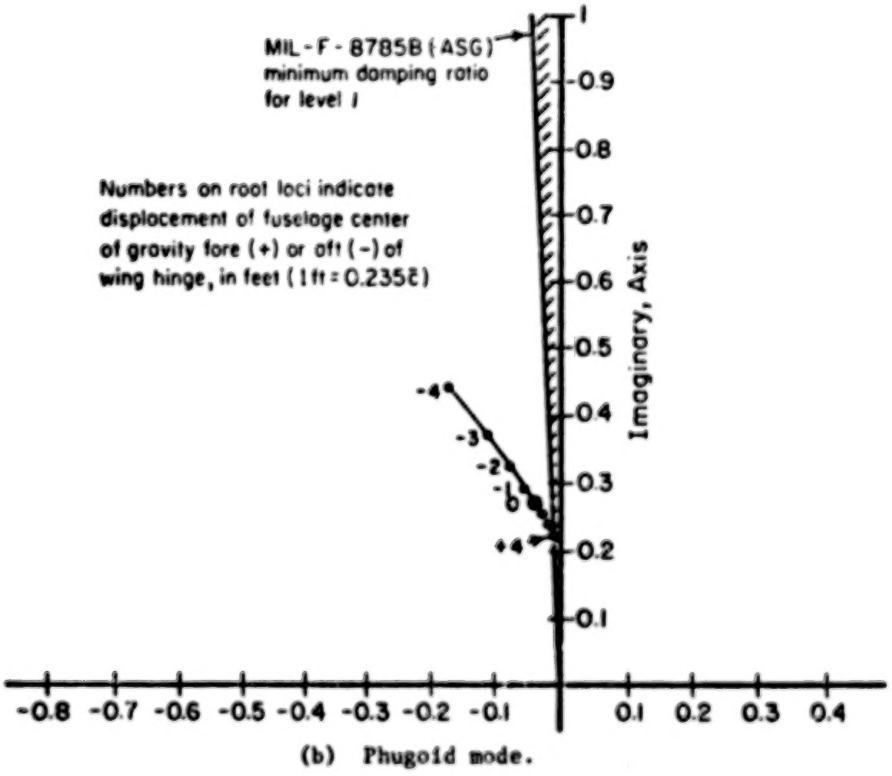

(b) Phugoid mode.

FIGURE 12. EFFECT OF FUSELAGE CENTER OF GRAVITY ON LARGE-TAIL VERSION OF CONFIGURATION 1C. CRUISE CONDITION WITH 10 PERCENT HINGE MARGIN.

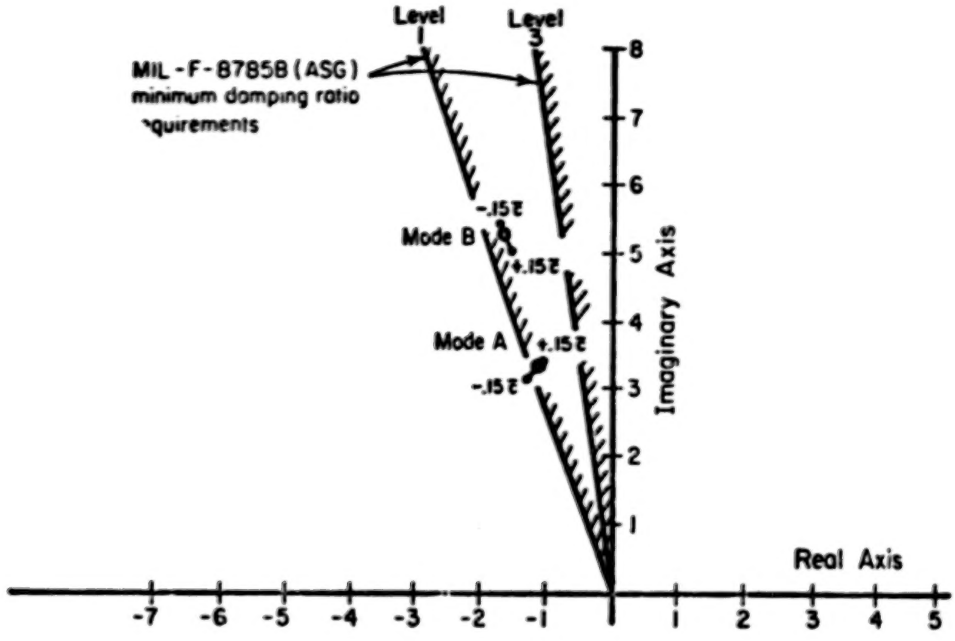

(a) Short-period modes.

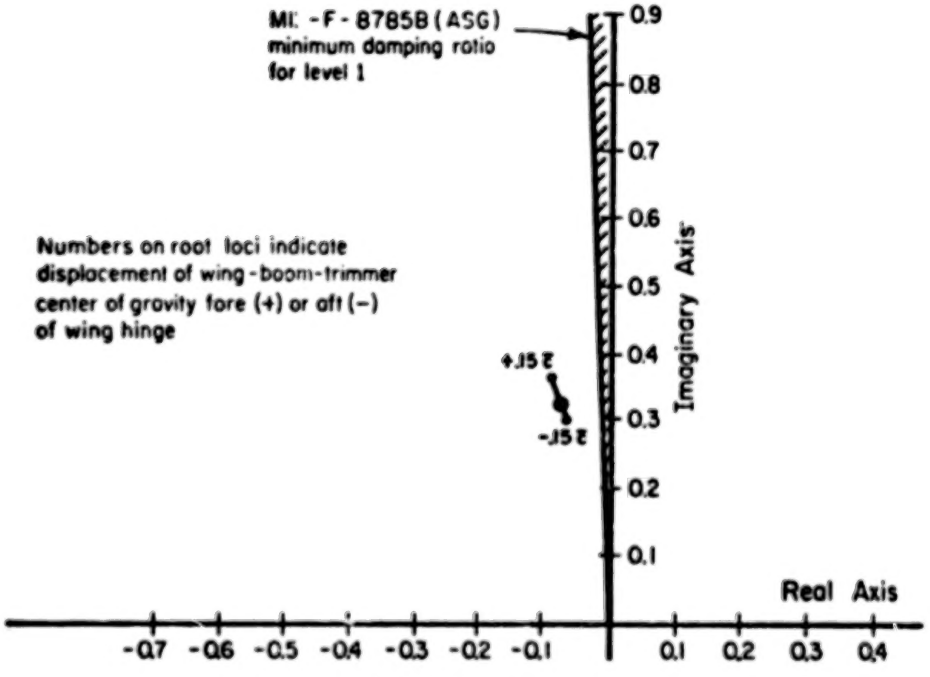

(b) Phugoid mode.

FIGURE 13. EFFECT OF WING/BOOM/TRIMMER IMBALANCE ON CHARACTERISTIC ROOTS OF CONFIGURATION 1C. CRUISE FLIGHT WITH 6 PERCENT HINGE MARGIN.

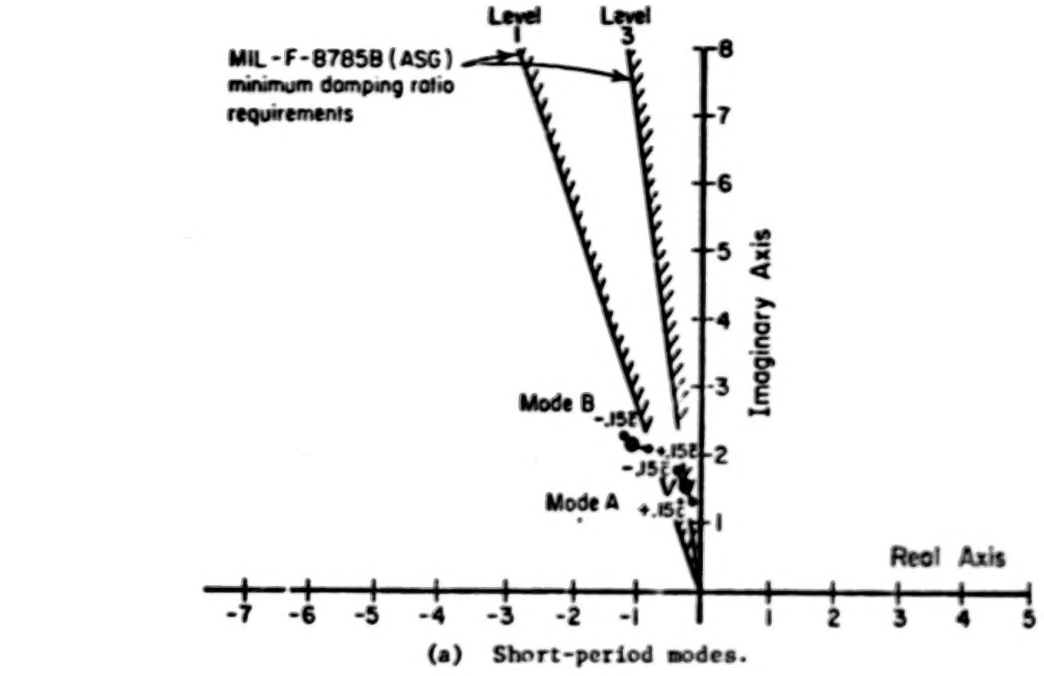

(a) Short-period modes.

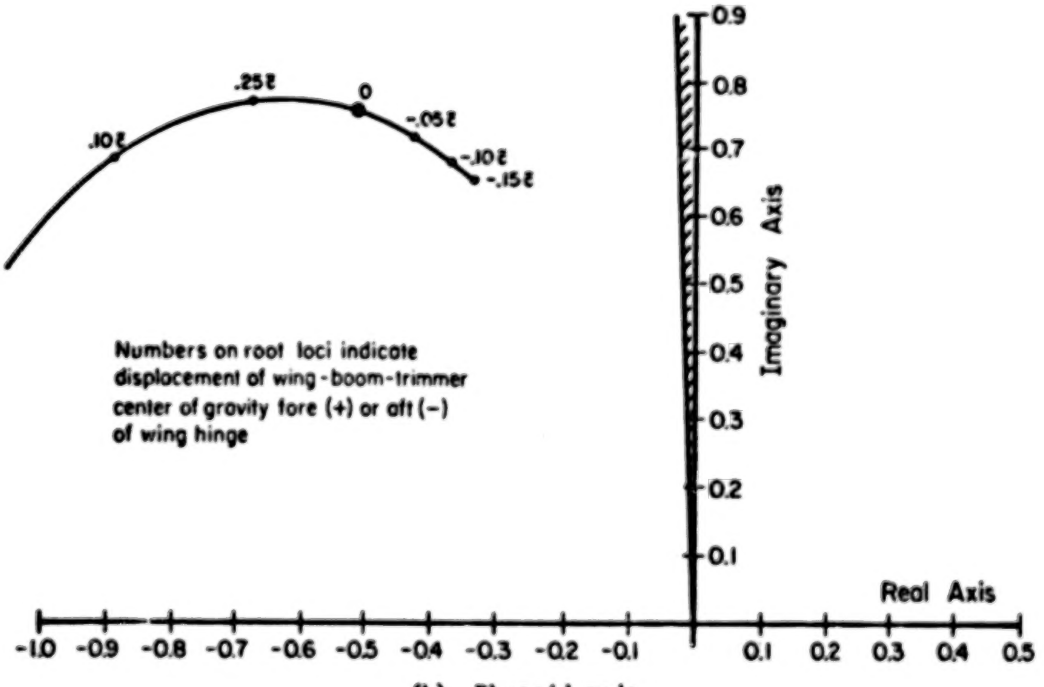

(b) Phugoid mode.

FIGURE 14. EFFECT OF WING/BOOM/TRIMMER IMBALANCE ON CHARACTERISTIC ROOTS OF CONFIGURATION 1C. APPROACH CONDITION WITH 4 PERCENT HINGE MARGIN.

Although the configuration under examination appears to be very tolerant to wing center of gravity displacement, the adverse effect of aft movement of the center of gravity during landing was not analyzed. In reference 2, it was concluded that an aft wing panel center of gravity would make a smooth landing very difficult because of the tendency for the free wing to pitch upward in response to a finite landing impact. The abrupt increase in angle of attack, in turn, would cause a bounce which could lead to a series of encounters with the runway before sufficient airspeed loss was achieved to remain on the ground. The landing impact simulation was not repeated for the free-wing/free-trimmer concept, but there is no reason to expect the results to be substantially different.

It may be concluded that small variations in wing center of gravity (of the order of a few percent of wing chord) will have no significant effect on the in-flight characteristic modes, but aft center of gravity locations should be avoided to facilitate smooth landings.

Trimmer imbalance. - The trimmer center of gravity was displaced up to 5 percent of the trimmer chord fore and aft of its hinge axis, and the characteristic modes were found to be very sensitive to this parameter.

An aft imbalance of the trimmer is especially to be avoided, as evidenced by the movement of the phugoid roots in figure 15 for cruise, and in the instability of mode A in figure 16 for the approach condition. For the latter case, an aft displacement of only 0.4 percent of the trimmer chord produces a dynamic instability. For forward center of gravity movement, greater tolerance is exhibited before the phugoid mode is destabilized for the approach condition.

Since the damping ratio of mode A in the approach condition is only marginally acceptable, even with no imbalance, further numerical experimentation was performed to insure that this significant result was not excessively configuration dependent. Again, the large-tail version of Configuration 1C was used. In this case, mode A improved but mode B became unstable, with an aft displacement only slightly in excess of 1 percent of the trimmer chord.

Because of the criticality of this parameter, the numerical experiment was repeated with a forward trimmer configuration to explore possible differences. Configuration 1A was selected with a forward surface at a moment

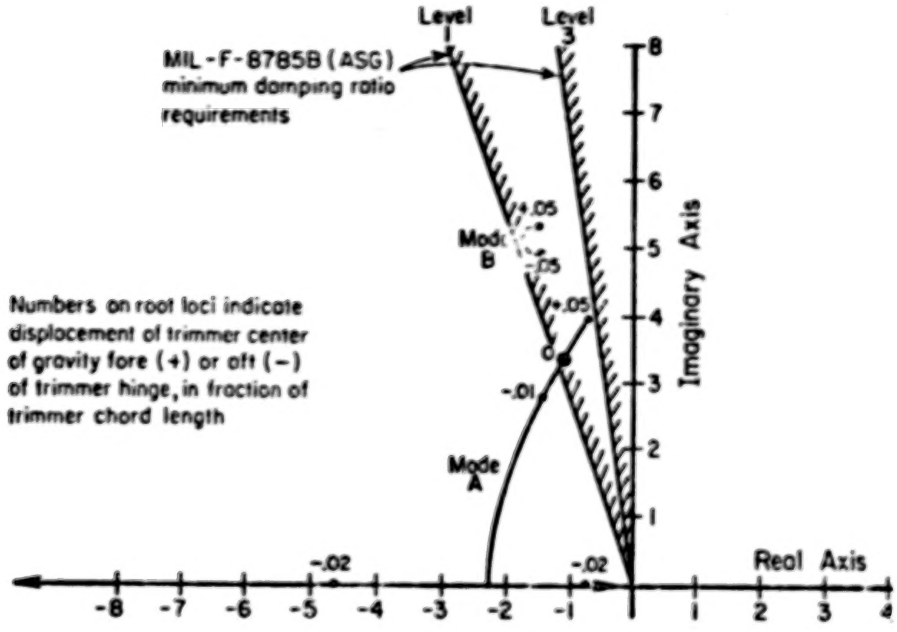

(a) Short-period modes.

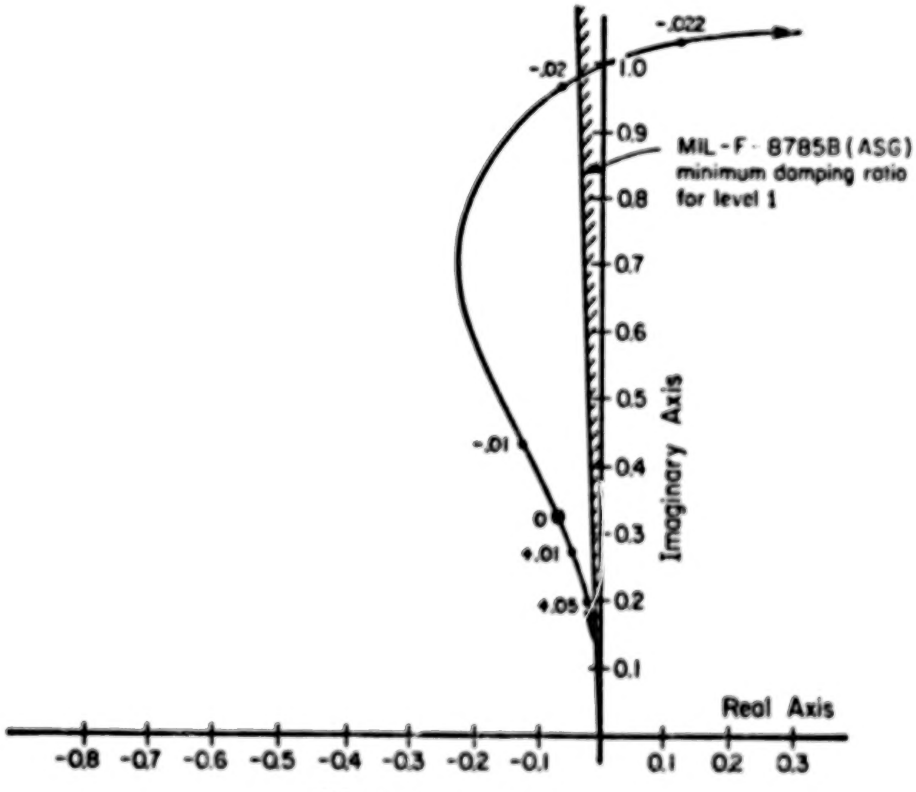

(b) Phugoid mode.

FIGURE 15. EFFECT OF TRIMMER IMBALANCE ON CHARACTERISTIC ROOTS OF CONFIGURATION 1C. CRUISE FLIGHT WITH 6 PERCENT WING HINGE MARGIN.

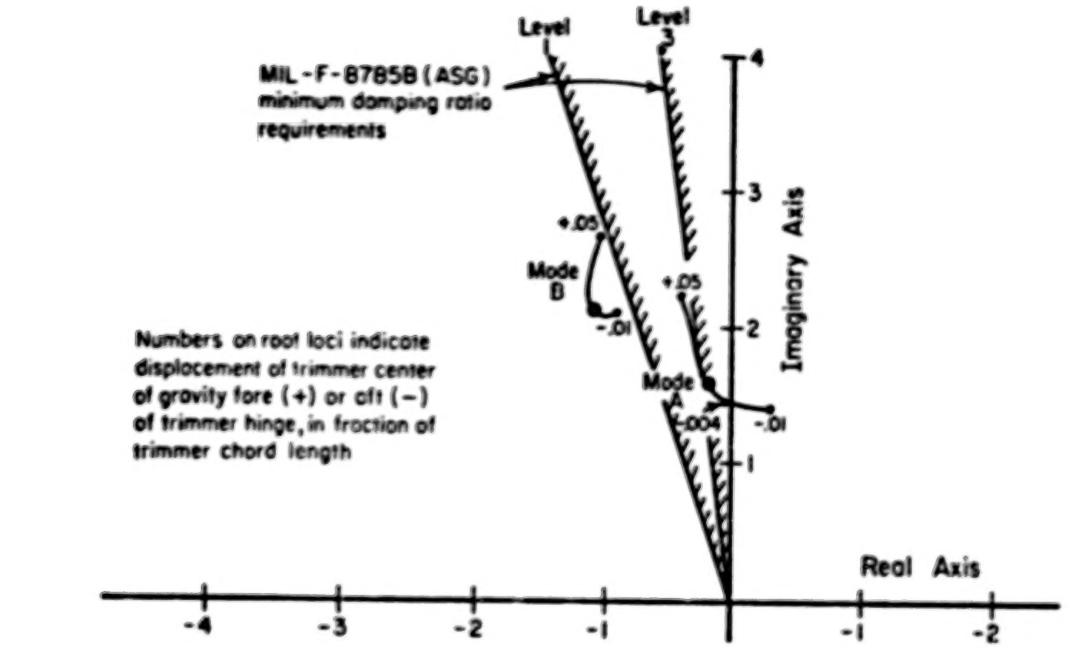

(a) Short-period modes.

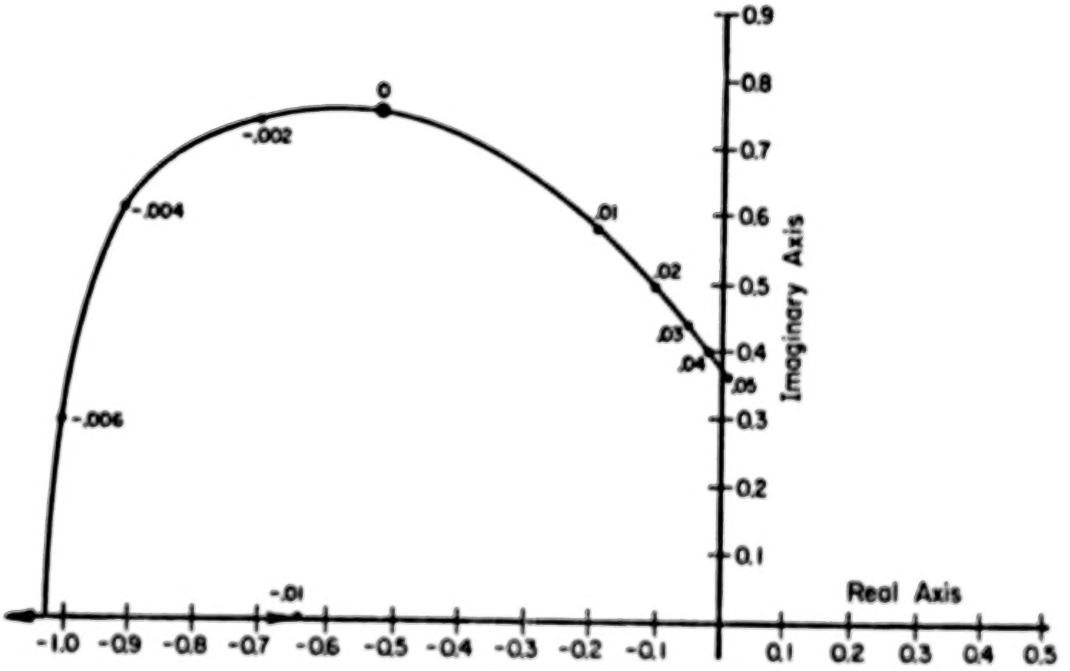

(b) Phugoid modes.

FIGURE 16. EFFECT OF TRIMMER IMBALANCE ON CHARACTERISTIC ROOTS OF CONFIGURATION 1C. APPROACH CONDITION WITH 4 PERCENT WING HINGE MARGIN.

arm of two wing chords. With regard to the consequences of aft trimmer imbalance, the results were virtually the same, a dynamic instability of mode B occurring with an aft imbalance of less than 1 percent of the trimmer chord.

It would appear that the effect of aft imbalance is the same whether the trimmer is located fore or aft of the wing hinge. A reasonable explanation for this observation is that, in both configurations, an aft imbalance of the panel tends to deflect the trimmer in the direction that enhances the angular acceleration of the wing.

In conclusion, no aft imbalance of the trimmer surface should be permitted. A small forward imbalance (of the order of one percent of trimmer chord) may be tolerated, although the effect may be felt in reduced damping of the phugoid at low speeds.

General Comments on Configuration Options

Although the forward trimmer configurations afford higher lift capabilities (fig. 8), the aft-trimmer configurations appear to offer inherently better gust alleviation. Furthermore, for the stick-fixed longitudinal motions analyzed in this study, the aft-trimmer configurations exhibit better dynamic behavior (compare fig. 6 and 7).

Figure 17 summarizes the normal load factor responses to continuous turbulence for both types of configurations for the cruise condition. Configuration 1C, with a tip-mounted aft trimmer with a moment arm of one chord length, was selected for the analysis of imbalance effects because it appears to be representative of promising configuration choices. For completeness, the turbulence responses were also calculated for the approach condition for this configuration; these responses are shown in figure 18.

The adverse effect of the free-wing principle on fuselage pitching response is consistent with the observations of references 1 and 2. The development of passive or active fuselage pitch dampers would be an interesting technical challenge because of the influence of fuselage characteristics on total aircraft behavior which has been noted for the free-wing/free-trimmer configurations.

One disadvantage of aft trimming surfaces is the necessity for greater ballast forward of the wing hinge to achieve mass balance of the wing

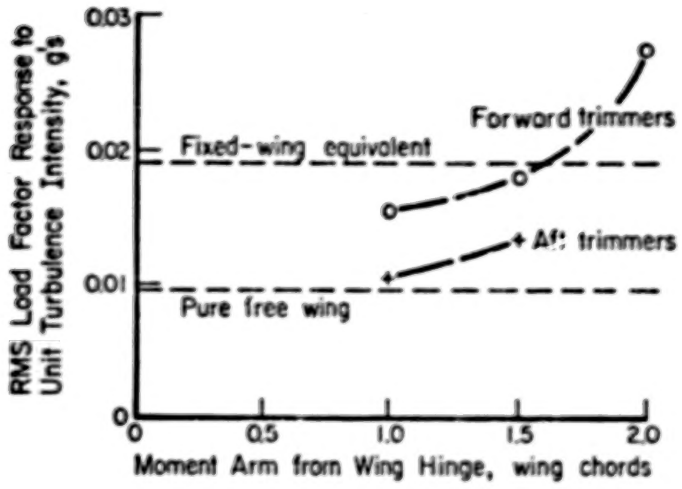

FIGURE 17. COMPARISON OF RESPONSES TO CONTINUOUS TURBULENCE.

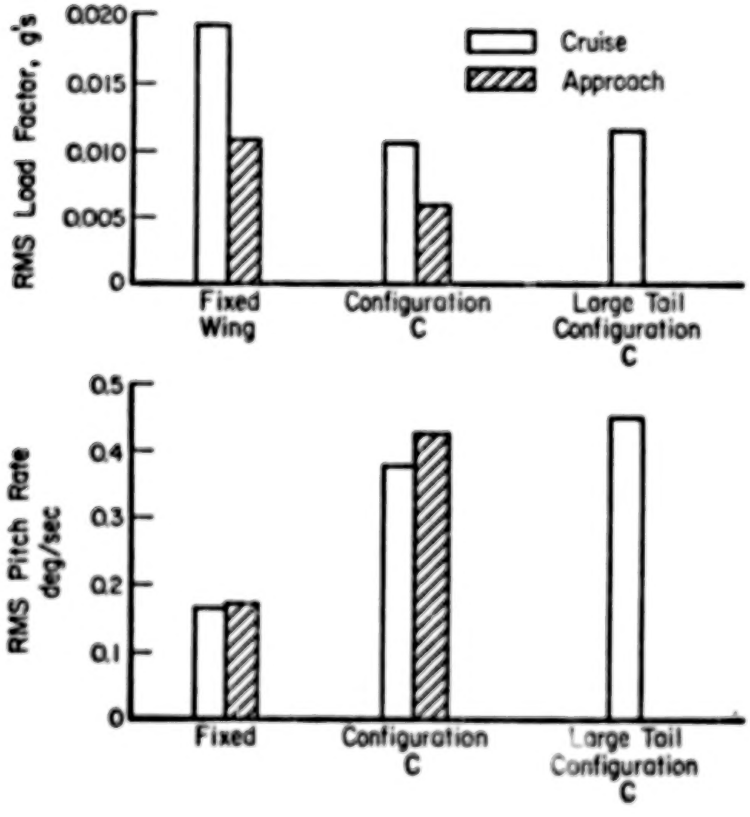

FIGURE 18. COMPARISON OF RESPONSES OF FIXED-WING AIRCRAFT AND TWO VERSIONS OF CONFIGURATION 1C.

assembly. It seems possible, however, to reduce the severity of this penalty by clever design of specific aircraft. For example, landing lights, avionics equipment, batteries, and other constant-mass fixed items of equipment could, in principle, be placed in the forward wingtip booms to reduce the required mass of additional inert weight. In addition, judicious choices of wing sweep and taper may move the wing center of gravity forward with respect to the wing hinge axis.

Another intriguing possibility for tip-mounted aft trimmers is the use of these surfaces for lateral control. Although no lateral-directional analysis was included in this study, the trimming surfaces, moved differentially, could be expected to provide powerful roll control.

CONCLUSIONS

The following conclusions may be drawn from this investigation:

(1) For the trimmer area ratio considered (1/6), the most promising configuration employs wingtip-mounted trimming surfaces placed aft of the wing hinge line with a moment arm of one wing chord length. Of the configurations examined in this study, this arrangement alone could provide excellent alleviation of vertical gust loads while exceeding the maximum lift capability of pure free-wing configurations, and while meeting fundamental criteria for the stability of the stick-fixed longitudinal modes.

(2) For vertical gust alleviation, forward trimmers are inferior to aft-mounted surfaces because of adverse wing pitching moments caused by transient aerodynamic forces on the trimming surfaces.

(3) Mass balancing of the trimmer surface about its hinge axis is vital for precluding adverse effects on the stability of the characteristic modes. In particular, aft imbalance must be avoided.

(4) Longitudinal displacement of the center of gravity of the fuselage assembly appears to be more significant for free-wing/free-trimmer configurations than for pure free-wing aircraft. Forward displacement decreases the damping of the phugoid mode while aft displacement decreases the damping of one of the short-period modes. The effect of fuselage imbalance is more pronounced for slow-speed flight, and the sensitivity depends upon the aerodynamic design of the fuselage assembly.

(5) Small variations in the wing assembly center of gravity (of the order of a few percent of wing chord) have no significant effect on the in-flight characteristic modes, but center of gravity locations aft of the wing hinge axis should be avoided to facilitate smooth landings.

(6) Forward-trimmer configurations are more efficient from a weight standpoint than aft trimmers, and could, if properly sized and placed, provide a lighter total wing weight than a pure free-wing. The aft-trimmer configuration incurs a higher weight penalty because of the additional counterweight needed to balance the wing assembly about its hinge axis.

APPENDIX A. DEVELOPMENT OF EQUATIONS OF MOTION

Introduction

In deriving the equations of motion, each free surface and the fuselage assembly are considered free bodies at first. After the individual sets of equations are written with respect to the most convenient axis systems, they are combined into a single set, referred to the wing hinge axis system. The equations are consolidated by eliminating the common forces and moments that act between the various components. The equations are then linearized for convenience in the analysis.

Symbols

Symbols that are defined each time they are used have been omitted from this list.

$\mathbf{a}$	linear acceleration, meters/second^2 (feet/second^2)
$\mathbf{F}$	force, newtons (pounds)
F	reversed effective force, newtons (pounds)
$\mathbf{g}$	acceleration due to gravity, meters/second^2 (feet/second^2)
$\dot{\mathbf{H}}$	angular momentum, radians/second
[I]	inertia tensor (shown in equation (31) for forward trimmer and after equation (44) for wing-boom assembly), kilogram-meters^2 (slug-feet^2)
M	moment, newton-meters (foot-pounds)
M	reversed effective moment, newton-meters (foot-pounds)
m	mass, kilograms (slugs)
p,q,r	roll rates about x,y,z axes, respectively, radians/second
$\ddot{\mathbf{R}}$	inertial linear acceleration, meters/second^2 (feet/second^2)
U,V,W	velocity vector components about x,y,z axes, respectively, meters/second (feet/second)
V	velocity, meters/second (feet/second)
X,Y,Z	stability axes
x_H, y_H, z_H	wing hinge axes
x',y',z'	wing panel axes
$X'_{CH}, Y'_{CH}, Z'_{CH}$	trimmer hinge axes

X",Y",Z"	trimmer panel axes
δ	deflection angle of surface, radians
ρ	position vector, meters (feet)
ω	angular velocity, radians/second
$\vec{1}_x, \vec{1}_y, \vec{1}_z$	unit vectors along x,y,z axes, respectively.

Subscripts and superscripts:

c	free trimmer surface
cg	center of gravity
CH	trimmer hinge
F	fuselage
H	wing hinge
O	wing hinge line intersection with aircraft plane of symmetry
O'	trimmer hinge line intersection with aircraft plane of symmetry
P	wing panel
W	wing
WB	wing/boom assembly
WH	wing hinge
x,y,z	axes other than stability
'	wing panel axis system
"	trimmer axis.

Coordinate Systems

The six coordinate systems described below were employed.

Conventional stability axis system. Following standard practice, the basic set of coordinates for describing the aircraft motion has its origin at the center of gravity of the complete aircraft. The x-axis is aligned with the velocity vector of the aircraft in the reference condition, the y-axis extends to the right of the plane of symmetry, and the z-axis completes the right-hand set. These coordinates are fixed in the aircraft and rotate with it. The orientation of the stability axis system with respect to an inertially fixed reference is defined by three standard Euler angles. The sequence of rotation used to define these angles is: (1) rotation about the z-axis through the yaw angle, ψ, (2) rotation about the y-axis through the pitch angle, θ, and (3) rotation about the x-axis through the roll angle, ϕ.

Hinge axis system. The hinge system of axes, x_H, y_H, z_H, has its origin in the plane of symmetry of the aircraft. The positive y_H-axis coincides with the axis of rotation of the right wing panel. For simplicity, the wing panels are assumed to have no geometric dihedral. Consequently, z_H lies in the plane of symmetry, and the negative y_H-axis coincides with the axis of rotation of the left wing panel. The hinge axis system is parallel to the stability axis system, and is therefore fixed in the fuselage assembly for a given flight condition.

Panel axis system. The panel axis system x', y', z', is similar to the hinge axis system, but rotates with the wing panels. When dealing with the wing panels, the panel axis system is rotated about the y_H-axis through the displacement angle δ_p.

Forward trimmer hinge axis system. The forward trimmer hinge axis system, X'_{CH}, Y'_{CH}, Z'_{CH} is fixed with respect to the wing panel axis system and varies from the stability axis system by δ_p only. Its origin is at the intersection of the forward trimmer hinge line and the aircraft plane of symmetry.

Forward trimmer panel axis system. The forward trimmer system of axes X", Y", Z" has its origin at the same point as the trimmer hinge axis system. The forward trimmer panel axis system, however, is fixed in the forward trimmer panel, its x-axis being the forward trimmer chord line at the aircraft plane of symmetry. This axis system is free to rotate from the forward trimmer hinge system through the displacement angle δ_c, only. The Y"- and Y'_{CH}-axes coincide and both are parallel to the y'-, y_H-, y_F-, and Y-axes at all times.

Fuselage axis system. The fuselage axis system x_F, y_F, z_F is fixed within the fuselage at the wing hinge. Its origin is at the intersection of the aircraft plane of symmetry and the wing hinge line, since this is the point about which the fuselage rotates. The x_F-axis is parallel to the fuselage reference line (FRL), positive forward. The axis y_F is coincident with y_H and y', and x_F and z_F vary from x_H and z_H by the fuselage pitch angle, ε. The fuselage pitch angle is usually small enough to be neglected. To assess the effect of fuselage pitch angle on aircraft characteristics, ε was initially set at a value other than zero and fuselage aerodynamic and inertial characteristics recalculated to reflect its static value.

Whenever equations of motion are to be formulated, they always derive from the application of two principles; namely, the principle of motion of the mass center and the principle of moment of momentum. The principle of motion of the mass center applies only to centers of gravity and this was carefully applied to each of the free bodies (fuselage, wing/boom and trimmer). The principle of moment of momentum is valid for points of rotation other than the mass center, if compensation is made for the offset center of gravity. This compensation was generally necessary for each free body, since the various auxiliary axis systems were not generally located at centers of gravity.

Unlike the case for a conventional aircraft, with the free-wing aircraft the equations of motion cannot be summarily referenced to the stability axes centered at the aircraft center of gravity. In fact, the location of the all-up aircraft center of gravity is variable, dependent upon the relative position of the wing/boom/trimmer. This variability has not been ignored in the current analysis. The hinge axis system can be used as the "principal reference" rather than the stability axis system. It is fixed with respect to the fuselage and parallel to the stability axis. All force and moment contributions from the various free bodies can be referenced/coordinated with respect to this axis system, even though it is not located at the aircraft center of gravity, nor at the center of gravity of any of the various free bodies.

Free-Body Equations

General procedure. To derive forward trimmer and wing panel force equations, first the position vector, ρ, from the panel hinge axis (coordinate system origin) to the panel center of gravity is written in the most convenient coordinate system. This allows the vector to be fixed. The position vector is then transferred to the wing hinge axis system and differentiated twice with respect to time. To this is then added the time differential of inertial velocity.

To derive forward trimmer and wing moment equations, first the position vector from the panel hinge axis to the panel center of gravity is written

in the appropriate axis system, as before. Then the momentum term, $\ddot{m\bar{R}}$, and the angular momentum term, $\dot{H}$, are written in the appropriate axis systems. The vector ρ, and the terms $\ddot{m\bar{R}}$ and $\dot{H}$ are transferred to the wing hinge axis system before being differentiated with respect to time as necessary to write the appropriate moment equations.

The above steps also apply to the fuselage moment equations, but these equations involve only the fuselage and stability axis systems.

The aircraft will be broken down into three free bodies for analysis: the forward trimmer, wing/boom assembly and fuselage.

Forward trimmer panel force equations. In the forward trimmer panel axis system in figure 19, the position vector of the forward trimmer panel center of gravity is as follows:

$$\rho_{ccg} = X''_{cg}\hat{i}_{x}'' + Y''_{cg}\hat{i}_{y}'' + Z''_{cg}\hat{i}_{z}'' \quad , \tag{11}$$

where, because of symmetry, $Y''_{cg} = 0$. This transfers to the forward trimmer hinge axis system (which is mutually parallel to the wing panel axis system) through the forward trimmer panel deflection angle, δ_c. This can be transferred to the wing hinge axis system through the wing panel deflection angle, δ_p. See figure 20.

Before the forward trimmer center of gravity position vector can be written in the wing hinge axis system, the forward trimmer hinge axis (origin of both forward trimmer axis systems), must be located with respect to the wing hinge axis (origin of both wing axis systems), so that

$$(\hat{\rho}_{ccg})_{WH} = \hat{\rho}_{ccg} + \hat{\rho}_{CH} = \rho_{xCH}\hat{i}_{xH} + \rho_{zCH}\hat{i}_{zH} \ .$$

The result is

$$(\hat{\rho}_{ccg})_{WH} = [X''_{cg}\cos(\delta_c + \delta_p) + Z''_{ccg}\sin(\delta_c + \delta_p) + X'_{CH}\cos\delta_p$$

$$+ Z'_{CH}\sin\delta_p]\hat{i}_{xH} + [-X''_{cg}\sin(\delta_c + \delta_p) - X'_{CH}\sin\delta_p + Z'_{CH}\cos\delta_p]\hat{i}_{zH}. \tag{12}$$

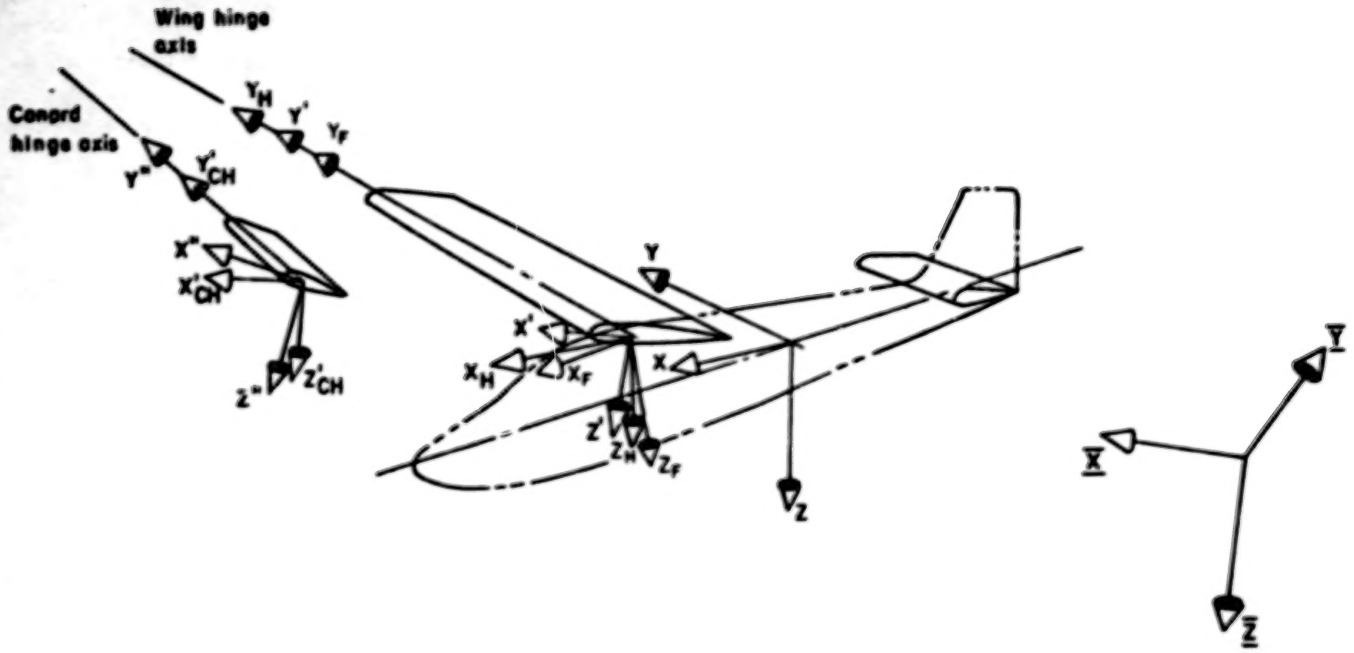

FIGURE 19. ILLUSTRATION OF AXIS SYSTEMS

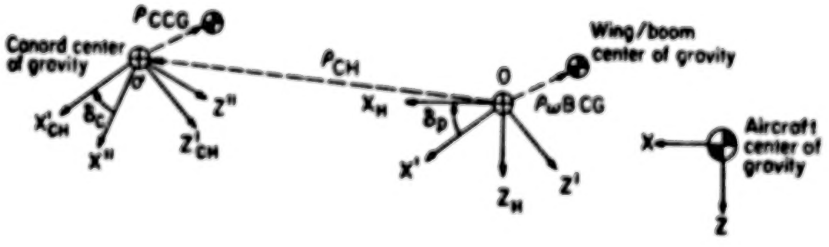

FIGURE 20. ANGULAR RELATIONSHIPS OF AXIS SYSTEMS

Since the vertical offset of the forward trimmer center of gravity from its hinge is effectively zero, the second term in the preceding equation may be dropped.

Now, define wing hinge velocity terms, $\vec{V}_H$ and $\vec{\omega}_H$, where $\vec{V}_H$ is inertial velocity and ω_H is angular velocity of the wing hinge in that system, or

$$\vec{V}_H = U\vec{1}_{xH} + V\vec{1}_{yH} + W\vec{1}_{zH} \; ; \tag{13}$$

and

$$\omega_H = p\vec{1}_{xH} + q\vec{1}_{yH} + r\vec{1}_{zH} \; . \tag{14}$$

Then the trimmer panel center of gravity inertial acceleration may be found in the wing hinge axis system as follows:

$$\vec{V}_{ccg} = (\dot{\vec{\rho}}_{ccg})_{WH} + \vec{V}_H \tag{15}$$

$$\vec{V}_{ccg} = (\dot{\rho}_{xCH} + U)\vec{1}_{xH} + V\vec{1}_{yH} + (\dot{\rho}_{zCH} + W)\vec{1}_{zH}$$

$$+ \rho_{xCH} \frac{d}{dt}(\vec{1}_{xH}) + \rho_{zCH} \frac{d}{dt}(\vec{1}_{zH}) \; . \tag{16}$$

$$\vec{a}_{ccg} = (\ddot{\rho}_{xCH} + \dot{q}\rho_{zCH} + q\dot{\rho}_{zCH} + \dot{U})\vec{1}_{xH} + (\dot{r}\rho_{xCH} + r\dot{\rho}_{xCH}$$

$$- \dot{p}\rho_{zCH} - p\dot{\rho}_{zCH} + \dot{V})\vec{1}_{yH} + (\ddot{\rho}_{zCH} - \dot{q}\rho_{xCH} - q\dot{\rho}_{xCH} + \dot{W})\vec{1}_{zH}$$

$$+ (\dot{\rho}_{xCH} + q\rho_{zCH} + U)\frac{d}{dt}(\vec{1}_{xH}) + (r\rho_{xCH} - p\rho_{zCH} + V)\frac{d}{dt}(\vec{1}_{yH})$$

$$+ (-q\rho_{xCH} + \dot{\rho}_{zCH} + W)\frac{d}{dt}(\vec{1}_{zH}) \; . \tag{17}$$

Unit vectors differentiate to:

$$\frac{d}{dt}(\hat{1}_{xH}) = r\hat{1}_{yH} - q\hat{1}_{zH}$$

$$\frac{d}{dt}(\hat{1}_{yH}) = -r\hat{1}_{xH} + p\hat{1}_{zH}$$

$$\frac{d}{dt}(\hat{1}_{zH}) = q\hat{1}_{xH} - p\hat{1}_{yH} \quad . \tag{18}$$

Therefore, the preceding expression for forward trimmer inertial acceleration becomes, upon expansion,

$$\begin{aligned}
(\hat{a}_{ccg})_x = \{&-\ddot{\delta}_c X''_{cg} \sin(\delta_c + \delta_p) - \dot{\delta}_c^2 X''_{cg} \cos(\delta_c + \delta_p) - \dot{\delta}_c \dot{\delta}_p X'' \cos(\delta_c + \delta_p) \\
&+ \ddot{\delta}_p[-X''_{cg} \sin(\delta_c + \delta_p) - X'_{CH} \sin\delta_p + Z'_{CH} \cos\delta_p] \\
&+ \dot{\delta}_p[-\dot{\delta}_c X''_{cg} \cos(\delta_c + \delta_p) - \dot{\delta}_p(X''_{cg} \cos(\delta_c + \delta_p) + X'_{CH} \cos\delta_p \\
&+ Z'_{CH} \sin\delta_p)] + (-r^2 - q^2)[X''_{cg} \cos(\delta_c + \delta_p) + X'_{CH} \cos\delta_p \\
&+ Z'_{CH} \sin\delta_p] + (\dot{q} + pr)[-X''_{cg} \sin(\delta_c + \delta_p) - X'_{CH} \sin\delta_p \\
&+ Z'_{CH} \cos\delta_p] + 2q[-\dot{\delta}_c X''_{cg} \cos(\delta_c + \delta_p) - \dot{\delta}_p(X''_{cg} \cos(\delta_c + \delta_p) \\
&+ X'_{CH} \cos\delta_p + Z'_{CH} \sin\delta_p)] + \dot{U} - rV + qW\}\hat{1}_{xH}
\end{aligned}$$

$$\begin{aligned}
(\hat{a}_{ccg})_y = \{&(pq + \dot{r})[X''_{cg} \cos(\delta_c + \delta_p) + X'_{CH} \cos\delta_p + Z'_{CH} \sin\delta_p] \\
&+ 2r[-\dot{\delta}_c X''_{cg} \sin(\delta_c + \delta_p) + \dot{\delta}_p(-X''_{cg} \sin(\delta_c + \delta_p) - X'_{CH} \sin\delta_p \\
&+ Z'_{CH} \cos\delta_p)] + (-\dot{p} + qr)[-X''_{cg} \sin(\delta_c + \delta_p) - X'_{CH} \sin\delta_p \\
&+ Z'_{CH} \cos\delta_p] - 2p[-\dot{\delta}_c X''_{cg} \cos(\delta_c + \delta_p) - \dot{\delta}_p(X''_{cg} \cos(\delta_c + \delta_p) \\
&+ X'_{CH} \cos\delta_p + Z'_{CH} \sin\delta_p)] + \dot{V} + rU - pW\}\hat{1}_{yH} \quad .
\end{aligned} \tag{19}$$

(Equation 19 continued)

$$(\hat{a}_{ccg})_z = \{(-\dot{q} + pr)[X''_{cg} \cos(\delta_c + \delta_p) + X'_{CH} \cos\delta_p + Z'_{ch} \sin\delta_p]$$

$$- 2q[-\dot{\delta}_c X''_{cg} \sin(\delta_c + \delta_p) + \dot{\delta}_p(-X''_{cg} \sin(\delta_c + \delta_p)$$

$$- X'_{CH} \sin\delta_p + Z'_{CH} \cos\delta_p)] + (-q^2 - p^2)[-X''_{cg} \sin(\delta_c + \delta_p)$$

$$- X'_{CH} \sin\delta_p + Z'_{CH} \cos\delta_p] - \ddot{\delta}_c X''_{cg} \cos(\delta_c + \delta_p)$$

$$+ \dot{\delta}_c^2 X''_{cg} \sin(\delta_c + \delta_p) + \dot{\delta}_c\dot{\delta}_p X''_{cg} \sin(\delta_c + \delta_p) - \ddot{\delta}_p[X''_{cg} \cos(\delta_c$$

$$+ \delta_p) + X'_{CH} \cos\delta_p + Z'_{CH} \sin\delta_p] - \dot{\delta}_p[-\dot{\delta}_c X''_{cg} \sin(\delta_c + \delta_p)$$

$$+ \dot{\delta}_p(-X''_{cg} \sin(\delta_c + \delta_p) - X'_{CH} \sin\delta_p + Z'_{CH} \cos\delta_p)] + \dot{W}$$

$$- qU + pV\}\hat{1}_{zH} . \qquad (19)$$

Finally, collecting terms by sines and cosines yields:

$$(a_{ccg})_x = -(\ddot{\delta}_c + \ddot{\delta}_p + \dot{q} + pr)[X''_{cg} \sin(\delta_c + \delta_p)] - [(\dot{\delta}_c + \dot{\delta}_p)^2 + 2q(\dot{\delta}_c + \dot{\delta}_p)$$

$$+ q^2 + r^2][X''_{cg} \cos(\delta_c + \delta_p)] + (\ddot{\delta}_p + \dot{q} + pr)(-X'_{CH} \sin\delta_p$$

$$+ Z'_{CH} \cos\delta_p) - [(q + \dot{\delta}_p)^2 + r^2](X'_{CH} \cos\delta_p + Z'_{CH} \sin\delta_p) + \dot{U}$$

$$- rV + qW$$

$$(a_{ccg})_y = -[2r(\dot{\delta}_c + \dot{\delta}_p) - \dot{p} + qr][X''_{cg} \sin(\delta_c + \delta_p)] + [2p(\dot{\delta}_c + \dot{\delta}_p)$$

$$+ pq + \dot{r}][X''_{cg} \cos(\delta_c + \delta_p)] + (2r\dot{\delta}_p - \dot{p} + qr)(-X'_{CH} \sin\delta_p$$

$$+ Z'_{CH} \cos\delta_p) + (2p\dot{\delta}_p + pq + \dot{r})(X'_{CH} \cos\delta_p + Z'_{CH} \sin\delta_p) + \dot{V}$$

$$- pW + rU \qquad (20)$$

(Equation 20 continued)

$$(a_{ccg})_z = [(\dot{\delta}_c + \dot{\delta}_p)^2 + 2q(\dot{\delta}_c + \dot{\delta}_p) + p^2 + q^2][X''_{cg}\sin(\delta_c + \delta_p)]$$

$$- (\ddot{\delta}_c + \ddot{\delta}_p + \dot{q} - pr)[X''_{cg}\cos(\delta_c + \delta_p)] - [(q + \dot{\delta}^2_p) + -[(q+\dot{\delta}_p)^2$$

$$+ p^2](-X'_{CH}\sin\delta_p + Z'_{CH}\cos\delta_p) - (\ddot{\delta}_p + \dot{q} - pr)(X'_{CH}\cos\delta_p$$

$$+ Z'_{CH}\sin\delta_p) + \dot{W} + pV - qU \quad . \tag{20}$$

Then, applying the fundamental Newtonian law, the three equations describing the forces at the origin of the wing hinge axis system that are associated with the acceleration of the forward trimmer panel are as follows:

$$(\vec{F}_{xH})_c = m_c(\vec{a}_{ccg})_x$$

$$(\vec{F}_{yH})_c = m_c(\vec{a}_{ccg})_y$$

$$(\vec{F}_{zH})_c = m_c(\vec{a}_{ccg})_z \quad . \tag{21}$$

Wing panel force equations. In the wing panel axis system in figure 19, the position vector of the wing panel plus boom center of gravity is:

$$\vec{\rho}_{WBcg} = X'_{cg}\hat{\imath}_{x'} + Y'_{cg}\hat{\imath}_{y'} + Z'_{cg}\hat{\imath}_{z'} \quad . \tag{22}$$

Again, $Y'_{cg} = 0$ because the free body is symmetrical about the x'-z' plane. The appropriate angular transfer must be made to write this position vector in the wing hinge axis system.

$$(\vec{\rho}_{WBcg})_{WH} = (X'_{cg}\cos\delta_p + Z'_{cg}\sin\delta_p)\hat{\imath}_{xH} + (-X'_{cg}\sin\delta_p$$

$$+ Z_{cg}\cos\delta_p)\hat{\imath}_{zH} \quad . \tag{23}$$

Simplifying momentarily to

$$\vec{\rho}_{WBcg} = \rho_{xH}\hat{\imath}_{xH} + \rho_{zH}\hat{\imath}_{zH} \tag{24}$$

yields, with V_H and ω_H the same as before,

$$\hat{V}_{WBcg} = (\hat{\dot{\rho}}_{WBcg})_{WH} + \hat{V}_H, \tag{25}$$

$$\hat{V}_{WBcg} = (\dot{\rho}_{xH} + U)\hat{i}_{xH} + V\hat{i}_{yH} + (\dot{\rho}_{zH} + W)\hat{i}_{zH} + \rho_{xH}\frac{d}{dt}(\hat{i}_{xH}) + \rho_{zH}\frac{d}{dt}(\hat{i}_{zH}). \tag{26}$$

$$\begin{aligned}\hat{a}_{WBcg} = {} & (\dot{U} + \dot{q}\rho_{zH} + q\dot{\rho}_{zH} + \ddot{\rho}_{xH})\hat{i}_{xH} + (\dot{V} - \dot{p}\rho_{zH} - p\dot{\rho}_{zH} + \dot{r}\rho_{xH} + r\dot{\rho}_{xH})\hat{i}_{yH} \\ & + (\dot{W} - \dot{q}\rho_{xH} - q\dot{\rho}_{xH} + \ddot{\rho}_{zH})\hat{i}_{zH} + (U + q\rho_{zH} + \dot{\rho}_{xH})\frac{d}{dt}(\hat{i}_{xH}) \\ & + (V - p\rho_{zH} + r\rho_{xH})\frac{d}{dt}(\hat{i}_{yH}) + (W - q\rho_{xH} + \dot{\rho}_{zH})\frac{d}{dt}(\hat{i}_{zH}) .\end{aligned} \tag{27}$$

Expanding this in its component form yields:

$$\begin{aligned}(a_{WBcg})_x = {} & [-(q + \dot{\delta}_p)^2 - r^2](X'_{cg}\cos\delta_p + Z'_{cg}\sin\delta_p) + (\ddot{\delta}_p + \dot{q} + pr) \\ & (-X'_{cg}\sin\delta_p + Z'_{cg}\cos\delta_p) + \dot{U} + qW - rV \\ (a_{WBcg})_y = {} & (2p\dot{\delta}_p + pq + \dot{r})(X'_{cg}\cos\delta_p + Z'_{cg}\sin\delta_p) + (2r\dot{\delta}_p - \dot{p} + qr) \\ & (-X'_{cg}\sin\delta_p + Z'_{cg}\cos\delta_p) + \dot{V} - pW + rU \\ (a_{WBcg})_z = {} & (-\ddot{\delta}_p + pr - \dot{q})(X'_{cg}\cos\delta_p + Z'_{cg}\sin\delta_p) + [-(q + \dot{\delta}_p)^2 \\ & - p^2](-X'_{cg}\sin\delta_p + Z'_{cg}\cos\delta_p) + \dot{W} + pV - qU .\end{aligned} \tag{28}$$

Again, applying the fundamental Newtonian law, the three equations describing the forces existing at the origin of the wing hinge axis system that are associated with acceleration of the wing panels are:

$$\begin{aligned}(\hat{F}_{xH})_{WB} &= m_{WB}(\hat{a}_{WBcg})_x \\ (\hat{F}_{yH})_{WB} &= m_{WB}(\hat{a}_{WBcg})_y \\ (\hat{F}_{zH})_{WB} &= m_{WB}(\hat{a}_{WBcg})_z .\end{aligned} \tag{29}$$

Trimmer-panel moment equations. The trimmer-panel moment equations will follow the general form for moments about offset points:

$$\hat{M} = \dot{\hat{H}} + (\hat{\rho}) \times m(\ddot{\hat{R}}) . \tag{30}$$

The first term will be referenced to the forward trimmer panel system where all inertias and angular velocities will be those of the forward trimmer panel about its hinge axis system. The position vector, ρ, will be expressed in the forward trimmer panel axis system initially, as will the linear momentum term, $m\ddot{\bar{R}}$. All of the terms will be transferred to the wing hinge axis system and combined at that time.

The angular momentum term is of the form:

$$\begin{Bmatrix} I_{xxc} & -I_{xyc} & -I_{xzc} \\ -I_{xyc} & I_{yyc} & -I_{yzc} \\ -I_{xzc} & -I_{yzc} & I_{zzc} \end{Bmatrix} \begin{Bmatrix} \omega_{x"} \\ \omega_{y"} \\ \omega_{z"} \end{Bmatrix} \begin{Bmatrix} \hat{I}_{x"} \\ \hat{I}_{y"} \\ \hat{I}_{z"} \end{Bmatrix} \tag{31}$$

Since the hinge axis system is composed of axes of mass symmetry, all products of inertia are zero. The angular velocity terms can be found by considering the relationship of the canard to the wing hinge axis. The only freedom the forward trimmer has with respect to this point is in pitch and is solely a function of the displacement angles δ_p and δ_c, such that

$$\hat{\omega}_{xyz"} = \omega_{x"}\hat{I}_{x"} + \omega_{y"}\hat{I}_{y"} + \omega_{z"}\hat{I}_{z"} \quad , \tag{32}$$

$$\hat{\omega}_{xyz"} = p\,\hat{I}_{xH} + (q + \dot{\delta}_c + \dot{\delta}_p)\hat{I}_{yH} + r\hat{I}_{xH} \quad . \tag{33}$$

H_o, can then be differentiated with respect to time to yield the first term in the moment equation.

The position vector, which is the arm to compute the moment of momentum, runs from the forward trimmer hinge point to the forward trimmer center of gravity and can be expressed as:

$$\hat{\rho}_{o'-ccg} = X"_{cg}\hat{I}_{x"} + Z"_{cg}\hat{I}_{z"} \quad .$$

To simplify this a bit, let $Z"_{cg} = 0$ to reflect the nominal difference in the z" coordinate of the forward trimmer center of gravity. Transferring this to the wing hinge axis system through the forward trimmer panel and wing panel axis systems yields

$$\hat{\rho}_{o'-ccg} = X"_{cg}\cos(\delta_c + \delta_p)\hat{I}_{xH} - X"_{cg}\sin(\delta_c + \delta_p)\hat{I}_{zH} \quad . \tag{34}$$

Next, the vector $\vec{R}_{o'}$ must be found.

$$\vec{R}_{o'} = \vec{a}_o + \vec{\rho}_{o-o'} \tag{35}$$

$$\vec{R}_{o'} = \dot{\vec{V}}_o + \frac{d^2}{dt^2}(X'_o \hat{I}_{x'} + Z'_o \hat{I}_{z'}) \tag{36}$$

$$\vec{R}_{o'} = \dot{\vec{V}}_o + \frac{d^2}{dt^2}[(X'_o \cos\delta_p + Z'_o \sin\delta_p)\hat{I}_{xH} + (-X'_o \sin\delta_p + Z'_o \cos\delta_p)\hat{I}_{zH}] \tag{37}$$

Now, for convenience, let

$$\begin{aligned} \rho_{o'x} &= X'_o \cos\delta_p + Z'_o \sin\delta_p \\ \rho_{o'z} &= -X'_o \sin\delta_p + Z'_o \cos\delta_p \quad . \end{aligned} \tag{38}$$

Then the vector becomes:

$$\vec{R}_{o'} = (\dot{U} + \ddot{\rho}_{o'x})\hat{I}_{xH} + \dot{V}\hat{I}_{yH} + (\dot{W} + \ddot{\rho}_{o'z})\hat{I}_{zH} + (U + 2\dot{\rho}_{o'x})\frac{d}{dt}(\hat{I}_{xH}) + V\frac{d}{dt}(\hat{I}_{yH}) + (W + 2\dot{\rho}_{o'z})\frac{d}{dt}(\hat{I}_{zH}) + \rho_{o'x}\frac{d^2}{dt^2}(\hat{I}_{xH}) + \rho_{o'z}\frac{d^2}{dt^2}(\hat{I}_{zH}) \quad . \tag{39}$$

Expanding yields,

$$\begin{aligned} \vec{R}_{o'x} &= \{-[(\dot{\delta}_p + q)^2 + r^2](X'_o \cos\delta_p + Z'_o \sin\delta_p) + (\ddot{\delta}_p + pr + \dot{q})(-X'_o \sin\delta_p + Z'_o \cos\delta_p) + \dot{U} + qW - rV\}\hat{I}_{xH} \\ \vec{R}_{o'y} &= [(2p\dot{\delta}_p + pq + \dot{r})(X'_o \cos\delta_p + Z'_o \sin\delta_p) + (2r\dot{\delta}_p + qr - \dot{p})(-X'_o \sin\delta_p + Z'_o \cos\delta_p) + \dot{V} + rU - pW]\hat{I}_{yH} \\ \vec{R}_{o'z} &= \{-(\ddot{\delta}_p - pr + \dot{q})(X'_o \cos\delta_p + Z'_o \sin\delta_p) - [(\dot{\delta}_p + q)^2 + p^2](-X'_o \sin\delta_p + Z'_o \cos\delta_p) + \dot{W} + pV - qU\}\hat{I}_{zH} \quad . \end{aligned} \tag{40}$$

Finally, since the mass involved is that of the forward trimmer alone, the moment equations become,

$$
\begin{aligned}
(\hat{\dot{M}}_o)_x = \{ & \Big[- p(\dot{\delta}_c + \dot{\delta}_p + q) I_{xx_c} + \dot{r} I_{zz_c} - m_c X''_{cg} [[- X'_o, (2r\dot{\delta}_p + qr - \dot{p}) \\
& + Z'_o, (2p\dot{\delta}_p + pq + \dot{r})] \sin \delta_p + [X'_o, (2p\dot{\delta}_p + pq + \dot{r}) + Z'_o, (2r\dot{\delta}_p \\
& + qr - \dot{p})] \cos \delta_p + \dot{V} + rU - pW] \Big] \sin (\delta_c + \delta_p) + [\dot{p} I_{xx_c} + r(\dot{\delta}_c \\
& + \dot{\delta}_p + q) I_{zz_c}] \cos(\delta_c + \delta_p) - r(\dot{\delta}_c + \dot{\delta}_p + q) I_{yy_c} \} \hat{\vec{I}}_{xH}
\end{aligned}
$$

$$
\begin{aligned}
(\hat{\dot{M}}_o)_y = \Big\{ & \Big[p^2 I_{xx_c} + r^2 I_{zz_c} + m_c X''_{cg} [[X'_o, (\ddot{\delta}_p + \dot{q} + pr) + Z'_o, [(\dot{\delta}_p \\
& + q)^2 + r^2]] \sin \delta_p + [X'_o, [(\dot{\delta}_p + q)^2 + r^2] - Z'_o, (\ddot{\delta}_p + \dot{q} \\
& + pr)] \cos \delta_p - \dot{U} + rV - qW \Big] \sin(\delta_c + \delta_p) + \Big[pr(I_{xx_c} - I_{zz_c}) \\
& + m_c X''_{cg} [[- X'_o, [(\dot{\delta}_p + q)^2 + p^2] + Z'_o, (\ddot{\delta}_p + \dot{q} - pr)] \sin \delta_p \\
& + [X'_o, (\ddot{\delta}_p + \dot{q} - pr) + Z'_o, [(\dot{\delta}_p + q)^2 + p^2]] \cos \delta_p + \dot{W} - qU \\
& + pV \Big] \cos (\delta_c + \delta_p) + (\ddot{\delta}_c + \ddot{\delta}_p + \dot{q}) I_{yy_c} \} \hat{\vec{I}}_{yH}
\end{aligned}
$$

$$
\begin{aligned}
(\hat{\dot{M}}_o)_z = \{ & [- \dot{p} I_{xx_c} - r(\dot{\delta}_c + \dot{\delta}_p + q) I_{zz_c}] \sin(\delta_c + \delta_p) + \Big[- p(\dot{\delta}_c + \dot{\delta}_p \\
& + q) I_{xx_c} + \dot{r} I_{zz_c} + m_c X''_{cg} [[- X'_o, (2r\dot{\delta}_p - \dot{p} + qr) + Z'_o, (2p\dot{\delta}_p \\
& + \dot{r} + pq)] \sin \delta_p + [X'_o, (2p\dot{\delta}_p + \dot{r} + pq) + Z'_o, (2r\dot{\delta}_p - \dot{p} \\
& + qr)] \cos \delta_p + \dot{V} + rU - pW] \Big] \cos(\delta_c + \delta_p) \\
& + p(\dot{\delta}_c + \dot{\delta}_p + q) I_{yy_c} \} \hat{\vec{I}}_{zH} \quad . \qquad (41)
\end{aligned}
$$

Wing/boom moment equations. The wing/boom moment equations are written most conveniently in the panel axis system (shown in figure 19), because in this system, the moments and products of inertia are constants. The moments are then transformed to the hinge axis system for later use.

An unusual feature of the panel axes is that the origin is displaced from the wing/boom center of gravity. Because of this, the more general form of the principle of the consdervation of moment of momentum must be used. This is:

$$\hat{M} = \dot{\hat{H}} + (\hat{\rho}) \times m(\ddot{\hat{R}}) \tag{42}$$

The components of the $\hat{H}$ vector are the inertial terms found in the conventional Euler equations for the rotation of a rigid body. These are not rederived here because they are developed in many texts. Their form is more general than that shown for the forward trimmer in equation (31) in that products of inertia are included.

The second term, caused by the offset center of gravity, requires the development outlined below.

In the wing panel axis system, the position vector to the wing/boom center of gravity, $\bar{\rho}$, is constant, and is given by

$$\hat{\rho}_{o\text{-}WBcg} = X'_{WB}\hat{i}_{X'} + Z'_{WB}\hat{i}_{Z'} \quad . \tag{43}$$

In the wing hinge system, this is

$$\hat{\rho}_{O\text{-}WBcg} = (X'_{WB} \cos \delta_p + Z''_{WB} \sin \delta_p)\hat{i}_{xH} + (-X'_{WB} \sin \delta_p + Z'_{WB} \cos\delta_p)\hat{i}_{zH} \; . \tag{44}$$

The angular momentum term will be, then, the time derivative of

$$\hat{H}_O = \left\{ \begin{bmatrix} I_{xxWB} & -I_{xyWB} & -I_{xzWB} \\ -I_{xyWB} & I_{yyWB} & -I_{yzWB} \\ -I_{xzWB} & -I_{yzWB} & I_{zzWB} \end{bmatrix} \begin{bmatrix} \omega_{xH} \\ \omega_{yH} \\ \omega_{zH} \end{bmatrix} \right\} \begin{bmatrix} \hat{i}_{xH} \\ \hat{i}_{yH} \\ \hat{i}_{zH} \end{bmatrix} .$$

Finally, the linear momentum can be found by noting that

$$\hat{R}_o = U\hat{i}_{xH} + V\hat{i}_{yH} + W\hat{i}_{zH} \quad . \tag{45}$$

$$\ddot{\vec{R}}_o = (\dot{U} + qW - rV)\vec{I}_{xH} + (\dot{V} + rU - pW)\vec{I}_{yH} + (\dot{W} + pV - qU)\vec{I}_{zH} \quad . \tag{46}$$

The moment equations can be written in their final forms by crossing $\vec{\rho}_{O\text{-}WBccg}$ into $\ddot{\vec{R}}_o$, multiplying by m_{WB}, and adding $\dot{\vec{H}}_o$ to obtain:

$$\begin{aligned}
(\vec{M}_o)_x &= [\dot{p}I_{xxWB} + (pr - \dot{q})I_{xyWB} - (pq + \dot{r})I_{xzWB} - qrI_{yyWB} + (r^2 - q^2)I_{yzWB} \\
&\quad + qrI_{zzWB} - m_{WB}(\dot{V} + rU - pW)(-X'_{WB} \sin\delta_p + Z'_{WB} \cos\delta_p)]\vec{I}_{xH} \\
(\vec{M}_o)_y &= [prI_{xxWB} - (qr + \dot{p})I_{xyWB} + (p^2 - r^2)I_{xzWB} + \dot{q}I_{yyWB} + (pq - \dot{r})I_{yzWB} \\
&\quad - prI_{zzWB} - m_{WB}[(\dot{W} + pV - qU)(X'_{WB} \cos\delta_p + Z'_{WB} \sin\delta_p) \\
&\quad + (\dot{U} + qW - rV)(-X'_{WB} \sin\delta_p + Z'_{WB} \cos\delta_p)]\ \vec{I}_{yH} \\
(\vec{M}_o)_z &= [-pqI_{xxWB} + (q^2 - p^2)I_{xyWB} + (qr - \dot{p})I_{xzWB} + pqI_{yyWB} \\
&\quad - (pr + \dot{q})I_{yzWB} + \dot{r}I_{zzWB} + m_{WB}(\dot{V} + rU - pW)(X'_{WB} \cos\delta_p \\
&\quad + Z'_{WB} \sin\delta_p)]\vec{I}_{zH} \quad .
\end{aligned} \tag{47}$$

Fuselage moment equations. Consider the fuselage as a weight suspended from a wing and connected to it by a single pin joint so that it is free to rotate about this point unless constrained by physical stops or aerodynamic forces on some auxiliary trimming surface attached to it. It should be apparent, then, that longitudinal motion will occur about this wing hinge axis for the fuselage as well as for the free wing/free trimmer combination. To describe the moments acting on the fuselage, it is again necessary to consider the general form of the equation for the conservation of angular momentum.

$$\vec{M}_F = \dot{\vec{H}} + (\vec{\rho}_F) \times m_F(\ddot{\vec{R}}_o) \quad . \tag{48}$$

Recall that there are three axis systems fixed at the intersection of the wing hinge line and the aircraft plane of symmetry: the wing panel axis system fixed in the wing, the wing hinge axis system mutually parallel to the

aircraft stability axis system, and the fuselage axis system with X_F positive forward and parallel to the fuselage reference line and Y_F positive right and coincident with the wing hinge line. Z_F is orthogonal to these two axes, positive downward. Both the fuselage center of gravity and the aircraft center of gravity are fixed points in the fuselage at any point in time and, hence, have fixed coordinates in the fuselage axis system. Assuming that the fuselage center of gravity lies in the aircraft plane of symmetry, the position vector from the wing hinge point to the fuselage center of gravity will be:

$$\vec{\rho}_F = X_{Fcg}\vec{1}_{xF} + Z_{Fcg}\vec{1}_{zF} \quad . \tag{49}$$

Since the linear velocity of the origin of the stability axis system is the velocity of the fuselage center of gravity,

$$\dot{\vec{R}}_o = U\vec{1}_X + V\vec{1}_Y + W\vec{1}_Z \quad . \tag{50}$$

However, the wing hinge axis system is parallel to the aircraft stability axis system, so

$$\dot{\vec{R}}_o = U\vec{1}_{xH} + V\vec{1}_{yH} + W\vec{1}_{zH} \quad , \tag{51}$$

and

$$\ddot{\vec{R}}_o = \dot{U}\vec{1}_{xH} + \dot{V}\vec{1}_{yH} + \dot{W}\vec{1}_{zH} + (\vec{\omega}_H) \times (\dot{\vec{R}}_o) \quad , \tag{52}$$

where

$$\vec{\omega}_H = p\vec{1}_{xH} + q\vec{1}_{yH} + r\vec{1}_{zH} \quad .$$

Then, the second term in equation (48) becomes:

$$\begin{aligned}(\vec{\rho}_F) \times m_F(\ddot{\vec{R}}_o) = &- m_F Z_{Fcg}(\dot{V} - pW + rU)\vec{1}_{xH} + m_f\,[Z_{fcg}\,(\dot{U} + qW - rV) \\ &- X_{fcg}\,(\dot{W} + pV - qU)]\vec{1}_{yH} + m_F X_{Fcg}(\dot{v} - pW + rU)\vec{1}_{zH} \quad .\end{aligned} \tag{53}$$

The remaining term on the right side of equation (48) is, as before, the inertial term found in the conventional Euler equations for the rotation of a rigid body.

The components of the applied fuselage moment defined by equation (48) become:

$$
\begin{aligned}
M_{xF} &= \dot{p}I_{xxF} + (pr - \dot{q})I_{xyF} - (pq + \dot{r})I_{xzF} + (r^2 - q^2)I_{yzF} \\
&\quad + qr(I_{zzF} - I_{yyF}) - m_F Z_{Fcg}(\dot{V} - pW + rU) \\
M_{yF} &= pr(I_{xxF} - I_{zzF}) - (qr + \dot{p})I_{xyF} + (p^2 - r^2)I_{xzF} + \dot{q}I_{yyF} \\
&\quad + (pq - \dot{r})I_{yzF} + m_F[-X_{Fcg}(\dot{W} + pV - qU) + Z_{Fcg}(\dot{U} + qW - rV)] \\
M_{zF} &= pq(I_{yyF} - I_{xxF}) + (q^2 - p^2)I_{xyF} + (qr - \dot{p})I_{xzF} \\
&\quad - (pr + \dot{q})I_{yzF} + \dot{r}I_{zzF} + m_F X_{Fcg}(\dot{V} - pW + rU)
\end{aligned}
\tag{54}
$$

The moments applied to the fuselage assembly, represented by the sides to the left in equations (54), contain contributions from the reversed effective forces and moments of the wing panels, booms, and trimmer. In actuality, they also contain gravity moments due to the weight of the fuselage, wing panels, booms, and trimmer.

Summation of Equations

Force equations. Summation of the force equations for the total aircraft will be simple and of the form:

$$
\begin{aligned}
F_{x,aero} + F_{x,thrust} - m_a g \sin\theta &= m_a(\dot{U} + qW - rV) \\
F_{y,aero} + F_{y,thrust} + m_a g \cos\theta \sin\phi &= m_a(\dot{V} + rU - pW) \\
F_{z,aero} + F_{z,thrust} + m_a g \cos\theta \cos\phi &= m_a(\dot{W} + pV - qU) \quad .
\end{aligned}
\tag{55}
$$

Moment equations. The moment equations will express that the sum of all externally applied moments, gravity moments, and moments generated by the

wing/boom/trimmer combinations on the fuselage must equal the fuselage inertial moments, or

$$\Sigma \hat{M}_{\substack{\text{applied to} \\ \text{fuselage}}} = \dot{\hat{H}}_F + (\hat{\omega}_F) \times m_F(\ddot{\hat{R}}_F) \quad . \tag{56}$$

Broken into components, the scalar equations are:

$$M_{x,aero} + M_{x,thrust} + M_{x,\substack{\text{fuselage} \\ \text{gravity}}} + M_{x,\substack{\text{wing/boom/trimmer} \\ \text{gravity}}}$$

$$+ M_{\substack{x,\text{due to reversed effective} \\ \text{moments at the hinge}}} + M_{\substack{x,\text{reversed effective forces} \\ \text{(inertial) at the hinge}}} \tag{57}$$

$$= \dot{p}I_{xxF} + (pr - \dot{q})I_{xyF} - (pq + \dot{r})I_{xzF} + (r^2 - q^2)I_{yzF}$$

$$+ qr(I_{zzF} - I_{yyF}) - m_a Z_{Fcg}(\dot{V} - pW + rU) \quad .$$

$$M_{y,aero} + M_{y,thrust} + M_{y,\substack{\text{fuselage} \\ \text{gravity}}} + M_{y,\substack{\text{wing/boom/trimmer} \\ \text{gravity}}}$$

$$+ M_{\substack{y,\text{reversed effective} \\ \text{moments at hinge}}} + M_{\substack{y,\text{reversed effective} \\ \text{forces at hinge}}} \tag{58}$$

$$= \dot{q}I_{yyF} + (pq - \dot{r})I_{yzF} - (qr + \dot{p})I_{xyF} + (p^2 - r^2)I_{xzF}$$

$$+ pr(I_{xxF} - I_{zzF}) - m_a [X_{Fcg}(\dot{W} + pV - qU) - Z_{Fcg}(\dot{U} + qW - rV)] \quad .$$

$$M_{z,aero} + M_{z,thrust} + M_{z,\substack{\text{fuselage} \\ \text{gravity}}} + M_{z,\substack{\text{wing/boom/trimmer} \\ \text{gravity}}}$$

$$+ M_{\substack{z,\text{reversed effective} \\ \text{moments at hinge}}} + M_{\substack{z,\text{reversed effective} \\ \text{forces at hinge}}} \tag{59}$$

$$= \dot{r}I_{zzF} + (qr - \dot{p})I_{xzF} - (pr + \dot{q})I_{yzF} + (q^2 - p^2)I_{xyF}$$

$$+ pq(I_{yyF} - I_{xxF}) + m_a X_{Fcg}(\dot{V} - pW + rU) \quad .$$

M_{aero} and M_{thrust} terms are dealt with in appendix B, and the gravity force terms appear below:

$$M_{x,\text{fuselage gravity}} = - Z_{Fcg} m_F g \cos\theta \sin\phi$$

$$M_{y,\text{fuselage gravity}} = - X_{Fcg} m_F g \cos\theta \cos\phi - Z_{Fcg} m_F g \sin\theta \qquad (60)$$

$$M_{z,\text{fuselage gravity}} = X_{Fcg} m_F g \cos\theta \sin\phi \; .$$

In deriving the reversed effective moment terms in equations (57) to (59), note that the y-components of these moments cannot be transmitted to the fuselage through the wing hinge, since by definition, the wing hinge is a frictionless pin joint. Practically speaking, friction forces would exist, but the calculation of their magnitude is beyond the scope of this work. The reversed effective moments at the hinge, then, will be:

$$M_{x,\text{reversed effective moments at hinge}} = - (M_{ox} + M_{o'x})$$

$$M_{z,\text{reversed effective moments at hinge}} = - (M_{oz} + M_{o'z}) \; . \qquad (61)$$

The total equation is:

$$\vec{M} = - (M_{ox} + M_{o'x})\vec{1}_{xH} + 0\vec{1}_{yH} - (M_{oz} + M_{o'z})\vec{1}_{zH} \; . \qquad (62)$$

Next, consider the moments due to reversed effective forces at the hinge. The inertial accelerations of the trimmer center of gravity and of the wing/boom center of gravity were expressed in the wing hinge coordinate system. The resulting reversed effective forces are, therefore, expressed in that system. These forces, in fact, act at the center of gravity of these two free bodies. It is possible to show how, with only one exception, they can be accounted for as acting at the hinge points of the trimmer and of the wing. Consider the explanation, by way of figure 21, as follows:

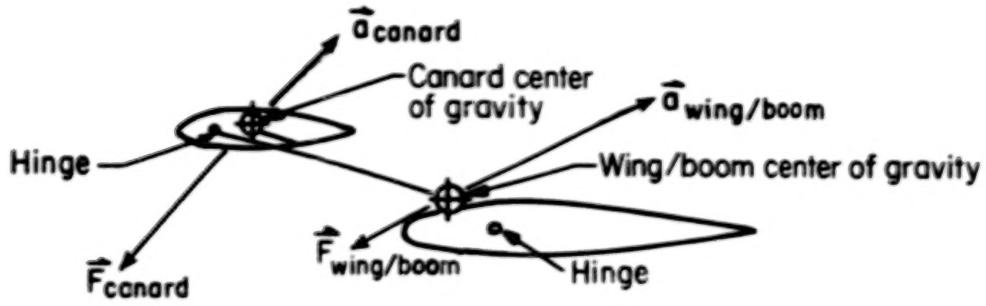

FIGURE 21. FORCES AND ACCELERATION VECTORS ACTING ON WING/BOOM/FORWARD TRIMMER ASSEMBLY

To the extent that these derivations have considered the "reversed effective moment" due to center of gravity offset in the moment-derivations $(\vec{\rho})$ x $m(\ddot{\vec{R}})$ about the hinge points, it would be redundant to consider it again. Therefore, both of the reversed effective forces can be shifted to their respective hinge points. For the wing/boom force, this is a complete step—the reaction is acting at the hinge and the moments resulting on the fuselage are calculable. For the trimmer force, the process is more involved. First, the force can indeed be viewed as acting at the trimmer hinge. Furthermore, it can then be shifted to the wing hinge as long as the gross moment due to this shift is also accounted for.

The process of getting the reactions at the wing hinge is, therefore, straightforward, except for this one moment. Note here that the y-components of this moment, as for the pure inertial moments, cannot be transmitted through to the fuselage.

In summary, the reversed effective force acting at the wing hinge is given by:

$$\vec{F}_{hinge} = -(F_{x,trimmer,H} + F_{xH})\vec{1}_{xH} - (F_{y,trimmer,H} + F_{yH})\vec{1}_{yH} - (F_{z,trimmer,H} + F_{zH})\vec{1}_{zH} \quad . \tag{63}$$

The reversed effective moments due to forces at the hinge, then, will be this force multiplied by its moment arm. In vector notation, this is:

$$\vec{M}_{\substack{\text{reversed effective}\\ \text{forces at hinge}}} = (\vec{\rho}) \times (\vec{F}_{\text{hinge}}) \quad , \tag{64}$$

where $\vec{\rho}$ is the position vector of the wing hinge axis with respect to the summation point—the wing/boom center of gravity:

$$\vec{\rho} = \bar{X}\hat{1}_{xH} + \bar{Z}\hat{1}_{zH} = 0 \quad . \tag{65}$$

Then, the moment due to reversed effective forces at the wing hinge becomes:

$$\begin{aligned}(\vec{\rho}) \times (\vec{F}_{\text{hinge}}) = {} & \bar{Z}(F_{y,\text{trimmer},H} + F_{yH})\vec{1}_{xH} + [\bar{X}(F_{z,\text{trimmer},H} + F_{zH}) \\ & - \bar{Z}(F_{x,\text{trimmer},H} + F_{xH})]\vec{1}_{yH} - \bar{X}(F_{y,\text{trimmer},H} \\ & + F_{yH})\vec{1}_{zH} = 0 \quad .\end{aligned} \tag{66}$$

The components of this yield partially the $M_{x,y,z}$ reversed effective forces for equations (57), (58), and (59). What is now necessary is the contribution from the cross-product of the position vector from the wing hinge to the trimmer hinge into the reversed effective force acting at the trimmer hinge. The force is just:

$$\begin{aligned}\vec{F}_{\substack{\text{trimmer hinge}\\ \text{reversed effective}\\ \text{force}}} = {} & - F_{x,\text{trimmer},H}\,\vec{1}_{xH} - F_{y,\text{trimmer},H}\,\vec{1}_{yH} \\ & - F_{z,\text{trimmer},H}\,\vec{1}_{zH} \quad .\end{aligned} \tag{67}$$

The necessary position vector is constant in the wing panel axis system, but it must be expressed in the wing hinge axis system. In the panel axis system, the vector is:

$$\vec{\rho}_{CH} = X'_{CH}\vec{1}_{x'} + Z'_{CH}\vec{1}_{z'} \quad . \tag{68}$$

The final form of these moments, due to the total reversed effective forces, is:

$$\hat{M}_{x,\text{reversed effective forces at hinge}} = [\bar{Z}(F_{y,\text{trimmer},H} + F_{yH}) + (Z'_{CH}\cos\delta_p - X'_{CH}\sin\delta_p)F_{y,\text{trimmer},H}]\hat{l}_{xH}$$

$$\hat{M}_{y,\text{reversed effective forces at hinge}} = [\bar{X}(F_{z,\text{trimmer},H} + F_{zH}) - \bar{Z}(F_{x,\text{trimmer},H} + F_{xH})]\hat{l}_{yH} \tag{69}$$

$$\hat{M}_{z,\text{reversed effective forces at hing}} = [-\bar{X}(F_{y,\text{trimmer},H} + F_{yH}) - (X'_{CH}\cos\delta_p + Z'_{CH}\sin\delta_p)F_{y,\text{trimmer},H}]\hat{l}_{zH} \ .$$

Last, the gravity moment must be calculated. The components of the gravity force are shown in equations (55). Defining a position vector from the wing hinge to the wing/boom/trimmer center of gravity as follows:

$$\hat{\rho}_{o\text{-}WBccg} = (\bar{X}_{WBccg}\cos\delta_p + \bar{Z}_{WBccg}\sin\delta_p)\hat{l}_{xH} + (-\bar{X}_{WBccg}\sin\delta_p + \bar{Z}_{WBccg}\cos\delta_p)\hat{l}_{zH} \ , \tag{70}$$

the moment due to gravity at the wing hinge is, with

$$\hat{W}_{WBC} = -m_{WBC}\,g\sin\theta\,\hat{l}_{zH} + m_{WBC}\,g\cos\theta\sin\phi\,\hat{l}_{yH} + m_{WBC}\,g\cos\theta\cos\phi\,\hat{l}_{zH}$$

$$(\hat{\rho}) \times (\hat{W}_{WBC}) = -(\bar{Z}_{WBC}\cos\delta_p - \bar{X}_{WBC}\sin\delta_p)m_{WBC}\,g\cos\theta\sin\phi\,\hat{l}_{xH} + (\text{non-transmittable y-terms}) + (\bar{X}_{WBC}\cos\delta_p + \bar{Z}_{WBC}\sin\delta_p)m_{WBC}\,g\cos\theta\sin\phi\,\hat{l}_{zH} \ . \tag{71}$$

Finally, all these parts may be summed to yield the total moments acting on the fuselage at the wing hinge due to inertial forces:

$$M_{x,aero} + M_{x,thrust} - [Z_{Fcg}m_F + (\bar{Z}_{WBC}\cos\delta_p - \bar{X}_{WBC}\sin\delta_p)m_{WBC}]g\cos\theta\sin\phi$$

$$- (M_{ox} + M_{o'x}) + [\bar{Z}(F_{y,trimmer,H} + F_{yH}) + (Z'_{CH}\cos\delta_p$$

$$- X'_{CH}\sin\delta_p)F_{y,trimmer,H}] = \dot{p}\,I_{xxF} + (pr - \dot{q})I_{xyF} - (pq + \dot{r})I_{xzF}$$

$$+ (r^2 - q^2)I_{yzF} + qr(I_{zzF} - I_{yyF}) - m_a Z_{Fcg}(\dot{V} - pW + rU) \quad .$$

$$M_{y,aero} + M_{y,thrust} - X_{Fcg}m_F g\cos\theta\cos\phi - Z_{Fcg}m_F g\sin\theta + [\bar{\bar{X}}(F_{z,trimmer,H}$$

$$+ F_{zH}) - \bar{\bar{Z}}(F_{x,trimmer,H} + F_{xH})] = \dot{q}I_{yyF} + (pq - \dot{r})I_{yzF} - (qr + \dot{p})I_{xyF} \qquad (72)$$

$$+ (p^2 - r^2)I_{xzF} + pr(I_{xxF} - I_{zzF}) - m_a\,[X_{Fcg}(\dot{W} + pV - qU) - Z_{Fcg}\,(\dot{U} + qW - rV)]$$

$$M_{z,aero} + M_{z,thrust} + [X_{Fcg}m_F + (\bar{\bar{X}}_{WBC}\cos\delta_p + \bar{\bar{Z}}_{WBC}\sin\delta_p)m_{WBC}]g\cos\theta\sin\phi$$

$$- (M_{oz} + M_{o'z}) + [-\bar{\bar{X}}(F_{y,trimmer,H} + F_{yH}) - (X'_{CH}\cos\delta_p - Z'_{CH}\sin\delta_p)$$

$$F_{y,trimmer,H}] = \dot{r}I_{zzF} + (qr - \dot{p})I_{xzF} - (pr + \dot{q})I_{yzF} + (q^2 - p^2)I_{xyF}$$

$$+ pq(I_{yyF} - I_{xxF}) + m_a X_{Fcg}\,(\dot{V} - pW + rU) \quad .$$

M_{ox}, M_{oy}, M_{oz} are given in their entirety in equations (47); $M_{o'x}$, $M_{o'y}$, $M_{o'z}$ are given in equations (41); trimmer forces are expressed in the wing hinge coordinate system in equations (21); and, finally, wing/boom force equations are given in the wing hinge system in equations (29).

APPENDIX B. DEVELOPMENT OF LINEARIZED LONGITUDINAL EQUATIONS OF MOTION

Introduction

The system is composed of three rigid bodies coupled together by geometric and kinematic constraints. The three bodies are the free trimmer panel, the wing/boom assembly, and the fuselage assembly.

Force and moment equations are developed for each free body in linearized form, with motion confined to the vertical plane. Although these individual equations implicitly contain the geometric and kinematic constraints, the forces transmitted through the trimmer hinge and the wing hinge are treated as separate, dependent variables. Furthermore, because of the complexity of the representation of unsteady aerodynamic forces, it is also convenient to treat the circulatory lift coefficients of the wing and trimmer surfaces as additional explicit variables.

As derived and employed in this study, the equations represent a departure from conventional analysis. Although the number of dependent equations could have been reduced, and all of the forces and moments could have been referred to the total aircraft center of gravity, as is customary, the physical significance and origins of the individual terms in the equations would have become obscure. In short, the individual equations are retained as they were derived to facilitate their verification — not a trivial consideration for such a complex system.

Coordinate Systems

Four coordinate systems were employed in the derivation of the linear longitudinal equations. These are identical to the systems used in the nonlinear derivation, but they are briefly described here for completeness.

Wing hinge axis system. The wing hinge axis system, x_h, y_h, z_h, is the primary axis system used to define the fuselage pitch angle, pitching rate, and translational velocity components of the total aircraft motion. The origin is at the intersection of the wing hinge axis and the plane of lateral symmetry of the aircraft. The x_h-axis is positive forward in the direction of flight, in the equilibrium condition. The y_h-axis is positive

toward the right wing. The z_h-axis completes the right-handed set, positive downward.

The wing hinge axes are fixed with respect to the fuselage assembly and rotate with the fuselage in pitch.

Wing panel axis system. In the wing panel axis system, x', y', z', the origin is coincident with the origin of the wing hinge axis system, but the panel axes are fixed to the wing and rotate in pitch with the wing panels. The x'-axis is parallel to a reference chord line in the wing and is positive toward the leading edge.

Trimmer hinge axis system. The trimmer hinge axis system, x_c, y_c, z_c, is parallel to the wing panel axis system, but the origin is at the intersection of the free-trimmer hinge axis and the plane of lateral symmetry.

Trimmer panel axis system. The trimmer panel axis system, x", y", z", is coincident with the origin of the trimmer hinge axis system, but is fixed in the free-trimmer surface and rotates in pitch with it. The x"-axis is parallel to a reference chord line in the trimmer and is positive toward the leading edge.

Symbols

a_{ccg}	acceleration of center of gravity of free trimmer, meters/second^2 (feet/second^2)
a_{Fcg}	acceleration of fuselage center of gravity, meters/second^2 (feet/second^2)
a_{WBcg}	acceleration of the center of gravity of wing boom assembly, meters/second^2 (feet/second^2)
$\bar{C}$	mean aerodynamic wing chord, meters (feet)
$\bar{C}_c$	mean free trimmer chord, meters (feet)
C_{D_F}	fuselage drag coefficient
$C_{D_{o_c}}$, $C_{D_{o_W}}$	profile drag coefficients of free trimmer and wing, respectively
C_{L_c}, C_{L_W}	lift coefficients of free trimmer and wing, respectively

$C_{L_{o_c}}$, $C_{L_{o_W}}$ — equilibrium lift coefficients of free trimmer and wing, respectively

$C_{L_{\alpha_c}}$, $C_{L_{\alpha_W}}$, $C_{L_{\alpha_F}}$ — lift-curve slopes per radian for free trimmer, wing, and fuselage, respectively, per radian

$C_{L_{\delta_t}}$ = $\partial C_L / \partial \delta_t$, per radian

C_m — pitching moment coefficient

$C_{m_{\alpha_F}}$ = $\partial C_m / \partial \alpha_F$, per radian

C_{m_ϵ} = $\partial C_m / \partial \epsilon$, per radian

C_{m_q} = $\partial C_m / \partial \left(\frac{q\bar{c}}{2U_o} \right)$, per radian

$C_{m_{\delta_t}}$ = $\partial C_m / \partial \delta_t$, per radian

$\frac{dC_D}{dC_L^2}$ — induced drag factor

E — ratio of wing semiperimeter to span

$F_{x_{c \to b}}$, $F_{z_{c \to b}}$ — components of force transmitted from free trimmer to wing boom, newtons (pounds)

$F_{x_{W \to F}}$, $F_{z_{W \to F}}$ — components of force transmitted from wing to fuselage newtons (pounds)

g — acceleration of gravity, meters/second^2 (feet/second^2)

G_{1_c}, G_{1_W} — transfer functions relating lift coefficient to angle of attack for free trimmer and wing, respectively

G_{2_c}, G_{2_W} — transfer functions relating lift coefficient to gust velocity for free trimmer and wing, respectively

I_{y_F} — pitching moment of inertia of fuselage assembly about wing hinge axis, kilogram-meters^2 (slug-feet^2)

I_y, — pitching moment of inertia of wing/boom assembly about wing hinge axis, kilogram-meters^2 (slug-feet^2)

I_y, — pitching moment of inertia of free trimmer about its hinge axis, kilogram-meters^2 (slug-feet^2)

ℓ_c — distance from quarter chord of wing to quarter chord of free trimmer, measured positive forward, meters (feet)

ℓ_t	distance from quarter chord of wing to quarter chord of fuselage mounted horizontal tail, measured positive rearward, meters (feet)
m_c, m_{WB}, m_F	mass of free trimmer, wing/boom assembly, and fuselage assembly, respectively, kilograms (slugs)
q	pitch rate of fuselage, radians/second
S	wing reference area, meters^2 (feet^2)
S_c	free trimmer reference area, meters^2 (feet^2)
U	true airspeed, meters/second (feet/second)
u	increment in airspeed divided by equilibrium airspeed
V_g	gust velocity, positive upward, meters/speed (feet/second)
W	component of velocity along z_h-axis, meters/second (feet/second)
X_{ac}	distance from leading edge to aerodynamic center of wing, meters (feet)
X_F	distance from wing hinge forward to fuselage center of gravity, meters (feet)
$\hat{X}_c$, $\hat{X}$	distance from hinge point to one-half chord point for free trimmer and wing, respectively, meters (feet)
X'_{CH}	x'-coordinate of trimmer hinge axis relative to wing hinge, meters (feet)
X'_{cg}	x'-coordinate of center of gravity of wing/boom, relative to wing hinge, meters (feet)
X''_{cg}	distance of free-trimmer center of gravity forward of hinge line, meters (feet)
Z_F	z_h-component of displacement of fuselage center of gravity with respect to wing hinge, meters (feet)
Z'_{CH}	z'-coordinate of trimmer hinge axis relative to wing hinge, meters (feet)
Z'_{cg}	z'-coordinate of center of gravity of wing/boom, relative to wing hinge, meters (feet)
α_c, α_F, α_W	angle of attack of free-trimmer, fuselage, and wing, respectively, radians
δ_c	displacement of free-trimmer with respect to wing, positive leading edge up, radians

δ_p	displacement of wing with respect to fuselage, positive leading edge up, radians
δ_t	displacement of control tab on free trimmer, positive trailing edge down, radians
ϵ	downwash angle, radians
θ	pitch angle of longitudinal fuselage axis with respect to horizon, radians
λ	Laplace operator, per second
ρ	atmospheric density, kilograms/meter^3 (slugs/foot^3)
$\rho_{x_{cg}}$, $\rho_{z_{cg}}$	coordinates of wing boom center of gravity in wing hinge axis system, meters
$\rho_{x_{H_c}}$, $\rho_{z_{H_c}}$	coordinates defined by equation (97)

Trimmer Free Body

The complete nonlinear expression for the acceleration of the center of gravity of the trimmer, expressed in the wing hinge axis system, is developed in appendix A. Eliminating the lateral-directional variables, the nonlinear expressions for the longitudinal acceleration are

$$\begin{aligned}(a_{ccg})_x = &-(\ddot{\delta}_c + \ddot{\delta}_p + \dot{q})[X''_{cg} \sin(\delta_c + \delta_p)] - [(\dot{\delta}_c + \dot{\delta}_p)^2 + 2q(\dot{\delta}_c + \dot{\delta}_p) + q^2] \\ &[X''_{cg} \cos(\delta_c + \delta_p)] + (\ddot{\delta}_p + \dot{q})(-X'_{CH} \sin\delta_p + Z'_{CH} \cos\delta_p) \\ &- [(q + \dot{\delta}_p)^2](X'_{CH} \cos\delta_p + Z'_{CH} \sin\delta_p) + \dot{U} + qW \\ (a_{ccg})_z = &[(\dot{\delta}_c + \dot{\delta}_p)^2 + 2q(\dot{\delta}_c + \dot{\delta}_p) + q^2][X''_{cg} \sin(\delta_c + \delta_p)] - \\ &(\ddot{\delta}_c + \ddot{\delta}_p + \dot{q})[X''_{cg} \cos(\delta_c + \delta_p)] - (q + \dot{\delta}_p)^2[-X'_{CH} \sin\delta_p \\ &+ Z'_{CH} \cos\delta_p] - (\ddot{\delta}_p + \dot{q})[X'_{CH} \cos\delta_p + Z'_{CH} \sin\delta_p] + \dot{W} - qU\end{aligned} \tag{73}$$

In the equilibrium state, all angular rates and accelerations are zero, as are all translational accelerations. Furthermore, the x-axis of the wing hinge system is aligned with the direction of motion.

Taking the differentials of equations (73), and denoting the equilibrium values of the variables by the subscript zero, the linearized form of the expressions for the acceleration of the trimmer center of gravity is:

TABLE OF CONTENTS

TABLE OF CONTENTS
(Continued)

TABLE OF CONTENTS
(Continued)

TABLE OF CONTENTS
(Continued)

LIST OF TABLES

LIST OF TABLES
(Continued)

LIST OF FIGURES

LIST OF FIGURES
(Continued)

LIST OF FIGURES
(Continued)

$$(a_{ccg})_x = \dot{U} + [Z'_{CH} \cos \delta_{p_o} - X'_{CH} \sin \delta_{p_o}](\dot{q} + \ddot{\delta}_p)$$
$$+ [-X''_{cg} \sin(\delta_{p_o} + \delta_{c_o})](\dot{q} + \ddot{\delta}_p + \ddot{\delta}_c)$$
$$(a_{ccg})_z = \dot{W} + [-U_o]q + [-Z'_{CH} \sin \delta_{p_o} - X'_{CH} \cos \delta_{p_o}] x \tag{74}$$
$$(\dot{q} + \ddot{\delta}_p) + [-X''_{cg} \cos (\delta_{p_o} + \delta_{c_o})](\dot{q} + \ddot{\delta}_p + \ddot{\delta}_c)$$

In equation (74) and in all subsequent linear equations, a variable without the zero subscript is understood to be a perturbation from the equilibrium value.

The forces acting on the trimmer surface to cause the acceleration defined by equation (74) are composed of aerodynamic forces, weight forces, and the force transmitted to the trimmer through its hinge.

The basic force equation for the trimmer is, then,

$$\vec{F}_{aero_c} + m_c \vec{g} + \vec{F}_{b \to c} = m_c \vec{a}_{ccg} \tag{75}$$

The circulation lift on the surface is based upon the angle of attack as defined at the one-half chord point by the velocity component normal to the surface.

In the trimmer panel axis system,

$$\tan \alpha_c = \frac{V_{z''}}{V_{x''}} \tag{76}$$

where $V_{z''}$ and $V_{x''}$ are the components of the inertial velocity at the one-half chord point.

Differentiating equation (76),

$$d(\tan \alpha_c) = \frac{1}{V_{x''_o}} [dV_{z''} - (\tan \alpha_o) dV_{x''}] \tag{77}$$

but

$$V_{x''_o} = U_o \cos (\delta_{p_o} + \delta_{c_o})$$
$$\tan \alpha_{c_o} = \frac{\sin (\delta_{p_o} + \delta_{c_o})}{\cos (\delta_{p_o} + \delta_{c_o})} \tag{78}$$

Substituting equation (78) into (77),

$$d(\tan \alpha_c) = \frac{dV_{z''} - \dfrac{\sin(\delta_{p_o} + \delta_{c_o})}{\cos(\delta_{p_o} + \delta_{c_o})}\, dV_{x''}}{U_o \cos(\delta_{p_o} + \delta_{c_o})} \tag{79}$$

The velocity components at the one-half chord point can be shown to be:

$$\begin{aligned} V_{x''} &= [U + (q + \dot{\delta}_p)(-X'_{CH} \sin \delta_p + Z'_{CH} \cos \delta_p)] \cos(\delta_p + \delta_c) \\ &\quad + [W - (q + \dot{\delta}_p)(X'_{CH} \cos \delta_p + Z'_{CH} \sin \delta_p)][-\sin(\delta_p + \delta_c)] \\ V_{z''} &= [U + (q + \dot{\delta}_p)(-X'_{CH} \sin \delta_p + Z'_{CH} \cos \delta_p)]\sin(\delta_p + \delta_c) \\ &\quad + [W - (q + \dot{\delta}_p)(X'_{CH} \cos \delta_p + Z'_{CH} \sin \delta_p)]\cos(\delta_p + \delta_c) \\ &\quad - \hat{X}_c(q + \dot{\delta}_p + \dot{\delta}_c) \end{aligned} \tag{80}$$

Taking differentials,

$$\begin{aligned} dV_{x''} &= -U_o \sin(\delta_{p_o} + \delta_{c_o})(\delta_p + \delta_c) + \cos(\delta_{p_o} + \delta_{c_o})[dU \\ &\quad + (-X'_{CH} \sin \delta_{p_o} + Z'_{CH} \cos \delta_{p_o})(q + \dot{\delta}_p)] - \sin(\delta_{p_o} + \delta_{c_o}) \times \\ &\quad [dW - (X'_{CH} \cos \delta_{p_o} + Z'_{CH} \sin \delta_{p_o})(q + \dot{\delta}_p)] \\ dV_{z''} &= U_o \cos(\delta_{p_o} + \delta_{c_o})(\delta_p + \delta_c) + \sin(\delta_{p_o} + \delta_{c_o})[dU \\ &\quad + (-X'_{CH} \sin \delta_{p_o} + Z'_{CH} \cos \delta_{p_o})(q + \dot{\delta}_p)] - \cos(\delta_{p_o} + \delta_{c_o}) \times \\ &\quad [dW - (X'_{CH} \cos \delta_{p_o} + Z'_{CH} \sin \delta_{p_o})(q + \dot{\delta}_p)] \\ &\quad - \hat{X}_c(q + \dot{\delta}_p + \dot{\delta}_c) \end{aligned} \tag{81}$$

Substituting equation (81) into (79), and recognizing that $\frac{dW}{U_o} = \alpha_F$, the angle of attack of the trimmer surface with respect to still air is

$$\alpha_c = \delta_p + \delta_c + \alpha_f - \left[\frac{X'_{CH} \cos \delta_{p_o} + Z'_{CH} \sin \delta_{p_o} + \hat{X}_c \cos(\delta_{p_o} + \delta_{c_o})}{U_o} \right] x$$

$$(q + \dot{\delta}_p) + \left[- \frac{\hat{X}_c}{U_o} \cos (\delta_{p_o} + \delta_{c_o}) \right] \dot{\delta}_c + \left[\frac{d\alpha_c}{dC_{L_W}} \right] C_{L_W} \qquad (82)$$

The last term in equation (82) is the induced angle of attack at the trimmer caused by the vortex system about the wing surface. It is evaluated using a vortex-lattice computer program for the particular wing-trimmer geometry being considered.

Note that no explicitly defined lag is included to allow for the induced velocity to propagate upstream (fwd trimmer) or downstream (aft trimmer) following a change in the bound vortex system on the wing. On the other hand, the C_{L_W} itself lags the change in angle of attack by a time constant dependent upon the ratio of wing chord to flight speed. Consequently, the induced angle of attack increment at the trimmer will lag any change in the wing angle of attack by the same time constant.

Equation (82) may be written

$$\alpha_c = \alpha_f + \delta_p + \delta_c + [C1]\dot{\delta}_p + [C2]q + [C3]\dot{\delta}_c + [C4]C_{L_W} \qquad (83)$$

where

$$C1 = C2 = - \frac{X'_{CH} \cos \delta_{p_o} + Z'_{CH} \sin \delta_{p_o} + \hat{X}_c \cos(\delta_{p_o} + \delta_{c_o})}{U_o}$$

$$C3 = - \frac{\hat{X}_c}{U_o} \cos(\delta_{p_o} + \delta_{c_o}) \qquad (84)$$

$$C4 = \frac{d\alpha_c}{dC_{L_W}}$$

In operational notation, where $q = \dot{\theta}$ and λ is the differential (LaPlace) operator,

$$[-1]\alpha_c + [1]\alpha_f + [1 + (C1)\lambda]\delta_p + [1 + (C3)\lambda]\delta_c + [(C2)\lambda]\theta + [C4]C_{L_W} = 0 \qquad (85)$$

Equation (85) is the first in the set of linear equations describing the total system. It represents the angle of attack increment of the free

trimmer caused by motion of the aircraft with respect to still air. The increment in angle of attack caused by a vertical gust is not included in equation (85) because the transient aerodynamic phenomena for gust penetration are different than for aircraft motion with respect to still air. For convenience, the vertical gust effects will be incorporated directly into the equation for trimmer lift coefficient.

The circulation lift on the trimmer surface arising from aircraft motion is based on the angle of attack of equation (85) plus an incremental camber caused by pitching and an effective increment caused by control tab deflection. The transient aerodynamic calculations and procedures are based on reference 5, and a discussion of the techniques as applied to the previous analyses is contained in appendix B of reference 1.

The circulatory lift caused by aircraft motion is

$$C_{L_{c_{mot.}}} = G_{1_c}(t)\left[\alpha_c + \frac{\bar{C}_c}{\pi U_o}\left(\dot{\delta}_p + q + \dot{\delta}_c\right) + \frac{C_{L_{\delta_t}}}{C_{L_{\alpha_c}}}\,\delta_t\right] \tag{86}$$

$G_{1_c}(t)$ is the lag function approximating the delay in the buildup of circulatory lift following a change in angle of attack. From reference 5, the lift function for an aspect ratio of 6, following a step change in angle of attack, is

$$C_{L_{circ.}} = C_{L_\alpha}\left[1 - 0.361e^{-0.598\frac{U_o}{\bar{C}}t}\right]\Delta\alpha \tag{87}$$

The corresponding transfer function relating lift coefficient to angle of attack is obtained by taking the LaPlace transform of the time derivative of equation (87) (ref. 6).

The desired transfer function is

$$G_{1_c}(\lambda) = \left[1 - \frac{0.361\lambda}{\lambda + 0.598\frac{U_o}{\bar{C}_c}}\right] C_{L_{\alpha_c}} \tag{88}$$

The circulation lift on the trimmer arising from a vertical gust is

$$C_{L_{c_{gust}}} = G_{2_c}(t)\frac{V_g}{U_o} \tag{89}$$

$G_{2_c}(t)$ is the function approximating the lag in circulatory lift build-up following the penetration of a vertical gust. Using the approximate indicial response function from reference 5, and following the procedure described above, the corresponding transfer function, in Laplace operator notation, is

$$G_{2_c}(\lambda) = C_{L_{\alpha_c}} \left[1 - \frac{0.488\lambda}{\lambda + 0.455\frac{U_o}{\bar{C}_c}} - \frac{0.272\lambda}{\lambda + 1.04\frac{U_o}{\bar{C}_c}} - \frac{0.193\lambda}{\lambda + 4.71\frac{U_o}{\bar{C}_c}}\right] \tag{90}$$

Since it is desirable to define the instantaneous gust velocity at the main lifting surface, the difference in gust velocity between the trimmer and the wing will be approximated by

$$\frac{V_{g_c}}{U_o} = \frac{V_g}{U_o} + \frac{\dot{V}_g}{U_o}\frac{\ell_c}{U_o} \tag{91}$$

Combining the various contributions the circulatory lift coefficient of the trimmer is

$$C_{L_c} = G_{1_c}(t)\left[\alpha_c + \frac{\bar{C}_c}{\pi U_o}(\dot{\delta}_p + q + \dot{\delta}_c) + \frac{C_{L_{\delta_t}}}{C_{L_{\alpha_c}}}\delta_t\right] + G_{2_c}(t)\left[\frac{V_g}{U_o} + \frac{\dot{V}_g}{U_o}\frac{\ell_c}{U_o}\right] \tag{92}$$

Letting

$$C5 = \frac{\bar{C}_c}{\pi U_o}$$

$$C6 = \frac{C_{L_{\delta_t}}}{C_{L_{\alpha_c}}} \tag{93}$$

and multiplying by the denominator of equation (88), the final expression, in operational form is:

$$
\begin{aligned}
&[-(\lambda + 0.598\frac{U_o}{\bar{c}_c})]C_{L_c} + [0.639C_{L_{\alpha_c}}\lambda + 0.598\frac{U_o}{\bar{c}_c}C_{L_{\alpha_c}}]\alpha_c \\
&+ [C_{L_{\alpha_c}}(C5)(0.639\lambda^2 + 0.598\frac{U_o}{\bar{c}_c})]\delta_p + [C_{L_{\alpha_c}}(C5)(0.639\lambda^2 \\
&+ 0.598\frac{U_o}{\bar{c}_c}\lambda)]\theta + [C_{L_{\alpha_c}}(C5)(0.639\lambda^2 + 0.598\frac{U_o}{\bar{c}_c}\lambda)]\delta_c \\
&= -[C_{L_{\alpha_c}}(C6)(0.639\lambda + 0.598\frac{U_o}{\bar{c}_c})]\delta_t - [C_{2_c}(\lambda + 0.598\frac{U_o}{\bar{c}_c})(\frac{\ell_g}{U_o}\lambda + 1)]\frac{V_g}{U_o}
\end{aligned}
\tag{94}
$$

Equation (94) is the second in the set of linearized equations describing the complete system.

The inertial pitching moment about the trimmer hinge axis can be obtained from equation (41) of appendix A. Ignoring the lateral-directional variables, the nonlinear expression for the pitching motion of the trimmer is

$$
\begin{aligned}
M_{y_{c_{aero}}} &= I_{y_c}(\ddot{\delta}_c + \ddot{\delta}_p + \dot{q}) + m_c X''_{cg}\{[X'_{CH}(\ddot{\delta}_p + \dot{q}) + Z'_{CH}(\dot{\delta}_p + q)^2]\sin\delta_p \\
&+ [X'_{CH}(\dot{\delta}_p + q)^2 - Z'_{CH}(\ddot{\delta}_p + \dot{q})]\cos\delta_p - \dot{U} - qW\}\sin(\delta_p + \delta_c) \\
&+ m_c X''_{cg}\{[-X'_{CH}(\dot{\delta}_p + q)^2 + Z'_{CH}(\ddot{\delta}_p + \dot{q})]\sin\delta_p + [X'_{CH}(\ddot{\delta}_p + \dot{q}) \\
&+ Z'_{CH}(\dot{\delta}_p + q)^2]\cos\delta_p - \dot{W} + qU\}\cos(\delta_p + \delta_c)
\end{aligned}
\tag{95}
$$

In linearized form, the fundamental trimmer pitching equation is, therefore

$$
\begin{aligned}
M_{y_{c_{aero}}} &= [I_{y_c}]\ddot{\delta}_c + [I_{y_c} + m_c\rho_{z_{H_c}}(Z'_{CH}\cos\delta_{p_o} - X'_{CH}\sin\delta_{p_o}) \\
&+ m_c\rho_{z_{H_c}}(Z'_{CH}\sin\delta_{p_o} + X'_{CH}\cos\delta_{p_o})]\ddot{\delta}_p + [I_{y_c} \\
&+ m_c\rho_{z_{H_c}}(Z'_{CH}\cos\delta_{p_o} - X'_{CH}\sin\delta_{p_o}) + m_c\rho_{x_{H_c}}(Z'_{CH}\sin\delta_{p_o} \\
&+ X'_{CH}\cos\delta_{p_o})]\dot{q} + [m_c\rho_{x_{H_c}}U_o]q + [m_c\rho_{z_{H_c}}U_o]\dot{U} + [-m_c\rho_{x_{H_c}}U_o]\dot{\alpha}_F
\end{aligned}
\tag{96}
$$

where

$$\rho_{x_{H_c}} = \ddot{X}''_{cg} \cos(\delta_{p_o} + \delta_{c_o})$$

$$\rho_{z_{H_c}} = -\ddot{X}''_{cg} \sin(\delta_{p_o} + \delta_{c_o}) \tag{97}$$

Aside from the circulatory lift of equation (94), a lift force arises from the apparent mass of air accelerated by the trimmer motion. This lift force, according to reference 5 , is

$$L_{m_c} = \frac{\rho U_o S_c \bar{C}_c}{E} \dot{\alpha}_c \tag{98}$$

Differentiating equation (83),

$$\dot{\alpha}_c = \dot{\alpha}_F + \dot{\delta}_p + \dot{\delta}_c + (C1)\ddot{\delta}_p + (C2)\dot{q} + (C3)\ddot{\delta}_c + (C4)\dot{C}_{L_W} \tag{99}$$

To compute the pitching moment acting on the trimmer, the apparent-mass lift is segregated into components arising from plunging acceleration (acting at the one-half chord point) and from pure rotation (acting at the three-quarter chord point).

Accordingly, the lift acting at the one-half chord point is

$$L_{m_{1/2}} = \frac{\rho U_o S_c \bar{C}_c}{E} (\dot{\alpha}_c - \dot{\delta}_p - \dot{\delta}_c) \tag{100}$$

and the lift acting at the three-quarter chord point is

$$L_{m_{3/4}} = \frac{\rho U_o S_c \bar{C}_c}{E} (\dot{\delta}_p + \dot{\delta}_c) \tag{101}$$

The forces acting on the free surface are shown in figure 22.

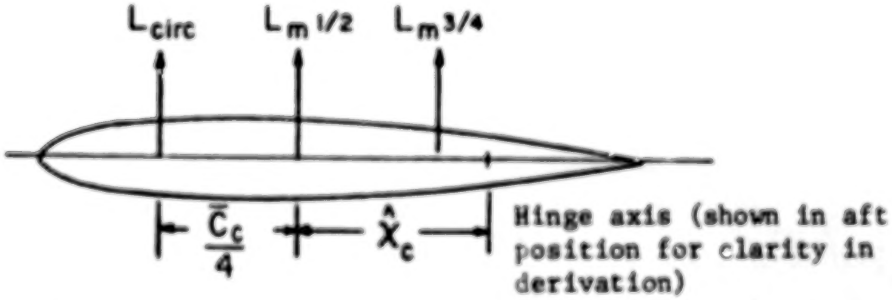

FIGURE 22. AERODYNAMIC FORCES ACTING ON FREE SURFACES

From the figure, the increment in aerodynamic pitching moment is:

$$M_{y_{c_{aero}}} = M_{\delta_t}\delta_t + L_{circ}(\hat{X}_c + \frac{\bar{C}_c}{4}) + L_{m_{1/2}}\hat{X}_c + L_{m_{3/4}}(\hat{X}_c - \frac{\bar{C}_c}{4}) \qquad (102)$$

or

$$M_{y_{c_{aero}}} = [C_{m_{\delta_t}}\frac{\rho U_o^2}{2}S_c\bar{C}_c]\delta_t + [\frac{\rho U_o^2}{2}S_c(\hat{X}_c + \frac{\bar{C}_c}{4})]C_{L_c}$$

$$+ [\frac{\rho U_o S_c \bar{C}_c}{E}\hat{X}_c](\dot{\alpha}_c - \dot{\delta}_p - \dot{\delta}_c) + [\frac{\rho U_o S_c \bar{C}_c}{E}(\hat{X}_c \qquad (103)$$

$$- \frac{\bar{C}_c}{4})](\dot{\delta}_p + \dot{\delta}_c)$$

Equations (103) and (96) can be combined. Combining terms and converting to operational notation, the trimmer pitching moment equation is:

$$[(C22)\lambda^2 + (C30 - C31)\lambda]\delta_c + [-(C30)\lambda]\alpha_c + [-C29]C_{L_c}$$

$$+ [(C27)\lambda]\alpha_F + [(C23)\lambda^2 + (C30 - C31)\lambda]\delta_p + [(C24)\lambda^2 \qquad (104)$$

$$+ (C25)\lambda]\theta + [(C26)\lambda]u = +[C28]\delta_t$$

where

$$C22 = I_{y''}$$

$$C23 = I_{y''} + m_c\rho_{z_{H_c}}(Z'_{CH}\cos\delta_{p_o} - X'_{CH}\sin\delta_{p_o})$$

$$+ m_c\rho_{x_{H_c}}(Z'_{CH}\sin\delta_{p_o} + X'_{CH}\cos\delta_{p_o})$$

$$C24 = C23$$

$$C25 = m_c\rho_{x_{H_c}}U_o$$

$$C26 = m_c\rho_{z_{H_c}}U_o \qquad (105)$$

$$C27 = -C25$$

$$C28 = C_{m_{\delta_t}}\,1/2\,\rho U_o^2 S_c\bar{C}_c$$

$$C29 = 1/2\ \rho U_o^2 S_c (\hat{X} + \frac{\bar{C}_c}{4})$$

$$C30 = \frac{\rho U_o S_c \bar{C}_c}{E} \hat{X}_c$$

$$C31 = \frac{\rho U_o S_c \bar{C}_c}{E} (\hat{X}_c - \frac{\bar{C}_c}{4})$$

Equation (104) is the third equation in the set describing the complete system.

The physical coupling between the free-trimmer and the wing is implicitly incorporated into equations (85), (94), and (104), but to depict the effect of the trimmer on the wing/boom assembly, the force acting at the trimmer hinge must be evaluated.

From equation (75), the force transmitted from the trimmer to the boom ($F_{c\to b}$) can be calculated, since

$$\vec{F}_{c\to b} = -\vec{F}_{b\to c} = \Delta\vec{F}_{aero_c} + \Delta m_c \vec{g} - m_c \vec{a}_c \tag{106}$$

If the aerodynamic force is computed in the wing hinge axis system, the trimmer lift force can be defined as acting solely in the $-z_h$ direction and the drag force as acting solely in the $-x_h$ direction.

Since we are dealing with perturbations from the nominal values in the linearized equations,

$$\Delta\vec{F}_{aero_c} = -\Delta L_c \vec{l}_{z_H} - \Delta D_c \vec{l}_{x_H} \tag{107}$$

The weight force, expressed in the wing hinge axis system, is

$$m_c \vec{g} = [-m_c g \sin\theta]\vec{l}_{x_H} + [m_c g \cos\theta]\vec{l}_{z_H} \tag{108}$$

So, in linearized form,

$$\Delta(m_c \vec{g}) = [-m_c g\theta]\vec{l}_{x_H} \tag{109}$$

From equations (109), (107), and (106), the x-component of the force transmitted from the trimmer to the boom is

$$F_{x_{c\to b}} = -\Delta D_c - m_c g\theta - m_c (a_{ccg})_x \tag{110}$$

The drag of the surface is

$$D_c = [C_{D_{o_c}} + \frac{dC_D}{dC_L^2} C_{L_c}^2]1/2\ \rho U_o^2 S_c \tag{111}$$

Taking differentials, the linearized form is

$$\Delta D_c = [(C_{D_{o_c}} + \frac{dC_D}{dC_L^2} C_{L_{o_c}}^2)\rho U_o^2 S_c]u + [\frac{dC_D}{dC_L^2} C_{L_{o_c}} \rho U_o^2 S_c]C_{L_c} \tag{112}$$

Incorporating equations (112) and (74) into equation (110),

$$F_{x_{c\to b}} = [C7]\dot{u} + [C9](\dot{q} + \ddot{\delta}_p) + [C10](\dot{q} + \ddot{\delta}_p + \ddot{\delta}_c) + [C11]u + [C12]C_{L_c} + [C13]\theta \tag{113}$$

where

$$\begin{aligned} C7 &= -m_c U_o \\ C9 &= -m_c (Z'_{CH} \cos \delta_{p_o} - X'_{CH} \sin \delta_{p_o}) \\ C10 &= -m_c [-X''_{cg} \sin(\delta_{p_o} + \delta_{c_o}) + Z''_{cg} \cos(\delta_{p_o} + \delta_{c_o})] \\ C11 &= -[C_{D_{o_c}} + \frac{dC_D}{dC_L^2} C_{L_{o_c}}^2]\rho U_o^2 S_c \\ C12 &= -\frac{dC_D}{dC_L^2} C_{L_{o_c}} \rho U_o^2 S_c \\ C13 &= -m_c g \end{aligned} \tag{114}$$

Finally, in operational notation, the x-component of the force transmitted from the trimmer to the boom is

$$[-1]F_{x_{c\to b}} + [C12]C_{L_c} + [(C9 + C10)\lambda^2]\delta_p + [C13 + (C9 + C10)\lambda^2]\theta + [(C10)\lambda^2]\delta_c + [C11 + (C7)\lambda]u = 0 \tag{115}$$

Equation (115) is the fourth of the set of equations describing the total system.

Similarly, the z_h component of the hinge force is

$$F_{z_{c\to b}} = -\Delta L_c - m_c (a_{ccg})_z \tag{116}$$

The increment of lift has contributions from the circulation lift (equation (92)), the apparent-mass lift (equation (98)), and airspeed changes:

$$\Delta L_c = C_{L_c}[1/2\ \rho U_o^2 S_c] + \frac{\rho U_o S_c \bar{C}_c}{E}\dot{\alpha}_c + [C_{L_{o_c}}\ \rho U_o^2 S_c]u \tag{117}$$

Substituting equations (117) and (74) into equation (116),

$$F_{z_{c\to b}} = [C14]\dot{\alpha}_F + [C15]q + [C17](\dot{q} + \ddot{\delta}_p) + [C18](\dot{q} + \ddot{\delta}_p + \ddot{\delta}_c) + [C19]C_{L_c} + [C20]\dot{\alpha}_c + [C21]u \tag{118}$$

where

$$\begin{aligned} C14 &= -m_c U_o \\ C15 &= -C14 \\ C17 &= m_c(Z'_{CH} \sin \delta_{p_o} + X'_{CH} \cos \delta_{p_o}) \\ C18 &= m_c[X''_{cg} \cos(\delta_{p_o} + \delta_{c_o})] \\ C19 &= -1/2\ \rho U_o^2 S_c \\ C20 &= -\frac{\rho U_o^2 S_c \bar{C}_c}{E} \\ C21 &= -C_{L_{o_c}}\ \rho U_o^2 S_c \end{aligned} \tag{119}$$

or, in operational notation,

$$\begin{aligned} &[-1]F_{z_{c\to b}} + [(C14)\lambda]\alpha_F + [(C15)\lambda + (C17 + C18)\lambda^2]\theta \\ &+ [(C17 + C18)\lambda^2]\delta_p + [(C18)\lambda^2]\delta_c + [C19]C_{L_c} \\ &+ [(C20)\lambda]\alpha_c + [C21]u = 0 \end{aligned} \tag{120}$$

Equation (120) is the fifth in the set of linear equations describing the total system.

Wing/Boom Assembly Free Body

The nonlinear expressions for the acceleration of the center of gravity of the wing/boom assembly are obtained by eliminating the lateral-

directional variables from equation (28) in appendix A.

$$(a_{WB_{cg}})_x = \dot{U} + qW - (q + \dot{\delta}_p)^2(X'_{cg} \cos \delta_p + Z'_{cg} \sin \delta_p) + (\ddot{\delta}_p + \dot{q})(-X'_{cg} \sin \delta_p + Z'_{cg} \cos \delta_p) \tag{121a}$$

$$(a_{WB_{cg}})_z = \dot{W} - qU - (q + \dot{\delta}_p)^2(-X'_{cg} \sin \delta_p + Z'_{cg} \cos \delta_p) - (\ddot{\delta}_p + \dot{q})(X'_{cg} \cos \delta_p + Z'_{cg} \sin \delta_p) \tag{121b}$$

In linearized form, these expressions become

$$(a_{WB_{cg}})_x = \dot{U} + [-X'_{cg} \sin \delta_{p_o} + Z'_{cg} \cos \delta_{p_o}](\dot{q} + \ddot{\delta}_p)$$

$$(a_{WB_{cg}})_z = \dot{W} + [-U_o]q + [-X'_{cg} \cos \delta_{p_o} - Z'_{cg} \sin \delta_{p_o}](\dot{q} + \ddot{\delta}_p) \tag{122}$$

Considering the wing/boom assembly as a free body, the motion is governed by the aerodynamic lift and drag forces, the force transmitted from the free trimmer to the boom through the trimmer hinge, the force transmitted from the fuselage to the wing through the wing hinge, and the force of gravity. Thus,

$$\vec{F}_{aero_{WB}} + \vec{F}_{c\to b} + \vec{F}_{F\to W} + m_{WB}\vec{g} = m_{WB}\vec{a}_{WB_{cg}} \tag{123}$$

The aerodynamic force on the wing/boom assembly can be represented as

$$\vec{F}_{aero_{WB}} = -\Delta D_{WB}\vec{i}_{x_H} - \Delta L_{WB}\vec{i}_{z_H} \tag{124}$$

By analogy to equation (112),

$$\Delta D_{WB} = [(C_{D_{\alpha_W}} + \frac{dC_D}{dC_{L_W}^2} C_{L_{\alpha_W}}^2)\rho U_o^2 S]u + [\frac{dC_D}{dC_{L_W}^2} C_{L_{\alpha_W}} \rho U_o^2 S]C_{L_W} \tag{125}$$

By analogy to equation (82), the geometrical angle of attack of the wing, in linearized form, based upon the normal velocity at the one-half chord point, is

$$\alpha_W = \alpha_F + \delta_p + [-\frac{\hat{X}}{U_o} \cos \delta_{p_o}](q + \dot{\delta}_p) + (\frac{d\alpha_W}{dC_{L_c}})C_{L_c} \tag{126}$$

The last term in equation (126) is the induced effective angle of attack increment caused by the vortex system on the free trimmer system.

Equation (126) will be written as

$$\alpha_W = \alpha_F + \delta_p + [C33](q + \dot{\delta}_p) + [C34]C_{L_c} \tag{127}$$

where

$$C33 = -\frac{\hat{X}}{U_o}\cos \delta_{p_o} \tag{128}$$

$$C34 = \frac{d\alpha_W}{dC_{L_c}}$$

So, in operational notation,

$$[1]\alpha_W + [1]\alpha_F + [1 + (C33)\lambda]\delta_p + [(C33)\lambda]\theta + [C34]C_{L_c} = 0 \tag{129}$$

Equation (129) is the sixth in the set of linearized equations representing the system.

As with the trimmer surface, the circulatory lift coefficient of the wing has contributions from the motion of the airplane and from the vertical gust velocity.

$$C_{L_W} = G_{1_W}(t)[\alpha_W + (C36)(q + \dot{\delta}_p)] + G_{2_W}(t)\frac{V_g}{U_o} \tag{130}$$

where

$$C36 = \frac{\bar{C}}{\pi U_o} \tag{131}$$

In operational notation,

$$G_1 = C_{L_{\alpha_W}}\left[\frac{0.639\lambda + 0.598\frac{U_o}{\bar{C}}}{\lambda + 0.598\frac{U_o}{\bar{C}}}\right] \tag{132}$$

$$G_2 = C_{L_{\alpha_W}}\left[1 - \frac{0.488\lambda}{\lambda + 0.455\frac{U_o}{\bar{C}}} - \frac{0.272\lambda}{\lambda + 1.04\frac{U_o}{\bar{C}}} - \frac{0.193\lambda}{\lambda + 4.71\frac{U_o}{\bar{C}}}\right] \tag{133}$$

Equations (132) and (133) are the operational equivalents of the indicial response function given in reference 5 for a wing of aspect ratio 6.

For computer mechanization of the homogeneous equations, it is desirable to eliminate the denominators of the coefficients. This is done by multiplying equation (130) by the denominator of equation (132).

The final expression for the wing lift coefficient is

$$-[\lambda + 0.598\frac{U_o}{\bar{C}}]C_{L_W} + [C_{L_{\alpha_W}}(0.639\lambda + 0.598\frac{U_o}{\bar{C}})]\alpha_W$$

$$+ [(C36)C_{L_{\alpha_W}}\lambda(0.639\lambda + 0.598\frac{U_o}{\bar{C}})]\delta_p + [(C36)C_{L_{\alpha_W}}\lambda(0.639\lambda \qquad (134)$$

$$+ 0.598\frac{U_o}{\bar{C}})]\theta = [-(\lambda + 0.598\frac{U_o}{\bar{C}})G_{2_W}]\frac{V_g}{U_o}$$

Equation (134) is the seventh in the set of linear equations describing the system.

The total wing lift force is made up of the circulatory lift defined by the lift coefficient of equation (134), and the lift due to the acceleration of the apparent mass of air surrounding the wing. The apparent mass lift is

$$L_{W_m} = \frac{\rho U_o S\bar{C}}{E}\dot{\alpha}_W = \underbrace{\frac{\rho U_o S\bar{C}}{E}(\dot{\alpha}_W - \dot{\delta}_p)}_{\text{Acts at 1/2 chord}} + \underbrace{\frac{\rho U_o S\bar{C}}{E}\dot{\delta}_p}_{\text{Acts at 3/4 chord}} \qquad (135)$$

In linear form, the increment of lift on the wing is

$$\Delta L_W = [1/2\ \rho U_o^2 S]C_{L_W} + [\frac{\rho U_o S\bar{C}}{E}]\dot{\alpha}_W + [C_{L_{\alpha_W}}\rho U_o^2 S]u \qquad (136)$$

Equations (136), (125), (115), (120), and (122) can be substituted into equation (123) to obtain explicit equations for the components of the force transmitted from the wing to the fuselage through the wing hinge. In operational notation, these are:

$$[-1]F_{x_{W\to F}} + [C38 + (C40)\lambda]u + [C39]C_{L_W} + [1]F_{x_{c\to b}}$$

$$+ [C43 + (C42)\lambda^2]\theta + [(C42)\lambda^2]\delta_p = 0 \qquad (137)$$

$$[-1]F_{z_{W\to F}} + [C44]C_{L_W} + [(C45)\lambda]\alpha_W + [C46]u$$

$$+ [1]F_{z_{c\to b}} + [(C47)\lambda]\alpha_F + [(-C47)\lambda + (C49)\lambda^2]\theta \qquad (138)$$

$$+ [(C49)\lambda^2]\delta_p = 0$$

where

$$C38 = -\left(C_{D_{o_W}} + \frac{dC_D}{dC_{L_W}^2} C_{L_{o_W}}^2\right)\rho U_o^2 S$$

$$C39 = -\frac{dC_D}{dC_{L_W}^2} C_{L_{o_W}} \rho U_o^2 S$$

$$C40 = -m_{WB} U_o$$

$$C42 = -m_{WB}(-X'_{cg} \sin \delta_{p_o} + Z'_{cg} \cos \delta_{p_o})$$

$$C43 = -m_{WB} g \tag{139}$$

$$C44 = -\ 1/2\ \rho U_o^2 S$$

$$C45 = -\frac{\rho U_o S\bar{C}}{E}$$

$$C46 = -C_{L_{o_W}} \rho U_o^2 S$$

$$C47 = C40$$

$$C49 = m_{WB}(X'_{cg} \cos \delta_{p_o} + Z'_{cg} \sin \delta_{p_o})$$

Equations (137) and (138) are the eighth and ninth equations in the linear set describing the system.

The pitching moment about the wing hinge caused by the force applied to the boom by the free trimmer is the cross-product of the vector from the wing hinge to the trimmer hinge and the applied force. The magnitude is

$$M_{F_c} = (-X'_{CH} \sin \delta_{p_o} + Z'_{CH} \cos \delta_{p_o}) F_{x_{c\to b}} - (X'_{CH} \cos \delta_{p_o} + Z'_{CH} \sin \delta_{p_o}) F_{z_{c\to b}} \tag{140}$$

For small displacements, the increment in pitching moment about the hinge axis due to gravity is

$$M_{weight} = [-m_{WB} g Z'_{cg}](\theta + \delta_p) \tag{141}$$

By analogy to equation (103), but allowing for the fact that the wing boom aerodynamic center may not be at the quarter-chord point, the aerodynamic moment on the wing is

$$M_{y_{aero}} = [1/2\ \rho U_o^2 S(\hat{X} + \frac{\bar{C}}{2} - \frac{X_{ac}}{\bar{C}}\bar{C})]C_{L_W} + [\frac{\rho U_o S\bar{C}}{E}\hat{X}](\dot{\alpha}_W - \dot{\delta}_p) + [\frac{\rho U_o S\bar{C}}{E}(\hat{X} - \frac{\bar{C}}{4})]\dot{\delta}_p \tag{142}$$

The inertial pitching moment on the wing boom assembly is obtained from equation (47) in appendix A by eliminating the lateral-directional terms:

$$M_{y_{inertial}} = I_y'(\ddot{\delta}_p + \dot{q}) - m_{WB}[(\dot{W} - qU)(X'_{cg}\cos\delta_p + Z'_{cg}\sin\delta_p) - (\dot{U} + qW)(-X'_{cg}\sin\delta_p + Z'_{cg}\cos\delta_p)] \tag{143}$$

In linearized form, this becomes:

$$M_{y_{inertial}} = I_y'\ddot{\delta}_p + I_y'\dot{q} + [m_{WB}\rho_{x_{cg}}U_o]q + [m_{WB}\rho_{z_{cg}}U_o]\dot{u} - [m_{WB}\rho_{x_{cg}}U_o]\dot{\alpha}_F \tag{144}$$

where

$$\rho_{x_{cg}} = X'_{cg}\cos\delta_{p_o} + Z'_{cg}\sin\delta_{p_o}$$
$$\rho_{z_{cg}} = -X'_{cg}\sin\delta_{p_o} + Z'_{cg}\cos\delta_{p_o} \tag{145}$$

Combining equations (140), (141), (142), and (143), the pitching moment equation for the wing boom assembly is, in operational form:

$$[C51 + (C56 - C59)\lambda + (C50)\lambda^2]\delta_p + [C51 + (C52)\lambda + (C56)\lambda^2]\theta + [(C53)\lambda]u + [C54]C_{L_W} + [-(C52)\lambda]\alpha_F + [(C55)\lambda]\alpha_W + [C57]F_{x_{c\to b}} + [C58]F_{z_{c\to b}} = 0 \tag{146}$$

Equation (146) is the tenth in the series of linear equations where

$$C50 = I_y'$$
$$C51 = m_{WB}gZ'_{cg} \tag{147a}$$
$$C52 = m_{WB}\rho_{x_{cg}}U_o$$

$$C53 = m_{WB} \rho_{z_{cg}} U_o$$

$$C54 = -1/2\ \rho U_o^2 S(\hat{X} + \frac{\bar{C}}{2} - \frac{X_{ac}}{\bar{C}} \bar{C})$$

$$C55 = -\frac{\rho U_o S\bar{C}}{E} \dot{X} \tag{147b}$$

$$C56 = -\frac{\rho U_o S\bar{C}}{E} (\hat{X} - \frac{\bar{C}}{4})$$

$$C57 = X'_{CH} \sin \delta_{p_o} - Z'_{CH} \cos \delta_{p_o}$$

$$C58 = X'_{CH} \cos \delta_{p_o} + Z'_{CH} \sin \delta_{p_o}$$

Fuselage Assembly Free Body

The inertial pitching moment about the wing hinge axis is given by equation (54) in appendix A. For longitudinal motion, the expression may be written

$$M_{y_{F_{inertial}}} = I_{y_F} \dot{q} + m_F[(\dot{U} + qW)Z_F - (\dot{W} - qU)X_F] \tag{148}$$

In linear form,

$$M_{y_{F_{inertial}}} = I_{y_F} \dot{q} + [m_F Z_F U_o]\dot{u} + [-m_F X_F U_o]\dot{\alpha}_F + [m_F X_F U_o]q \tag{149}$$

The applied moments on the fuselage assembly arise from aerodynamic moments and the weight moment caused by the offset center of gravity.

The weight force vector is

$$\hat{\bar{F}}_F = (-m_F g \sin \theta)\hat{i}_{x_H} + (m_F g \cos \theta)\ \hat{i}_{z_H} \tag{150}$$

The pitching moment caused by the weight force is the cross-product of the position vector from the wing hinge to the fuselage center of gravity and the weight force vector:

$$M_{y_{F_{weight}}} = -m_F g Z_F \sin \theta - m_F g X_F \cos \theta \tag{151}$$

Or, in linearized form, with $\theta_o = 0$,

$$M_{y_{F_{weight}}} = [-m_F g Z_F]\theta \tag{152}$$

The aerodynamic moments on the fuselage will be assumed to have contributions from α_F, q, δ_p, V_g, and $\dot{V}_g$.

For the angle of attack contribution,

$$\Delta M_{aero_\alpha} = C_{m_{\alpha_F}} \; 1/2 \; \rho U_o^2 S\bar{C}(\alpha_F + \alpha_{gust}) \tag{153}$$

where

$$\alpha_{gust} = \frac{V_g}{U_o} - \frac{\ell_t}{U_o}\frac{\dot{V}_g}{U_o} \tag{154}$$

Since most of the moment arises from the horizontal tail on the fuselage, it is reasonable to use the gust velocity adjusted for the penetration time from the wing to the tail. Therefore, the pitching moment contribution from fuselage angle of attack is

$$\Delta M_{aero_\alpha} = 1/2 \; \rho U_o^2 S\bar{C} C_{m_{\alpha_F}} \left(\alpha_F + \frac{V_g}{U_o} - \frac{\ell_t}{U_o}\frac{\dot{V}_g}{U_o}\right) \tag{155}$$

The aerodynamic pitch damping term includes a contribution from the gust gradient

$$\Delta M_{aero_q} = 1/4 \; \rho U_o S\bar{C} C_{m_q} \left(q - \frac{\dot{V}_g}{U_o}\right) \tag{156}$$

The downwash angle at the horizontal tail can be expressed in terms of wing circulatory lift coefficient as follows:

$$\epsilon = \frac{d\epsilon}{d\alpha} \; \frac{1}{C_{L_{\alpha_W}}} \; C_{L_W} \tag{157}$$

Thus, the effect of wing lift on the fuselage pitching moment will be

$$\Delta M_{aero_{C_L}} \; \Delta C_{m_\epsilon} \; 1/2 \; \rho U_o^2 S\bar{C} \; \frac{\frac{d\epsilon}{d\alpha}}{C_{L_{\alpha_W}}} \; \Delta C_{L_W} \tag{158}$$

Combining the applied moments and setting those equal to the inertial pitching moment, the fuselage pitching equation becomes, in operational notation,

$$[C62 + (C65 - C61)\lambda - (C59)\lambda^2]\theta + [(C60)\lambda]u + [C63 + (C61)\lambda]\alpha_F$$

$$+ [C66]C_{L_W} + \{[C63] + [(C64)(C63) - C65]\lambda\}\frac{V_g}{U_o} = 0 \tag{159}$$

where

$$C59 = I_{y_F}$$

$$C60 = -m_F Z_F U_o$$

$$C61 = m_F X_F U_o$$

$$C62 = -m_F g Z_F$$

$$C63 = 1/2\ \rho U_o^2 S\bar{C} C_{m_{\alpha_F}} \tag{160}$$

$$C64 = -\frac{\ell_t}{U_o}$$

$$C65 = 1/4\ \rho U_o S(\bar{C})^2 C_{m_q}$$

$$C66 = (C_{m_\varepsilon}\ 1/2\ \rho U_o^2 S\bar{C})(\frac{\frac{d\varepsilon}{d\alpha}}{C_{L_{\alpha_W}}})$$

Equation (159) is the eleventh in the set of linear equations describing the system.

The components of the acceleration of the center of gravity of the fuselage can be expressed in the wing hinge axis system as:

$$(a_{F_{cg}})_x = \dot{U} + qW + Z_F\dot{q} - q^2 X_F$$

$$(a_{F_{cg}})_z = \dot{W} - qU - X_F\dot{q} - q^2 Z_F \tag{161}$$

In linearized form, with $q_o = w_o = 0$,

$$(a_{F_{cg}})_x = \dot{U} + Z_F\dot{q}$$

$$(a_{F_{cg}})_z = \dot{W} - U_o q - X_F\dot{q} \tag{162}$$

The dynamic equation for motion in the x_h direction is,

$$M_F(a_{F_{cg}})_x = F_{x_{W\to F}} + \Delta F_{x_{aero}} - m_F g\theta \tag{163}$$

And,

$$\Delta F_{x_{aero}} = -\Delta D_F = -[C_{D_F}\rho U_o^2 S]u \tag{164}$$

Substituting equations (164) and (162) into (163), the airspeed equation is obtained. In operational form, this is:

$$[C69 - (C67)\lambda]u + [C70 + (C68)\lambda^2]\theta + [1]F_{x_{W\to F}} = 0 \tag{165}$$

where

$$\begin{aligned} C67 &= m_F U_o \\ C68 &= -m_F Z_F \\ C69 &= -C_{D_F}\rho U_o^2 S \\ C70 &= -m_F g \end{aligned} \tag{166}$$

Equation (165) is the twelfth in the set of equations describing the total system.

The equation of motion in the z_h direction is

$$m_F(a_{F_{cg}})_z = F_{z_{W\to F}} + \Delta F_{z_{aero}} \tag{167}$$

The aerodynamic force increment in the z_h direction is assumed to be dependent upon α_f, u, and V_g.

$$\Delta F_{z_{aero}} = -[C_{L_{\alpha_F}} 1/2\ \rho U_o^2 S]\alpha_F + [C_{L_{F_o}}\rho U_o^2 S]u + [C_{L_{\alpha_F}} 1/2\ \rho U_o^2 S]\frac{V_g}{U_o} \tag{168}$$

Substituting equation (168) and (162) into (167), and writing in operational form, the thirteenth and last of the set of linear equations is obtained:

$$\begin{aligned} &[C72 - (C67)\lambda]\alpha_F + [(C67)\lambda + (C71)\lambda^2]\theta + [1]F_{z_{W\to F}} \\ &+ [C73]u = -[C72]\frac{V_g}{U_o} \end{aligned} \tag{169}$$

where

$$C67 = m_F U_o$$

$$C71 = -Y_F X_F$$

$$C72 = -C_{L_{\alpha_F}} 1/2\ \rho U_o^2 S \tag{170}$$

$$C73 = -C_{L_{F_o}} \rho U_o^2 S$$

Matrix Form

As derived, the state vector of the system has 13 components. These are:

$$\bar{X} = \begin{bmatrix} \alpha_c \\ C_{L_c} \\ \delta_c \\ F_{x_{c\to b}} \\ F_{z_{c\to b}} \\ \alpha_W \\ C_{L_W} \\ \delta_p \\ F_{x_{W\to F}} \\ F_{z_{W\to F}} \\ \theta \\ u \\ \alpha_F \end{bmatrix} \tag{171}$$

In matrix form, the equations of motion are:

$$[A]\bar{X} = [B]\delta_t + [C]\frac{V_g}{U_o} \tag{172}$$

In the last equation, [A] is a 13 x 13 matrix of the coefficients of the homogeneous equations, and [B] and [C] are column matrices through which the control tab displacement and gust velocities are introduced to perturb the system.

Conversion to First-Order Form

The numerical integration of the equations of motion requires that an explicit solution be developed for the highest derivative required for each variable.

Although two of the variables of equation (172), α_c and α_w, appear in nonderivative form, their first derivatives are used elsewhere in the set of equations because of the unsteady aerodynamic functions.

To modify equation (172) for direct numerical integration, the α_c and α_w equations were replaced by their time derivatives, and all lower order derivative terms were moved to the right side of the equality sign.

In the computer subroutine for evaluating the derivatives at each instant of time, it was necessary to perform a simultaneous solution for the 13 highest-order derivatives of the modified equations. This solution, combined with another 12 direct integrations for the lower order variables, yielded the current values of all quantities needed in the integration process.

Aerodynamic Coefficients

The aerodynamic coefficients of the representative aircraft were estimated from two primary sources. A vortex-lattice program, modified at Battelle Columbus Laboratories by using the method described in reference 7, was used to predict the static wing and free-trimmer characteristics; the approach outlined in reference 8 was used to estimate the primary contributions of the fuselage and fuselage-mounted stabilizing surface.

Geometrical data for the analyses were obtained from the three-view drawings of the candidate aircraft contained in the main body of the report.

Static Wing/Trimmer Coefficients

Lift-curve slope. The lift-curve slopes for the isolated wing and trimmer surfaces were obtained from the vortex lattice program by using 12 spanwise vortex elements per semispan. For aspect ratio 6, the resulting value was 4.276 per radian.

Profile drag coefficients. The section profile drag coefficient for both surfaces was broadly estimated to be 0.01.

Mutual interference coefficients. Because of their close proximity, the wing and trimmer have significant mutual interference effects. To account for this phenomenon, the effective induced angle of attack on each surface was computed as a function of the lift coefficient on the other surface.

Using the appropriate relative geometry of the surfaces, the influence coefficients were computed from:

$$\frac{d\alpha_c}{dC_{L_W}} = \frac{C_{L_c} - C'_{L_c}}{C'_{L_{\alpha_c}}} \frac{1}{C_{L_W}}$$

$$\frac{d\alpha_W}{dC_{L_c}} = \frac{C_{L_W} - C'_{L_W}}{C'_{L_{\alpha_W}}} \frac{1}{C_{L_c}} \qquad (173)$$

In equations (173), the prime superscript denotes the value obtained without the presence of the other lifting surface.

Representative values, so obtained, are given in table XV for an area ratio of 1/6.

TABLE XV. MUTUAL INTERFERENCE COEFFICIENTS

$\frac{X'_{CH}}{\bar{c}}$	$\frac{Z'_{CH}}{\bar{c}}$	$\frac{d\alpha_c}{dC_{L_W}}$	$\frac{d\alpha_W}{dC_{L_c}}$
2.0	-0.50	0.0226	-0.0140
0.75	-0.364	0.0778	-0.0122
-0.75*	0	0.0898	0.00585
-1.50*	0	0.02772	0.004473

* Tip-mounted aft trimmers.

Induced drag coefficients. The induced drag coefficients for both the wing and trimmer surfaces were estimated to be 0.0624.

Fuselage Coefficients

The aerodynamic coefficients of the fuselage and fuselage-mounted horizontal stabilizer were estimated by assuming an equivalent circular body with area distribution as used in the aircraft shown in figure 2 of the main body of the report.

Following the method of reference 8, the lift and moment contributions of the fuselage and horizontal tail were determined. The reference point for the moment coefficients was the wing hinge axis.

Fuselage-tail lift-curve slope. The lift coefficient of the fuselage-tail assembly, as a function of fuselage angle of attack is estimated to be:

$$C_{L_F} = 0.00751(\alpha_F - 4°) + 0.000033(\alpha_F - 4°) + (0.0104)(0.55\alpha_F) \qquad (174)$$

From which $C_{L_{\alpha_F}} = 0.758$ per radian.

Fuselage static angle of attack stability. Similarly, the slope of the fuselage moment coefficient with respect to angle of attack is

$$C_{m_{\alpha_F}} = -0.006 - 0.00015\alpha_F \text{ per degree} \qquad (175)$$

From which $C_{m_{\alpha_F}} = -0.344$ per radian. (176)

Pitch damping coefficient. The pitch damping coefficient was estimated on the assumption that all damping arises from the forces on the horizontal tail. On this basis, $C_{m_q} = -4.76$ per radian.

APPENDIX C. METHOD OF COMPUTING TURBULENCE RESPONSES

Symbols

L scale length of turbulence, meters (feet)

U airspeed, meters/second (feet/second)

σ_x rms value of variable x

Φ power spectral density function

Ω spatial frequency, radians/meter

Responses to Continuous Turbulence

Equation (1) in this report describes the deterministic response of the longitudinal system to the vertical gust velocity.

For random turbulence responses, the frequency response function is used to compute the spectrum of the response for each variable of interest. The output spectrum for a variable, x, is given by the following equation (ref 6):

$$\Phi_x(\Omega) = \left|\frac{x}{V_g}\right|^2 \Phi(\Omega) \tag{177}$$

where $\frac{x}{V_g}$ is the modulus of a frequency response function which defines the response of the variable to the gust velocity.

The root-mean-square response of the variable is the quantity of interest, and it is then computed from:

$$\sigma_x = \left[\int_0^\infty \Phi_x(\Omega)\, d\Omega\right]^{1/2} \tag{178}$$

In the numerical integration of equation (178), the actual limits of integration were from spatial frequencies corresponding to temporal frequencies ranging from 0.3 to 40 radians per second, using the relationship

$$\Omega = \frac{\omega}{U_o} \tag{179}$$

Only vertical gust components were considered, and the Dryden power spectral density function was used with a scale length of 533.4 meters (1750 feet) and an rms gust intensity of 0.305 meters per second (1 foot per second). The Dryden spectrum is given by

$$\Phi(\Omega) = 0.0283\, \sigma_g^2\, \frac{L}{\pi}\, \frac{1 + 3\Omega^2L^2}{(1+\Omega^2L^2)^2} \tag{180}$$

The frequency response function was computed directly at each frequency by setting the gust velocity equal to $j\omega$ in the equations of motion. In this way, the steady-state sinusoidal response of each variable of interest was computed for each value of the sinusoidal gust velocity frequency, ω. The absolute magnitude of the response function was then computed, as a function of frequency, to obtain the required frequency response function for use in equation (177).

REFERENCES

1. Porter, Richard F.; and Brown, Joe H., Jr.: Evaluation of the Gust-Alleviation Characteristics and Handling Qualities of a Free-Wing Aircraft. NASA CR-1523, July 1970.

2. Porter, Richard F.; Luce, Ross G.; and Brown, Joe H., Jr.: Investigation of the Applicability of the Free-Wing Principle to Light General Aviation Aircraft. NASA CR-2046, June 1972.

3. Schuldenfrei, Marvin J.: Wind-Tunnel Investigation of an NACA 23012 Airfoil With a Handley-Page Slat and Two Flap Arrangements. NACA WR L-261, 1942.

4. Abbott, Ira H.; and von Doenhoff, Albert E.: Theory of Wing Sections. Dover Publications, Inc., New York, 1959.

5. Jones, Robert T.: The Unsteady Lift of a Wing of Finite Aspect Ratio. NACA Report 681, 1940.

6. Etkin, Bernard: Dynamics of Flight. John Wiley & Sons, Inc., New York, 1959.

7. Margason, Richard J.; and Lamar, John E.: Vortex Lattice Fortran Programs for Estimating Subsonic Aerodynamic Characteristics of Complex Planforms. NASA TN D-6142, 1971.

8. Wolowicz, Chester H.; and Yancey, Roxanah B.: Longitudinal Aerodynamic Characteristics of Light, Twin-Engine, Propeller-Driven Airplanes. NASA TN D-6800, 1972.

1. Report No.	2. Government Accession No.	3. Recipient's Catalog No.
NASA CR-2946		

4. Title and Subtitle	5. Report Date
ANALYTICAL STUDY OF A FREE-WING/FREE-TRIMMER CONCEPT	February 1978
	6. Performing Organization Code

7. Author(s)	8. Performing Organization Report No.
Richard F. Porter, David W. Hall, Joe H. Brown, Jr., and Gerald M. Gregorek	
	10. Work Unit No.

9. Performing Organization Name and Address	11. Contract or Grant No.
Battelle Columbus Laboratories 505 King Avenue Columbus, Ohio 43201	NAS4-2378
	13. Type of Report and Period Covered
12. Sponsoring Agency Name and Address	Contractor Report - Final
National Aeronautics and Space Administration Washington, D.C. 20546	14. Sponsoring Agency Code

15. Supplementary Notes

NASA Technical Monitor: Shu W. Gee, Dryden Flight Research Center

16. Abstract

Previous studies have indicated substantial gust-alleviation and other benefits for aircraft employing an unconventional wing, free to pivot about a spanwise axis and trimmed by a trailing-edge control surface. A shortcoming of the basic concept is the relatively low trimmed lift coefficient that is attainable.

The free-wing/free-trimmer is a NASA-conceived extension of the free-wing concept intended to permit the use of high-lift flaps. Wing pitching moments are balanced by a smaller, external surface attached by a boom or equivalent structure. The external trimmer is, itself, a miniature free wing, and pitch control of the wing-trimmer assembly is effected through a trailing-edge control tab on the trimmer surface.

This report describes an analytical study of the longitudinal behavior of representative small free-wing/free-trimmer aircraft. Aft-mounted trimmer surfaces are found to be superior to forward trimmers, although the permissible trimmer moment arm is limited, in both cases, by adverse dynamic effects. It is concluded that aft-trimmer configurations can provide excellent gust alleviation and meet fundamental stick-fixed stability criteria while exceeding the lift capabilities of pure free-wing configurations.

17. Key Words (Suggested by Author(s))	18. Distribution Statement
Free wing Aerodynamics Aircraft design	Unclassified - Unlimited

19. Security Classif. (of this report)	20. Security Classif. (of this page)	21. No. of Pages	22. Price*
Unclassified	Unclassified	129	$4.50

*For sale by the National Technical Information Service, Springfield, Virginia 22161

NASA-Langley, 1978


50

END

8-18-78